Preclinical evaluation of TRAIL combined with PAC-1 to control granulosa cell tumour

by

Powel Crosley

A thesis submitted in partial fulfillment of the requirements for the degree of

Master of Science

in

Cancer Sciences

Department of Oncology
University of Alberta

© Powel Crosley, 2019

ABSTRACT

Granulosa cell tumour (GCT) is a malignant sex-cord stromal cell form of ovarian cancer that constitutes ~5% of ovarian neoplasms. Current chemotherapy regimens are not effective enough in controlling recurrent GCT, and as a result ~80% of women who relapse will die of disease. Procaspase-activating compound 1 (PAC-1) is a small-molecule activator of procaspase-3 that has shown efficacy in treating several cancers either alone or in combination with other agents. Here we investigated the effectiveness of PAC-1 in treating GCT *in vitro*, and the amount of synergy displayed by combining PAC-1 with selected apoptosis-inducing agents. We found that while tumour necrosis factor-related apoptosis-inducing ligand (TRAIL) was only marginally toxic to GCT, combining it with PAC-1, even at low doses, was strongly synergistic in killing an established GCT cell line. The combination was also toxic to patient samples of primary and recurrent GCT cells. Based on those results we sought to overcome known limitations in the clinical effectiveness of TRAIL through generation of a novel recombinant oncolytic vaccinia virus that secretes human TRAIL (VACV^{TRAIL}). Infection and replication by our virus was efficient, it generated significant levels of TRAIL, and it displayed strong cytotoxicity in GCT model cell line KGN. Our attempt to develop a xenograft mouse model using KGN cells for *in vivo* testing of PAC-1 and VACV^{TRAIL} was unsuccessful. While we did see small lesions in mice injected with KGN cells expressing Runx3, the extended time required for development of tumours and their small size currently limits the model's utility as a test platform. Never the less, we propose that the novel combination of this TRAIL-expressing oncolytic virus and caspase-activator PAC-1 has potential as a GCT treatment, and warrants further investigation in models of GCT that are under development.

DEDICATION

This work is dedicated to my late wife, Sladjana M. Crosley.

ACKNOWLEDGEMENTS

My strongest gratitude goes to my supervisor, Dr. Mary Hitt: firstly for allowing me to join her lab and pursue my personal objective of working to find a treatment for this rare cancer; secondly for her continued guidance and support during my graduate program. Dr. Hitt always made herself available to answer my questions, talk through my ideas, and ensure that my experiments were scientifically sound. I would also like to thank my committee members: Dr. YangXin Fu, who has shown keen interest in granulosa cell tumour research and aided my attempt to develop animal models of the disease; and Dr. Ing Swie Goping, who first piqued my interest in investigating apoptosis during a classroom lecture and has been intently supportive of my work. In addition, I thank Dr. Rob Ingham for serving as the external examiner during my thesis defence, and Dr. Gordon Chan for serving as Chair of the examination committee. Also, I thank Dr. Rachel Milner (University of Alberta) and Dr. Ann Dorward (Memorial University) for their support of my application to the Experimental Oncology Graduate Program.

In the lab, I would like to thank Kate Agopsowicz, who trained me on proper lab techniques, provided assistance in the animal work, and served as a sounding board and friend. My lab colleagues have been numerous throughout my time here, but most important to my progress is Dr. Kyle Potts, who served as my great friend and personal Wikipedia any time I had a question or an idea come into my head. It was during a conversation with him in 2015 that we first formulated the concept of using a recombinant vaccinia virus to deliver TRAIL to tumour cells, and his knowledge of and enthusiasm for generating recombinant virus was critical to the success I have achieved. I also thank: Dr. Shyam Chaurasiya, who was a good friend and interested supporter of my work with PAC-1; Quinn Storozynsky, who started the

graduate program with me and has been a friend and sounding board to talk through issues; and the various undergrad and visiting students who have worked in our lab including current members Shae Komant and Xuefei Han. They brought enthusiasm for research and working to help them learn lab processes sharpened my own understanding. I also want to thank the lab technicians Darcy Robillard and Colleen Dluzewski who work to provide us basic reagents, take care of glassware and autoclaving and many other small tasks that we will not appreciate until we have to do them for ourselves.

I also thank colleagues in the Department of Medical Microbiology & Immunology starting with Dr. David Evans whose expertise and support in generating recombinant vaccinia virus was invaluable. I also thank Nicole Favis and Megan Desaulniers for assistance with the various animal experiments; and Dr. Ryan Noyce who eagerly assisted in final design of the vaccinia shuttle plasmid, sequencing of the final recombinant virus, and was always willing to talk through issues that arose.

I also acknowledge the research funding I have received during this project including: a Brian & Gail Heidecker Oncology Graduate Student Travel Award; the Faculty of Medicine and Dentistry 75th Anniversary Graduate Student Award; an Innovation Grant funded by generous supporters of the Lois Hole Hospital for Women through the Women and Children's Health Research Institute; and a Pilot Award from the Sladjana M. Crosley Fund for GCT Research.

Finally, I want to thank all the faculty, staff and trainees in the Department of Oncology for their eager support throughout my program. Their friendship, willingness to help, provide feedback and general camaraderie made my work easier and more enjoyable.

TABLE OF CONTENTS

LIST OF TABLES

LIST OF FIGURES

LIST OF ABBREVIATIONS

AGCT	Adult granulosa cell tumour
ANOVA	Analysis of variance
APAF-1	Apoptotic protease activating factor 1
Asp	Aspartate
Bak	BCL2-antagonist/killer
Bax	BCL2-associated x protein
BCA	Bicinchoninic acid assay
BCG	Bacille Calmette Guerin bacteria
Bid	BH3 interacting domain
BIR	Baculoviral IAP repeat
BPES	Blepharophimosis-ptosis-epicanthus inversus syndrome
BRCA1	Breast cancer gene 1
BRCA2	Breast cancer gene 2
BSA	Bovine serum albumin
CAD	Caspase-activated DNAse
CASP3	Caspase-3
CASP7	Caspase-7
CASP8	Caspase-8
CASP9	Caspase-9
cDNA	Complementary DNA
CDX	Cell-line derived xenograft
ctDNA	Circulating tumour DNA
Cys	Cysteine
DAPI	4',6-Diamidino-2-Phenylindole
DIABLO	Direct IAP binding protein with low isoelectric point
DISC	Death-inducing signaling complex
DMEM	Dulbecco's modified Eagle's medium
DNA	Deoxyribonucleic acid
dNDP	Deoxynucleotide diphosphate
dNMP	Deoxynucleotide monophosphate
dNTP	Deoxynucleotide triphosphate
DR4	Death receptor 4
DR5	Death receptor 5
EDTA	Ethylenediaminetetraacetic acid
ER	Endoplasmic reticulum
EV	Enveloped virus
F12	Nutrient mixture F12

FACS	Fluorescence-activated cell sorting
FADD	FAS-associated death domain
FBS	Fetal bovine serum
FDA	Food and Drug Administration (U.S.)
FIGO	International Federation of Gynecology and Obstetrics
FITC	Fluorescein isothiocyanate
FOXL2	Forkhead box L2
GC	Granulosa cell
GCT	Granulosa cell tumour
GEM	Genetically engineered model
GFP	Green fluorescent protein
GM-CSF	Granulocyte macrophage - colony stimulating factor
gpt	Xanthine phosphoribosyltransferase gene
GSK3-β	Glycogen synthase kinase 3, isoform beta
His	Histidine
IAP	Inhibitor of apoptosis
ICAD	Inhibitor of caspase activated DNAse
IFN	Interferon
IL-2	Interleukin-2
ILZ	Isoleucine zipper
i.p.	Intraperitoneal
JGCT	Juvenile granulosa cell tumour
miRNA	Micro RNA
MOI	Multiplicity of infection
MOMP	Mitochondrial outer membrane permeabilisation
MPA	Mycophenolic acid
mRNA	Messenger RNA
MSC	Mesenchymal stromal cell
MUC1	Mucin 1
MV	Mature virus
OV	Oncolytic virus
PARP	poly(ADPribose) polymerase
PBS	Phosphate buffered saline
PDX	Patient derived xenograft
PFU	Plaque-forming units
p.i.	Post-injection or post-infection
PVDF	Polyvinylidene difluoride
R1	RNR large subunit
R2	RNR small subunit

RFU	Relative fluorescent unit
rhTRAIL	recombinant human TRAIL
RIPA	Radioimmunoprecipitation assay
RNA	Ribonucleic acid
RNR	Ribonucleotide reduction
RT	Radiotherapy
s.c.	Subcutaneous
SCCOHT	Small cell carcinoma of the ovary hypercalcemic type
SD	Standard deviation
SDS	Sodium dodecyl sulfate
SDS-PAGE	Sodium dodecyl sulfate-polyacrylamide gel electrophoresis
SEM	Standard error of the mean
shCASP3	Short hairpin CASP3
SMAC	Second mitochondria-derived activator of caspase
StAR	Steroidogenic acute regulatory protein
sTRAIL	Soluble TRAIL
tBid	Truncated Bid
TK	Thymidine kinase
TRAIL	Tumour necrosis factor-related apoptosis-inducing ligand
TRAIL-R1	TRAIL receptor-1
TRAIL-R2	TRAIL receptor-2
UPR	Unfolded protein response
UV	Ultraviolet
VACV	Vaccinia virus
VACV^{TRAIL}	Vaccinia virus expressing TRAIL
VACV^{YFP}	Vaccinia virus expressing YFP
VGF	Vaccinia virus growth factor
WR	Western Reserve
WT	Wild-type
XIAP	X-Linked inhibitor of apoptosis
YFP	Yellow fluorescent protein
ΔF4L	Vaccinia virus lacking F4L gene
ΔF4LΔJ2R	Vaccinia virus lacking F4L and J2R genes
ΔJ2R	Vaccinia virus lacking J2R gene

CHAPTER 1. INTRODUCTION

1.1 Granulosa cell tumour

The Canadian Cancer Society reports that in 2017, approximately 2,800 women were diagnosed with ovarian cancer and 1,800 women died from the disease [6]. Granulosa cell tumour (GCT) is a non-epithelial, malignant, sex-cord stromal cell form of ovarian cancer that constitutes 5 - 8% of ovarian neoplasms [7, 8] suggesting that annually there are upwards of 140 new cases of GCT in Canada. The disease was first identified 1859 [9], and there are two categories of GCT, adult (AGCT) and juvenile (JGCT), with 95% of GCTs being AGCT [10]. The general incidence of GCT ranges from 0.47 cases/100,000 women in Finland, to 0.99/100,000 in United States/Europe, to 1.7/100,000 in a range of other countries [8, 11-13]. There is no known association between GCT and germline mutations in BRCA1 and BRCA2, known to increase the risk of developing epithelial ovarian cancer [14, 15]. Standard of care treatment for GCT is surgical resection, both for primary and recurrent disease if the recurrence is localized. In the case of advanced-stage disease or widespread recurrence chemotherapy or hormonal therapy may be utilised although results are inconsistent [16].

1.1.1 Epidemiology of GCT

The primary roles for the ovary are to develop mature oocytes for ovulation, and to generate bioactive molecules such as the steroids oestrogen and progestin [17]. GCT originates in granulosa cells which form the follicle around an oocyte and interact with endocrine factors that control maturation of the follicle from a primordial to pre-ovulatory state (Figure 1.1). During fetal development there are several million oocytes/primordial follicles in the developing ovary, but by the time gestation is complete the number of primordial follicles has been reduced to ~400,000, of which only ~400 will ever be selected for ovulation. During

gestation, loss of primordial follicles is largely driven by oocyte quality whereas after puberty follicle loss is regulated by hormone signaling during the menstrual cycle.

Upon initial presentation GCT is almost always confined to one ovary and tumours are commonly large (>10 cm in the greatest dimension) with surgery as the primary treatment modality [18]. The majority (~90%) of GCT cases are classified as FIGO stage I (Table 1.1) [7, 10] but they present a clinical conundrum: five-year survival for early-stage disease is cited as >90% but that is a somewhat misleading metric because GCT is known for late (>5 years) recurrence with 10 – 20 years post-diagnosis not uncommon [19, 20]. Stenwig, *et al.*, reported in 1979 that the average time from diagnosis to recurrence was 8.9 years, and the mean time between recurrence and death from disease was 2.6 years [21]. Multiple retrospective studies have concluded that stage of disease, along with tumour size, to be the leading prognostic factor [22]. Although no causative effect has been inferred, it has been reported that there is a tendency towards increased incidence of breast cancer, another hormonally-driven disease, in women with GCT [23]. The dichotomy between JGCT and AGCT is interesting in that one occurs in young, oocyte-replete women and the other occurs in older, more oocyte-depleted women.

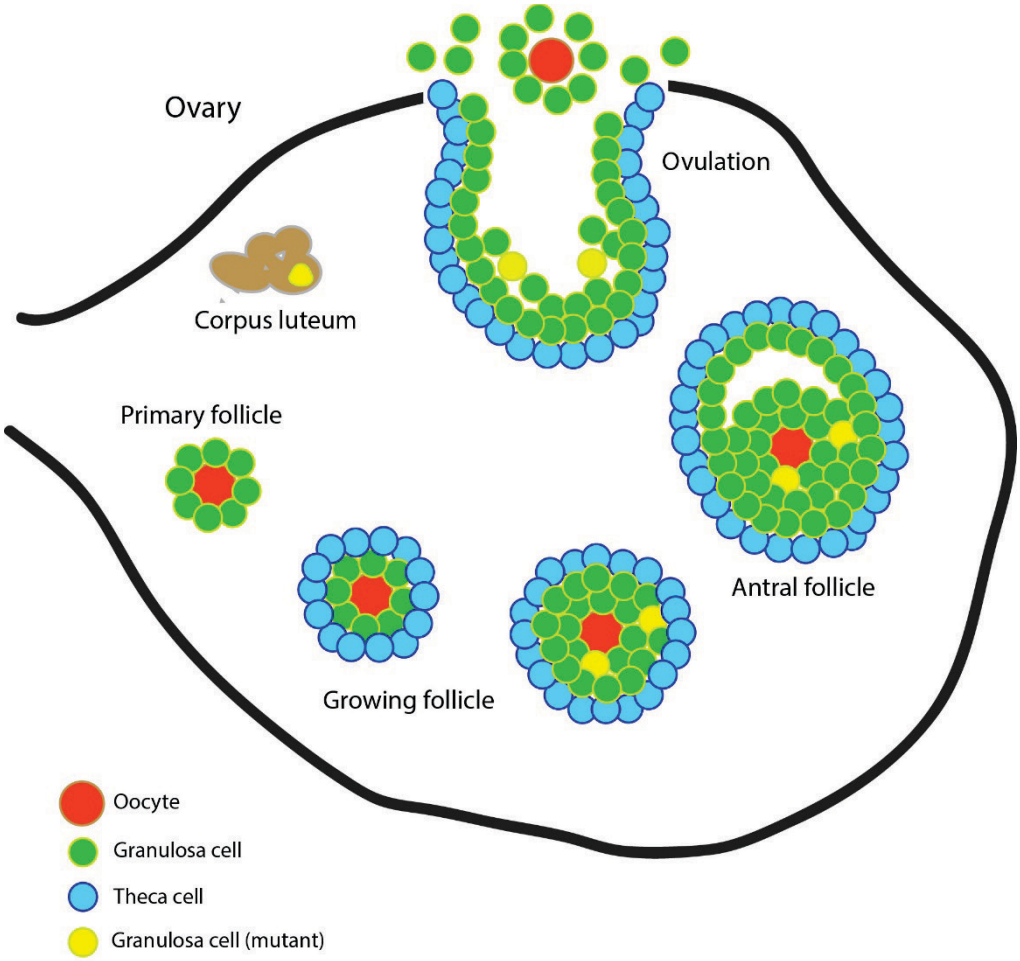

Figure 1.1 - Granulosa cells encapsulate and interact with the oocyte throughout follicular development. GCT may develop initially as mutated GCs that avoid apoptosis during follicular atresia.

Table 1.1- International Federation of Gynecology and Obstetrics (FIGO) staging for ovarian cancer

FIGO stages (National Comprehensive Cancer Network (U.S.), 2005)			
Stage	Description	Sub-category	Condition
I	Tumour confined to ovaries	A	Limited to 1 ovary; capsule intact; no tumour on ovarian surface
		B	Tumour involves both ovaries; capsules intact; no tumour on ovarian surface
		C	Capsule(s) ruptured or tumour on ovarian surface or malignant cells in washings
II	Tumour involves pelvic extension	A	Extensions on uterus or tubes, no malignant cells in peritoneal washings
		B	Extensions on other pelvic tissues, no malignant cells in peritoneal washings
		C	Extensions with malignant cells in peritoneal washings
III	Tumour spread to peritoneum or retroperitoneal lymph nodes	A	Microscopic peritoneal metastases
		B	Macroscopic peritoneal metastases less than 2 cm
		C	Peritoneal metastases > 2 cm and/or regional lymph node involvement
IV	Distant metastases		Excludes peritoneal disease

1.1.1.1 Adult GCT

AGCT is the result of somatic mutations and it tends to occur in post or peri-menopausal women with a median age at diagnosis of 48 - 54 years [8, 24]. During the course of any given menstrual cycle there will be several follicles undergoing development until the dominant follicle is selected for ovulation (Figure 1.1). As the follicle develops, an anti-apoptotic microenvironment is created in response to hormones produced under the influence of steroidogenic acute regulatory protein (StAR) [25], which also serves as a marker for granulosa cell differentiation. Post-ovulation the dominant follicle forms a corpus luteum and the cells undergo apoptosis and autophagy. For those developing follicles that were not selected, hormone signaling shifts to induce follicular atresia which requires granulosa cells to undergo apoptosis. Granulosa cells that have somatic mutations will be resistant to apoptotic processing and, eventually, proliferate to the point of being detected as GCT.

Clinically AGCT is often categorized as a slow-growing, indolent disease of low malignant potential [8, 17, 24, 26, 27]. Common clinical symptoms include endocrine-driven manifestations such as irregular vaginal bleeding, and non-specific complaints such as abdominal pain, abdominal distension, and bloating with tumour size commonly being over 10 cm. Tumours tend to be a mixture of solid and cystic components, and can include hemorrhagic areas due to high vascularization of the tumour.

1.1.1.2 Juvenile GCT

JGCT represents only 5% of GCT cases and while it may visually appear similar to AGCT, it has distinct histopathologic differences and affects a different age group with a reported median age at diagnosis of 3 – 8 years including patients less than 1-year old [28, 29]. As with

AGCT, bilateral disease is very rare and most cases are presented as stage I disease [26]. Common symptoms are reported to be precocious puberty due to oestrogen secretion, abdominal pain and abdominal distension [30, 31]. In general, girls experiencing precocious puberty do not experience ovulation [32]. Interestingly, Dorward, *et al.*, has reported that SWXJ-9 recombinant inbred mice that are used as a model for JGCT only develop disease between 3 and 5 weeks of age [33]. Beyond that the mice are no longer at risk, which suggests that JGCT is the result of early, possibly *in utero*, somatic events whereas AGCT is the result of later, acquired somatic events. This might also be reflected by the propensity for JGCT to occur pre-puberty in women [26], whereas prepubescent girls almost never develop a case of AGCT [32]. While overall rates for recurrence are favourable for patients with early-stage JGCT, advanced-stage disease tends to be more rapidly aggressive than AGCT [26, 34, 35].

1.1.2 FOXL2

FOXL2, a member of the forkhead–winged-helix family of transcription factors, is a single-exon gene that is known to interact with proteins involved in regulating cell-cycle arrest, cell adhesion, genome stability, and apoptosis [36]. FOXL2 is also the earliest marker of ovarian differentiation and is expressed in granulosa cells of the early follicle [37, 38]. FOXL2 regulates granulosa cell proliferation by repressing StAR along with other genes involved in steroidogenesis and cell cycle control [39]. Germline mutations in FOXL2 contribute to conditions such as blepharophimosis-ptosis-epicanthus inversus syndrome (BPES) and premature ovarian failure [38]. In 2009, using whole-transcriptome paired-end RNA sequencing, Shah, *et al.*, discovered a unique somatic mutation in AGCT ($FOXL2^{C134W}$) that was present in 97% of cases and in the model cell line for GCT (KGN) [37] meaning the mutation can

be used for diagnostic purposes [40]. While research continues to fully decipher the role of FOXL2^{C134W} in GCT oncogenesis, it has been found that the mutation persists in recurrent disease lending credence to its importance in oncogenesis [41]. FOXL2 has been found to be missing or expressed at very low levels in most JGCTs emphasizing the fact that AGCT and JGCT are two distinct diseases arising from the same cell type [42, 43]. For women with AGCT, it has been shown that FOXL2^{C134W} can be detected in circulating tumour DNA (ctDNA) and may represent an effective, non-invasive means for clinical surveillance of recurrence with the ability to detect disease before elevation of other serum markers [44].

1.1.3 Current treatment options

Surgery is the cornerstone for clinical treatment of GCT, both primary and recurrent disease. The extent of surgical intervention depends on the extent of the woman's disease, her age and fertility status. At a minimum, conservative surgery will involve unilateral salpingo-oophorectomy and clinical guidelines recommend that surgical staging be performed even if it is presumed to be early-stage disease [45, 46]. Post-menopausal women will typically be advised to undergo bilateral salpingo-oophorectomy or total abdominal hysterectomy, but younger women may wait on more radical intervention in order to preserve their fertility [47, 48].

Clinical guidelines recommend chemotherapy for GCT only in the case of advanced-stage or recurrent disease [46, 49]. Currently the most-used regimens for patients are combinations of bleomycin, etoposide and cisplatin (BEP), or carboplatin and paclitaxel. Reported results have varied in terms of clinical response, but there has been general inability to sustain durable response in patients, which contributes to the high mortality (~80%) in

patients with recurrent disease [7, 19, 26]. In fact, multiple retrospective analyses of case history data conclude that there is no survival advantage between adjuvant chemotherapy, radiotherapy, or observation [45, 50, 51].

Radiotherapy (RT) is a less commonly used treatment option as adjuvant therapy. It was reported to be somewhat useful for control of recurrent GCT in a limited retrospective analysis [52], although a larger, 45 year retrospective assessment in Canada concludes there is no demonstration of survival advantage with use of RT [53]. Choan, *et al.*, suggest that the problem assessing RT effectiveness partly lies in differences between eras of RT methodology, dosing levels, and inconsistent or lack of sectional imaging to assess treatment effect [54].

1.1.4 Factors impacting research on GCT

As a rare disease, GCT presents limitations on the ability to robustly research both the nature of the disease and the effectiveness of treatment regimes. Clinically, there have been numerous retrospective studies of GCT patients attempting to analyse treatment outcomes [22, 45, 55-57]. Most of them have low sample numbers; involve incorporating data from multiple treatment centers with inconsistent record-keeping; and/or cover a study period that may be too short—given the tendency for late recurrence of GCT—or so long that specific treatment practices could have changed but not be captured in data (e.g., records indicating chemotherapy was used, but not the number of cycles) (Table 1.2). As a result posted findings can be confusing with wide variations in individual parameters reported such as: age at diagnosis; stage of disease; recurrence rate; time to recurrence; and effectiveness of treatment. Prospective trials investigating adjuvant chemotherapy is especially needed for GCT, but rarity

of the disease and need for long-term follow-up means that such trials would have difficulty reaching statistical power, especially if looking at incremental changes in survival [55].

Pre-clinical research faces a more basic limitation in that there is only one established cell line for GCT (KGN) that carries the FOXL2^{C134W} mutation [58, 59] that differentiates AGCT from other ovarian malignancies, and there are no cell lines definitively characterized as JGCT after the COV434 cell line was determined to display markers more typical of small-cell carcinoma of the ovary, hypercalcemic type (SCCOHT) [60, 61]. To complicate matters further there is no established xenograft animal model for GCT. There have been only a few reports on the establishment of tumours from the human adult GCT cell line KGN (which contains the FOXL2^{C134W} mutation [62]) [63-65] but in these reports endpoints varied considerably and tumours were very small, thus not ideal as a model for testing therapeutics (Table 1.3). The conclusions reached by these reports also vary from suggesting: betaglycan moderates tumourigenesis of KGN [63]; GCT is the result of GSK3-β-mediated post-translational phosphorylation of FOXL2^{C134W} on S33 [66]; KGN spontaneously transforms into an aggressive phenotype with advanced passages [64]; and GCT oncogenesis is promoted by microRNA-10a through downregulation of PTEN and, interestingly, GSK3-β [65].

Table 1.2 - Selected retrospective studies of GCT cases

Study	NCDB	Bryk	Mangili	Sun	Uygun	Haupsy	Suri	Babarovic
N	2660	187	97	176	45	103	201	36
Study period (yr)	15	56	43	26	19	45	15	18
Median age	53	53	51	46	46	47	47	54
Stage 1 (%)	64	89	72	77	52	77	86	100
Recurrence (n)	--	54	33	37	9	39	17	4
Deaths[1]	417	27	5	5	18	10	--	2
Median follow-up (yr)	5.9	13.7	7.3	5.1	7	6.1	3.4	9.8
Tumour size (cm)	9	10	--	10.4	--	10	--	6.6
Chemo (n)	610	32	23	28	30	0	41	3
Rad (n)	39	23	2	--	11	31	--	--
Median time to recurrence (yr)	--	7	4.4	4.8	1.6	--	--	3.3
Reference	***[55]***	***[67]***	***[68]***	***[22]***	***[69]***	***[45]***	***[45]***	***[70]***

[1] Patient death from disease

Table 1.3 - Reported attempts to generate KGN xenograft animal models

Study	Reference	Injected cells	Mice age	Endpoint	Tumour size	Notes
Bilandzic	[63]	5 x 10^6	6 wk	16 wk	24 mm^3	*a, b, c*
Kim	[66]	2 x 10^7 (x2)	5 wk	4 wk	10 mm^3	*a, b, c*
Imai	[64]	5 x 10^6	6 wk	12 wk	13.5 mm^3	*a, b, d, e*
Tu	[65]	5 x 10^6 1 x 10^6	4–6 wk 4–6 wk	8 wk 4 wk	6 mm (diameter) Not reported	*a, c?, f* *c?, g, h*

a – Size/volume estimated from graph data or published image
b – Subcutaneous injection using KGN cells
c – Model was Balb/$c^{nu-/nu-}$ female mice (nude)
d – Model was BALB/c $^{Foxn1/Foxn1}$ female mice (nude)
e – Cells were advanced passage (p58) KGN cells
f – Cells were dox-inducible miR-10a KO KGN cells
g – Orthotopic injection into ovarian bursa of nude mice
h – Cells were pLVTHM-miR10a (miR10a overexpressing) KGN cells

1.2 Programmed cell death – Apoptosis

1.2.1 Apoptotic pathways

One of the main objectives for most cancer treatments is overcoming a long-established hallmark of cancer: resistance to the cellular process of programmed cell death, apoptosis [71, 72]. First defined in 1972 [73], the process of apoptosis is part of the normal lifecycle of cells as it allows for deletion of damaged or aged cells, and recycling of constituents, without disrupting nearby tissue and without inflammation. Apoptosis is activated in response to irreparable DNA damage, external stimuli, or other cellular stresses [74-76]. In response to these stimuli the cell undergoes distinctive morphological changes resulting in condensation of nuclei, cytoskeletal restructuring, and the blebbing of small apoptotic bodies that eventually undergo phagocytosis [77]. There are multiple pathways for execution of apoptosis within a cell, with separate triggering events. What all apoptotic pathways have in common is that they are largely regulated by caspases (cysteine-dependent aspartate-specific proteases), a family of proteolytic enzymes [78].

Within the group of caspases involved there are two classifications: initiator (caspase-2, -8, -9, 10), and effector caspases (caspase-3, -6, -7) [79, 80]. In general, initiator caspases are activated by upstream biologic events and they in turn activate the effector caspases. The effector caspases then execute their proteolytic functionality leading to demolition of the cell [81]. Each caspase initially exists as an inactive zymogen and transforms into an active multimeric conformation [82]. The zymogen is almost all localized to the cytoplasm while active forms of some caspases traffic to the nucleus to execute part of their role [83, 84]. Because of the potential for detrimental effects from incidental activation of caspase functions,

the cell maintains an equally robust complex of anti-apoptotic proteins that are often upregulated in cancer cells leading to resistance to therapy and proliferation of cancer cells [76]. There are also caspases that fill roles outside apoptosis, primarily dealing with inflammation (caspase-1, -4, -5) [85], which is a research area outside the scope of this report. What follows is a brief description of three apoptotic pathways relevant to this report.

1.2.1.1 Intrinsic pathway

The intrinsic pathway is initiated in response to stress stimuli signaling that irreparable DNA damage has occurred. This induces oligomerization of BCL2-antagonist/killer (Bak) and BCL2-associated X protein (Bax) in the mitochondrial outer membrane creating pores through which cytochrome c and second mitochondria-derived activator of caspase/direct IAP binding protein with low isoelectric point (SMAC/DIABLO) are released (Figure 1.2) [76]. Cytochrome c binds with apoptotic protease activating factor 1 (APAF-1) and recruits/activates caspase-9 (CASP9) to form the apoptosome heptamer [80, 86]. CASP9 then cleaves/activates caspase-3 (CASP3), the primary effector caspase. CASP9, CASP3, and CASP7 can be directly inhibited by X-linked inhibitor of apoptosis (XIAP) which has three baculoviral IAP repeat (BIR) domains that specifically bind the caspases (BIR2 binds CASP3/CASP7; BIR3 binds CASP9) [87-89]. SMAC/DIABLO inhibits XIAP from binding caspases through competitive binding to the BIR domains, allowing apoptosis to occur. Two other cellular inhibitor of apoptosis proteins (cIAP1/cIAP2) share homology with XIAP but are only weak inhibitors of CASP3 and CASP7. It is thought that their anti-apoptotic role may partly be to act as a protein sink by binding pro-apoptotic proteins such as SMAC/DIABLO [90].

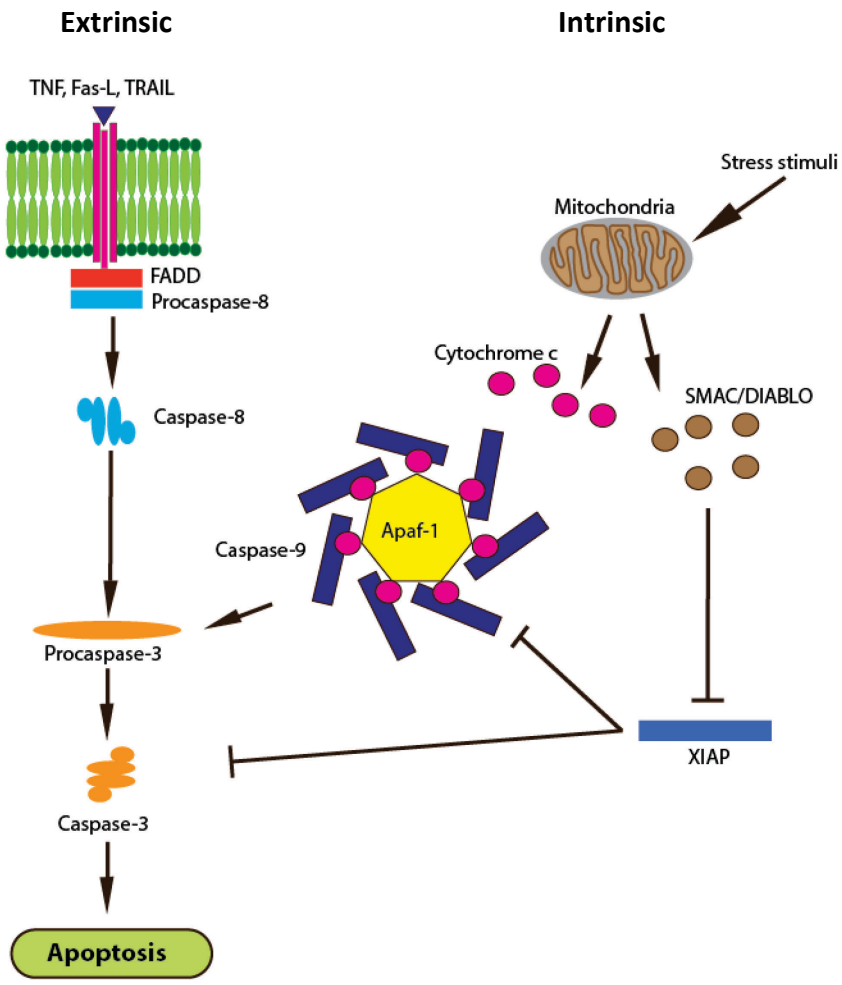

Figure 1.2 – Primary apoptotic pathways. Ligands such as TRAIL bind death receptors to induce the extrinsic pathway while stress stimuli such as irreparable DNA damage induce the intrinsic pathway. Both pathways converge with caspase-3-activated apoptosis.

1.2.1.2 Extrinsic pathway

The cellular membrane contains a number of death receptors belonging to the tumour necrosis factor (TNF) family. Among these are receptors for tumour necrosis factor-related apoptosis-inducing ligand (TRAIL), death receptors 4 and 5 (DR4/DR5) [76, 91]. The receptors have extracellular, transmembrane, and cytosolic domains. When ligands bind the receptor, signals recruit Fas-associated via death domain (FADD) and caspase-8 (CASP8) to the receptor's cytosolic death domain forming the death-inducing signaling complex (DISC). CASP8 is then activated to cleave CASP3 and also truncates BH3 interacting domain death agonist (tBid), a pro-apoptotic protein. tBid then induces oligomerization of BAK and BAX resulting in mitochondrial outer membrane permeabilisation and release of cytochrome c and SMAC/DIABLO as described for the intrinsic pathway [92].

1.2.1.3 Endoplasmic reticulum (ER) stress response

The ER is a fundamentally important organelle where synthesized secreted proteins undergo post-translational modification prior to being released from the cell to carry out their cellular function [93, 94] and where calcium ions are stored for release into the cytosol [95]. Changes in ER homeostasis result in a state of ER stress, which if not rectified leads to apoptotic cell death [93, 94]. Response to ER stress is called unfolded protein response (UPR), which initially helps the cell adapt to stressful conditions such as hypoxia [95]. If the ER stress is protracted, however, the UPR signals a switch to pro-apoptotic processes, leading to cell death through activation of caspase-12 (CASP12) which then cascades activation of CASP9 and CASP3 [93, 95, 96].

1.2.2 Caspase-3

CASP3 is the primary effector of apoptosis in most cells. Once activated it begins proteolytic cleavage of substrates leading to controlled demolition of the cell and distinctive morphological signs of apoptosis, such as membrane blebbing [77, 78]. CASP3 also translocates to the nucleus to cleave inhibitor of caspase-activated DNase (ICAD) and poly(ADPribose) polymerase (PARP) [97]. Cleavage of ICAD frees up caspase-activated DNase (CAD) which then carries out DNA fragmentation [85].

As a zymogen, CASP3 consists of three domains: a small prodomain, a large subunit (P17) and a small subunit (P12) with a polypeptide linker between the two subunits. The P17 subunit contains the active site which is a Cys – His catalytic dyad. Once the interunit linker is cleaved the P17 and P12 subunits form a dimer which the combines with another P17/P12 dimer to form the final active heterodimer (Figure 1.3) [79, 85, 98, 99].

Paradoxically, CASP3 expression is elevated in many cancers even though the cancer cells show resistance to endogenous death-signaling and signaling induced by chemotherapeutic agents [100]. The cancer cell employs endogenous anti-apoptotic pathways to evade cell death including proteins such as XIAP, and in the case of CASP3 Zn^{2+} ions. Specifically in the case of CASP3, Zn^{2+} sterically limits access to the active site (near His121) and may interfere with conformational exposure of the IETD inter-subunit cleavage site (at Asp175) [101, 102].

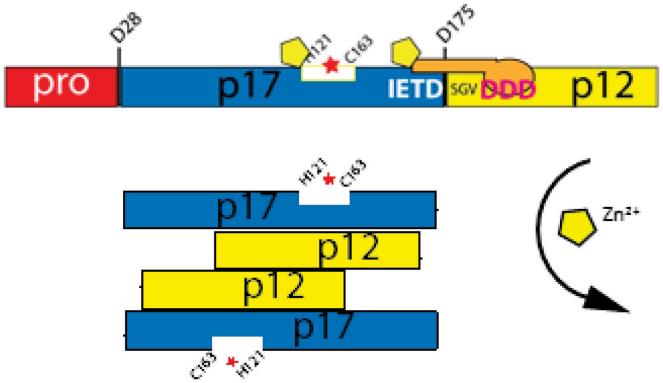

Figure 1.3 - Procaspase-3 matures into an active heterotetramer. Procaspase-3 is inhibited by Zn^{2+} ions (yellow pentagon) near its active site (red star) and triaspartic acid 'safety catch' (DDD). The cleavage site in procaspase-3 (IETD) generates a large/small subunit (p17/p12) dimer, with the fully mature caspase-3 forming a heterotetramer with two catalytically active sites.

1.2.3 Procaspase activating compound-1 (PAC-1)

Procaspase activating compound-1 (PAC-1) is a small-molecule compound that was identified through a high-throughput screen of ~20,500 small-molecule compounds for the ability to activate procaspase-3 *in vitro* [100]. Later it was determined that PAC-1 prepares CASP3 for activation by sequestering labile inhibitory Zn^{2+} ions from the zymogen allowing it to undergo either auto-maturation into an active state or cleavage by initiator caspases, caspase-8 and caspase-9 (CASP8/CASP9) [103]. The ability of CASP3 to auto-mature means that sequestration of Zn^{2+} potentiates activation of apoptosis even when upstream signals are defective, in a manner directly proportional to the concentration of procaspase-3 in the cell, explaining PAC-1 selectivity for cancer [100, 104]. PAC-1 has shown efficacy as an anti-cancer agent *in vitro* and *in vivo,* and has minimal activity towards other zinc-dependent enzymes [105], which may account in part for its demonstrated safety. PAC-1 is currently in phase I trials for advanced malignancies and in combination with temozolomide for recurrent malignant glioma (NCT02355535, NCT03332355) [106].

1.2.4 Tumour necrosis factor-related apoptosis inducing ligand (TRAIL)

TRAIL is a 281-amino-acid transmembrane protein whose extracellular domain (aa 114-281) binds TRAIL-R1 or TRAIL-R2 (also known as death receptor-4 or -5, respectively (DR4/DR5)) triggering apoptotic pathways [107, 108]. TRAIL executes the extrinsic apoptotic pathway through CASP8 activation of CASP3. It augments induction of apoptosis through the intrinsic pathway by truncating Bid, which induces mitochondrial outer membrane permeabilisation (MOMP) and subsequent activation of CASP3 by CASP9 (Figure 1.2) [109, 110]. Full-length

TRAIL can act in an autocrine manner to bind DR4/5, or the extracellular domain can be cleaved to form soluble TRAIL to act in a paracrine manner. In either form TRAIL is only active once it forms a trimer, causing trimerization of the ligated death receptor. Physiologic TRAIL is stabilized in the trimeric form through non-covalent interaction of Cys230 with a Zn^{2+} ion [111].

TRAIL has been reported to be selective for cancer cells without causing toxicity in normal cells [112] and clinically it has been well-tolerated by patients, both alone and in combination with other drugs in clinical trials [111-115]. There is some debate as to whether the full-length or soluble form of TRAIL is more effective as a cancer therapy [116-118]. Perplexingly however, clinical trials with soluble TRAIL have failed to display efficacy [119]. Assessment of results has identified a short half-life *in vivo*, lack of drug stability and inability to reach therapeutic concentration at the tumour site as limiting factors along with a significant reduction in effectiveness as a monomer or homodimer versus as a homotrimer [120, 121].

TRAIL and TRAIL-R2 (DR5) have been found to be expressed in human fetal ovaries from the 11^{th} week of gestation onward [122] indicating its role in normal ovarian apoptosis such as occurs with follicular atresia [25]. While normal granulosa cells have been found to be resistant to TRAIL-induced apoptosis, follicles undergoing atresia have upregulated expression of TRAIL mRNA [123]. It has also been shown that KGN cells undergo apoptosis in a dose-dependent manner when treated with rhTRAIL [122]. Using a panel of patient-derived GCT tissue, Färkkilä, *et al.*, found variable amounts of TRAIL mRNA expression and no correlation to tumour size [124]. Immunohistochemistry of tumour tissue displayed diffuse staining of tumour cells but stronger staining in tumour stroma. TRAIL protein expression was inversely correlated with

tumour size for tumours > 10 cm, suggesting that reduction of TRAIL production in the stroma might support progression of GCT. It has also been reported that in GCT expression of GATA4 protects against TRAIL-induced apoptosis [125] and high GATA4 expression is associated with more aggressive disease [126].

1.3 Development of vaccinia viruses for treating cancer

1.3.1 History of oncolytic viruses (OV)

The interaction between viruses and cancer was first noted anecdotally by George Dock in 1904. He initially noticed that a patient with leukemia had a decreased leukocyte count after contracting influenza. The use of viruses as cancer therapy was largely unexplored, however, due to a poor understanding of viral biology, until the late 1940s when it was observed that two patients with Hodgkin's lymphoma had a sustained partial anti-tumour response after contracting hepatitis [127-129]. That led to the first clinical trial involving 22 patients with Hodgkin's lymphoma. This was followed by multiple trials with diverse viruses, all of which were ineffective and the use of virus as cancer therapy waned until advances in recombinant deoxyribonucleic acid (DNA) technology provided the opportunity to engineer viruses that were more selective for tumour cells, which enhanced their safety. Since then, OVs have developed into a widely studied field due to their selectivity for cancer without causing harm to normal issue.

OV offer several means for killing cancer cells, such as: direct lysing of the cells; release tumour antigens that activate an anti-tumour immune response; destruction of tumour vasculature; and delivery of cytotoxic transgenes that are amplified/expressed by the infected cell [130]. Once the infected cell is lysed, amplified viral progeny spread through the tumour to

repeat the cycle. As of April 15 2019 there are 81 clinical trials registered in the NIH clinical trials database (clinicaltrials.gov) for oncolytic virus use against cancers, of which 47 are (or soon will be) active. To date, only one oncolytic virus (talimogene laherparepvec, Imlygic) has received US FDA approval (for unresectable melanoma). Another oncolytic virus (pexastimogene devacirepvec, Pexa-vec) is currently in phase 3 trials for liver cancer.

1.3.2 Biology of vaccinia virus (VACV)

VACV is a large, enveloped double-stranded DNA virus that belongs to the *Poxviridae* family of viruses. VACV encodes many of the proteins required for viral replication including proteins involved in DNA synthesis. This allows VACV to complete its lifecycle entirely within the cytoplasm of infected cells following construction of membrane-bound factories [131, 132]. VACV has been well-characterized due to its use as the vaccine that eradicated smallpox and has an established safety profile. Because of its large size, VACV may preferentially locate in tumours due to the leaky nature of tumour vasculature [133, 134]. VACV can be in one of two forms of infectious particles: mature virion (MV) and enveloped virion (EV). MV have a single wrapping membrane and primarily collect in the cell until released by cell lysis. EV are formed by transportation of MV through the Golgi apparatus where it is wrapped with another membrane on its way to being extruded from the cell [135]. It is thought that the wrapping of host membrane around the EV helps it avoid immune detection [136].

As reviewed in [135], VACV enter a cell either through macropinocytosis or by membrane fusion with the cell membrane. After cell entry the viral core is released into the cytoplasm and early transcription takes place controlled by viral RNA polymerase, which produces mRNA that is translated by host ribosomes. Among the early products are proteins

for DNA replication and intermediate gene transcription. As the viral core is uncoated, viral factories are established. In the viral factory, DNA replication will begin which also signals the start of intermediate and late gene transcription. Late gene products are largely structural or associated with enzymes required for viral entry and early transcription following the next round of infection. As virion assembly begins crescent structures made of lipids and proteins enclose the genome and core proteins, and these will become MV. Most MVs remain within the cell until lysis, however some are trafficked through the Golgi network and pick up an additional membrane layer to become EV. The EV then fuses with the plasma membrane and is released to the extracellular space, or is extruded by an actin-tail polymerization to enter a neighboring cell [135].

VACV is attractive as an oncolytic vector because it is very efficient both in DNA replication and in cell-to-cell spread of virus. Within two h of infection, early genes are already being synthesized and viral assembly begins as soon as six h post-infection [137]. VACV generates two forms progeny. The EV then fuses to the cell membrane and is either extruded by an actin tail to infect a nearby cell, or released as free virions. Importantly, the host-membrane-wrapped EV is relatively stable in blood, able to resist antibody and complement-mediated neutralization when administered intravenously [133, 138].

1.3.3 Development of more tumour-selective VACV

Normal cells limit virus production and spread via control pathways aimed at restricting viral gene expression thereby disrupting viral DNA replication. In addition, cells release cytokines, such as interferon (IFN), to signal other cells of an infection and generate an immune

response [139]. These control pathways are often deregulated in tumour cells, which allows a foothold for OVs to replicate, achieving tumour selectivity [139, 140].

The availability of a pool of 2'-deoxyribonucleotides (dNTP) are critical for DNA replication, such as is carried out by proliferating cancer cells [141]. DNA synthesis is also crucial for replication of OV. Maintenance of dNTP pools is carried out through two parallel pathways: the *de novo* or the salvage pathway (Figure 1.4). In *de novo* synthesis of dNTPs, ribonucleotide reductase (RNR) catalyzes precursor molecules to generate purine and pyrimidine nucleosides. RNR is a heterotetramer made of large (R1) and small (R2) subunits (Figure 1.5A). Of the two subunits, R2 is the rate-limiting enzyme [2, 142]. While the level of R1 within a cell is relatively constant throughout the cell cycle, the level of R2 is cell-cycle dependent and rises during DNA replication [141]. The salvage pathway recycles purine and pyrimidine nucleosides and, as an example, cellular thymidine kinase (TK) is a key enzyme in the thymidine salvage pathway [131, 143].

VACV encodes viral homologues for TK (J2R), R1 (I4L), and R2 (F4L) and they are able to combine with cellular R1/R2 to form a chimeric RNR complex [2] (Figure 1.5B). To increase selectivity of VACV for cancer cells, there is commonly mutation or deletion of the viral TK gene (ΔJ2R), including in VACV that are currently in clinical trials [144]. Gammon, *et al.*, showed that in the *de novo* pathway, the R2 subunit homologue F4, but not R1 subunit I4, was critical for

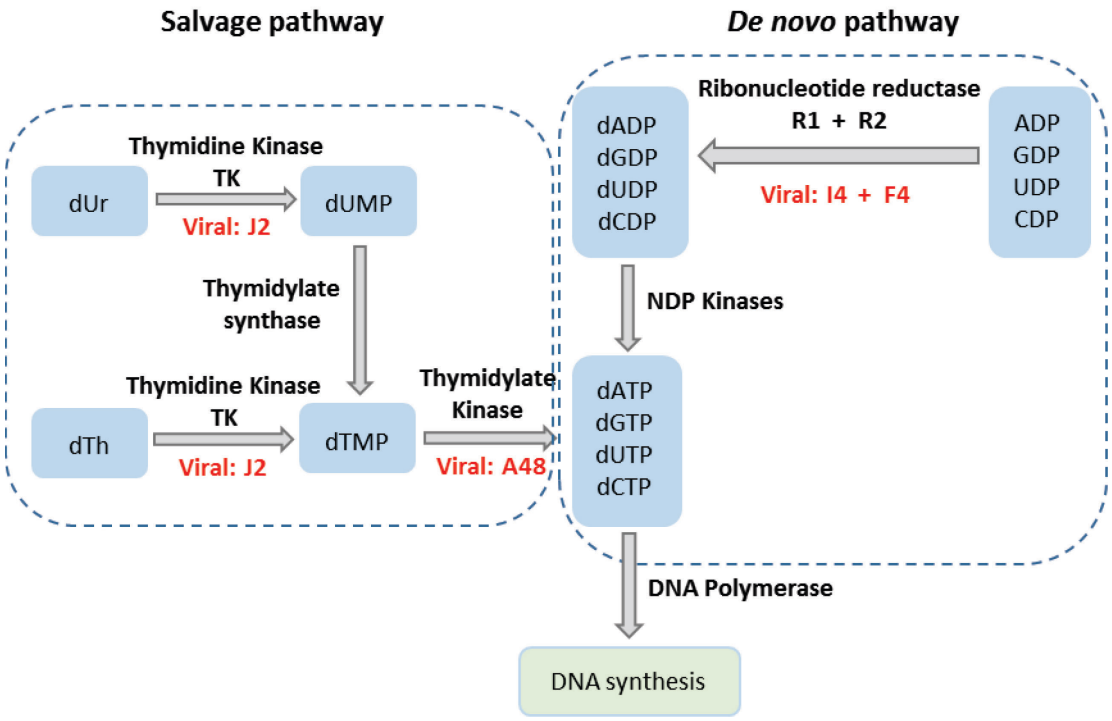

Figure 1.4 – Nucleotide biosynthesis pathways.

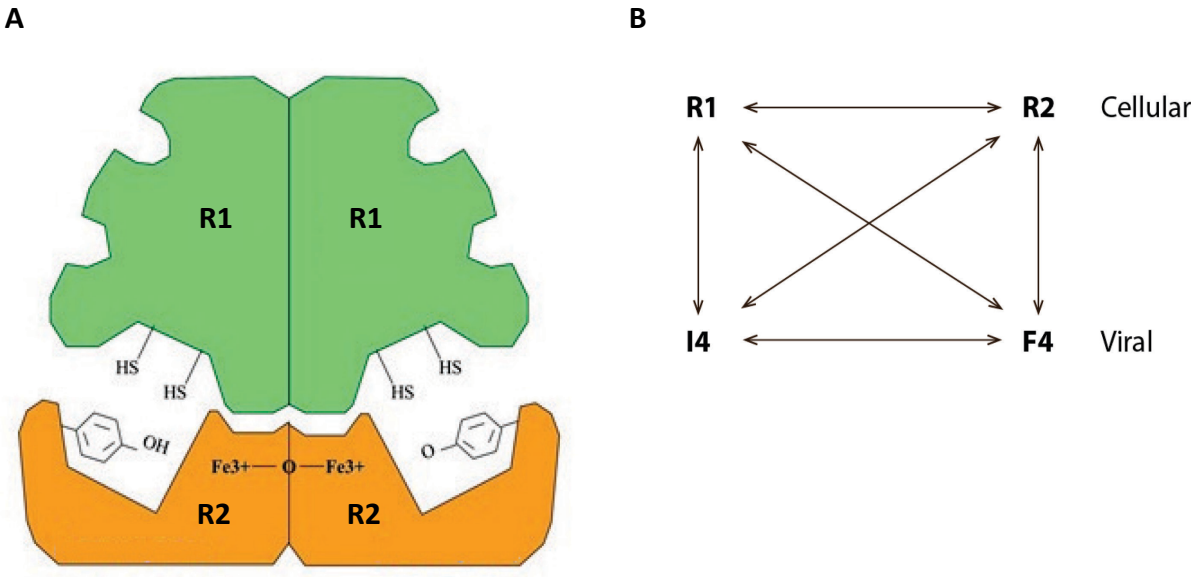

Figure 1.5 – The ribonucleotide reductase (RNR) complex. (A) RNR is a heterotetrameric complex composed of large (R1) and small (R2) subunits. **(B)** VACV encodes viral homologues of the large (I4) and small (F4) subunits and can combine with the cellular homologues to form functional chimeras. Adapted from [113] with permission from AACR.

VACV replication both *in vitro* and *in vivo* [2]. Potts, *et al.*, further showed that the combined western reserve-based (WR) VACV$^{\Delta F4L\Delta J2R}$ was able to control BCG-resistant bladder cancer *in vivo* and generate a lasting anti-tumour immune response [145]. The result is that recombinant VACV lacking two key genes for viral DNA synthesis provides an improved safety profile while maintaining efficacy both *in vitro* and *in vivo*.

1.3.4 Arming VACV for delivery of gene therapy

Gene therapy is the general term for treatments that involve inserting foreign DNA into a patient's cell. The introduced gene may be intended to correct a mutated gene in the patient's own genome, introduce a new gene to fight the disease, or to knock-out a gene that is acting improperly. Among the potential advantages of gene therapy in treating cancer are the possibility of high dose and longer-term expression of a drug; localized delivery of drug with minimal toxicity to other cells [146]. VACV is an excellent vector for gene therapy in cancer treatment. As described earlier, VACV is highly efficient at infecting cells; rapidly begins viral replication; is able to travel safely to tumour sites through vasculature; is tumour-selective; and is able to encode a large range of transgenes for expression in infected cells [138]. Design of a transgene under the control of a VACV early viral promoter allows for rapid expression of the transgene, and use of an early/late promoter will allow for robust expression throughout the viral lifecycle. To date, there are, or have been, clinical trials using VACV-mediated gene therapy for expression of: granulocyte-macrophage colony-stimulating factor (GM-CSF) (SillaJen Pexa-vec); Mucin 1 (MUC1) and interleukin-2 (IL-2) (Transgene TG4010); a proprietary gene (FCU1) for conversion of prodrug 5-FC into 5-FU (Transgene TG6002) [147-150].

1.4 Animal models in cancer research

Animal models of cancer have become a standard tool for researchers looking to understand both the etiology of cancer, and to assess the efficacy of potential new treatments [151]. Animal models of human cancer, xenograft models, are either cell-line-derived or patient-derived (CDX and PDX, respectively) and are generated in immunocompromised animals. They have an advantage in that the models can develop tumours that mimic at least some aspects of the human tumours from which they were generated. A disadvantage of CDX and PDX models is that the animals lack, or have severe defects in, their immune system and it is therefore not possible to assess what the immune response to a treatment may be [152].

Models of immunocompetent animals can fall into several categories, most commonly syngeneic or genetically-engineered models (GEM). Syngeneic mouse models, for example, allow allografts of mouse cancer cell lines allowing rapid, scalable and economic assessment of potential therapies. One drawback to the widespread use of syngeneic models, however, is the limited number of cell lines available for use in these models, which is especially the case for many rare or less-researched cancers. GEM, on the other hand, provide potential opportunity to investigate the role of cell-specific genes in tumourigenesis through development of models that can be induced to, or spontaneously develop cancer. These models can also provide a more physiologically-relevant microenvironment for the developing tumour and the ability to assess the immune response *in vivo*. There are drawbacks to GEMs including: GEM may have lower mutational burden because the tumours are generated as the result of a select set of mutations and gene expression may exceed patient-relevant levels [152]; there will be latency

and variable penetrance in disease development [153]; and costs tend to be higher due to animal numbers required for animal cross-breeding [152].

1.5 Project rationale

GCT is an especially troublesome diagnosis for women because: it often presents as early-stage disease, which might otherwise suggest a favourable prognosis; is clinically considered an indolent disease of low malignant potential; is known for late relapse (> 5 years after diagnosis); and has repeatedly shown itself to be highly resistant and/or refractory to standard chemotherapy. Even in the case of early-stage disease women must be vigilant for the remainder of their life due to the fact that currently, 80% of women who have recurrence of GCT die of disease.

In an attempt to address this lack of effective treatments for recurrent GCT, here we report on the testing of a novel small-molecule CASP3 activator (PAC-1) in combination with an activator of the extrinsic apoptotic pathway (TRAIL). The combination of clinically-relevant doses of PAC-1 and rhTRAIL resulted in effective control of both model GCT cell line KGN, and cultured patient-derived GCT cells *in vitro*. The combination of rhTRAIL with PAC-1 displayed a synergistic drug interaction in GCT yet was less toxic to normal cells indicating a potential safety profile in keeping with those reported for the individual agents.

Based on those results, we generated a unique recombinant VACV that lacks the viral *F4L* and *J2R* genes normally used for nucleotide biosynthesis, and expresses soluble TRAIL ($VACV^{TRAIL}$). That combination results in a VACV that is tumour-selective and delivers TRAIL directly to the tumour site. Combining $VACV^{TRAIL}$ with PAC-1 resulted in more effective killing of

GCT cells *in vitro* than VACV^{TRAIL} alone, and supernatant from infected cells contained effective levels of soluble TRAIL that was cytotoxic to GCT even in the absence of active virus.

This thesis demonstrates the potential for a novel combination of oncolytic VACV, gene therapy, and small-molecule activation of apoptosis in cancer cells (Figure 1.6). Recurrent disease, especially metastatic disease, is the bane of cancer therapy and GCT is known to have a poor prognosis once relapse occurs. With its tropism for replicating cells, VACV^{TRAIL} could be effective in clearing micro sites of tumour cells allowing for more sustained disease-free survival and decreased recurrence rates.

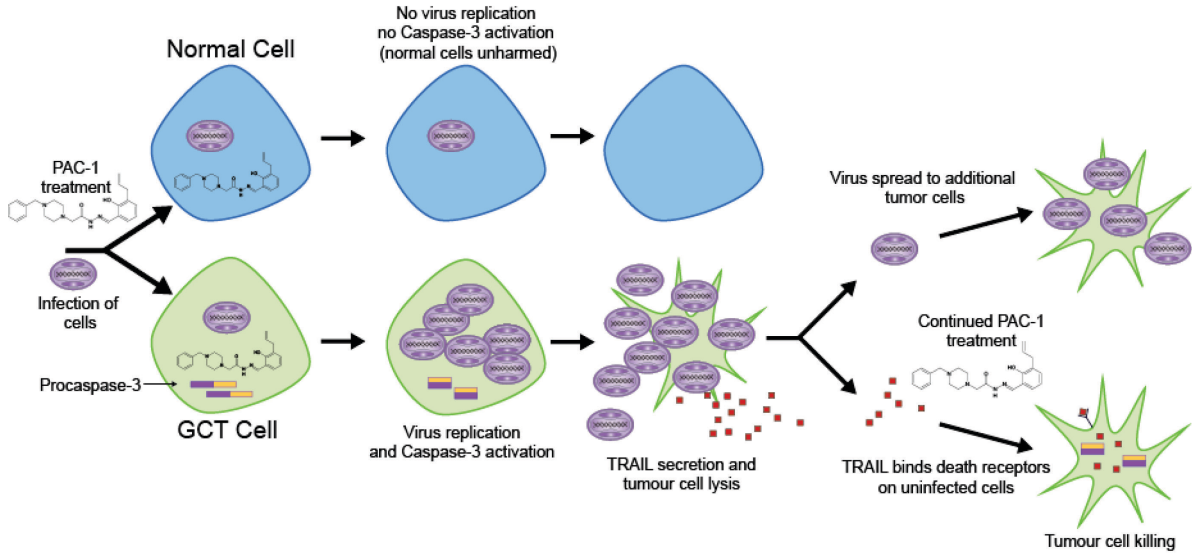

Figure 1.6 - Graphical abstract. Treatment with PAC-1 along with infection by VACV^{TRAIL} will result in self-amplifying control of GCT cells while normal cells are left unaffected. Modified from: Potts, et al., EMBO Molecular Medicine (2017) e201607296

CHAPTER 2. PAC-1 COMBINATION WITH TRAIL AS TREATMENT FOR GRANULOSA CELL TUMOUR

PREFACE

A portion of this chapter has been submitted for publication in the manuscript: Crosley, P., Potts, K., Agopsowicz, K., Farkkila, A., Pihlajoki, M., Heikinheimo, M., Fu, Y., Hitt, M. Procaspase-activating compound-1 synergizes with TRAIL to induce cytotoxicity in established granulosa cell tumor cell line KGN and in primary granulosa cell tumor cells *in vitro*. (Submitted) 2019.

Contributions:

I designed and performed experiments (except experiments with primary patient GCT samples), analyzed the data, and prepared the manuscript. Dr. Kyle Potts provided guidance in experimental design, data interpretation, and manuscript preparation.

2.1 Introduction

Granulosa cell tumour (GCT) is a malignant sex-cord stromal cell form of ovarian cancer that constitutes ~5% of ovarian neoplasms. Current chemotherapy regimens are not effective enough in controlling recurrent GCT, and as a result ~80% of women who relapse will die of disease. Procaspase-activating compound 1 (PAC-1) is a small-molecule activator of procaspase-3 that has been extensively studied both *in vitro* and *in vivo* for many types of cancer both as a single agent and in combination with other drugs [78-80, 124], but never with GCT and not in combination with tumour necrosis factor-related apoptosis-inducing ligand (TRAIL). Here we investigated the effectiveness of PAC-1 in treating GCT *in vitro*, and the existence of synergy displayed by combining PAC-1 with selected apoptosis-inducing agents. We found that while TRAIL was only marginally toxic to GCT, combining it with PAC-1, even at low doses, was strongly synergistic in an established GCT cell line, and induced a significant increase in CASP3 activity in patient samples of primary and recurrent GCT cells. We propose that the novel combination of these two pro-apoptotic agents warrants further investigation as a potential GCT treatment.

2.2 Materials and Methods

2.2.1 Cell culture and reagents

The human GCT cell line, KGN (Riken Biosciences) was cultured in Dulbecco's Modified Eagle's Medium/Nutrient Mixture F12 (DMEM/F12, Sigma-Aldrich) with 5% fetal bovine serum (FBS, Gibco). Adenovirus E1- and SV40 T antigen-transformed human embryonic kidney cell line 293T (generously provided by Dr. Gordon Chan, University of Alberta), human breast cancer cell lines MCF7 (ATCC® HTB-22), $MCF7_{CASP3}$ (MCF7 stably-transformed with CASP3 cDNA, generously

provided by Dr. Shairaz Baksh, University of Alberta), normal human fibroblast cell lines F202 and N60 (generously provided by Dr. Ted Tredget, University of Alberta), and normal human kidney epithelial cell line NKC (generously provided by Dr. Ronald Moore, University of Alberta) were cultured in DMEM/high glucose (Sigma-Aldrich) with 10% FBS. All culture media were supplemented with 2 mM L-glutamine, 100 U/mL penicillin, and 100 U/mL streptomycin) (Gibco). Cell line authentication was performed for KGN and MCF7 (and their derivatives) using short tandem repeat DNA profiling (Promega's GenePrint 10 System; [125]) at the Genetic Analysis Facility at the Centre for Applied Genomics of The Hospital for Sick Children (Toronto, Ontario, Canada). All lines were routinely tested for and found free of mycoplasma either by Hoechst 33342 staining (Thermo Fisher Scientific) and fluorescence imaging, or using the Mycoplasma PCR Detection Kit (Applied Biological Materials, Inc.).

PAC-1 was generously provided by Dr. Paul Hergenrother (University of Illinois) and Hoechst 33342 was generously provided by Dr. Linda Pilarski (University of Alberta). Other chemicals include recombinant human TRAIL (sTRAIL/Apo2L, Peprotech #310-04); carboplatin (Enzo Life Sciences #400-041); resazurin sodium salt (R7017), embelin (E1406), and gemcitabine hydrochloride (G6423-10) from Sigma-Aldrich; NucView 488 Caspase-3 substrate (Biotium #30029); and RevertTM Total Protein Stain (#926-11010) and Odyssey blocking buffer (#927-50003) from Li-COR Biosciences. Western blot antibodies for beta-tubulin (#2146), caspase-3 (#9662), survivin (#2808), BID (#2002), SMAC (#2954) and Jurkat positive control lysate (#2043) were purchased from Cell Signaling. Secondary antibodies (#926-68, #926-68070) and Chameleon Duo protein ladder (#928-60000) were purchased from Li-COR Biosciences. PE-

conjugated antibodies for flow cytometry against DR4 (TRAIL-R1, #FAB347P), DR5 (TRAIL-R2, FAB6311P) or isotype controls (mouse IgG1 (#IC002P) or IgG2B, #IC0041P) were purchased from R&D Systems.

2.2.2 Lentiviral transduction of KGN cell lines

KGN-shCASP3 and KGN-shScramble cells were generated by lentivirus transduction of KGN cells as described by Campeau *et al.* [154]. Briefly, 293T cells were plated in 100 mm dishes to be 50-60% confluent at the time of transfection. 15 µg plasmid pLKO.1-puro-U6-TRCN0000003549; TRCN0000003550; or TRCN0000003551 (Dharmacon [126]) expressing an shRNA against CASP3 (generously provided by Dr. Maya Shmulevitz, University of Alberta), 15 µg pMDLg/pRRE (Addgene #12251), 6 µg pRSV-REV (Addgene #12253), and 3 µg pMD2.G (Addgene #12259) were mixed with OPTI-MEM (Thermo Fisher) to a final volume of 1.5 mL. 1.5 mL of a 1:50 dilution of Lipofectamine 2000 (Thermo Fisher) in OPTI-MEM was added to the plasmid mixture. The mixture was incubated at room temperature for 25 min, then added to cells plated in 7 ml of OPTI-MEM. After incubating at 37^{o} C for ~6 h the medium was replaced with 7 mL of DMEM medium supplemented with 10% fetal bovine serum (FBS), 2 mM L-glutamine, 100 U/mL penicillin, 100 U/mL streptomycin, and 0.25 µg/mL Fungizone® (Gibco). Viral supernatant was collected 48 h and 72 h post-transfection (7 mL medium was added back after collecting at 48 h). Supernatants were filtered through a low protein binding PVDF 0.44 µM filter (Millipore) and this crude vector stock was stored at -80^{o} C. To construct the knockdown cell lines KGN cells in 6-well plates were infected with 1 mL of undiluted vector stock containing polybrene 6 µg/mL (Thermo Fisher). Transduction efficiency was determined in a parallel infection with a GFP-expressing vector. After 18 h incubation at 37^{o} C the inoculum

was aspirated and cells washed twice with PBS before adding normal growth medium. 72 h post-infection cells were selected with puromycin 4 μg/mL and after 5 days of drug selection cells were single-cell sorted into a 96-well plate by FACS. Three clones were expanded, assayed for reduction of CASP3 expression and the cell line with most effective knock-down of CASP3 was selected for use in assays.

2.2.3 Cell viability/metabolism assay

5000 cells/well were seeded in triplicate wells of a 96-well plate containing a range of doses of selected compounds and incubated at 37° C with 5% CO_2 for the time indicated. Resazurin (final concentration 44 μM) was then added to the medium and cells incubated up to four h at 37° C. Reduction of resazurin was measured on a BMG FLUOStar Omega microplate reader (544 nm excitation/590 nm emission). Blank-corrected relative fluorescence units (RFUs) were normalised to untreated control wells. Each assay was repeated at least 3 times.

2.2.4 Caspase-3 activity assay

5000 KGN cells/well in black 96-well plates were stained with 0.1 μg/mL Hoechst 33342 and 1 μM NucView-488 Caspase-3 substrate for 30 min in the dark at 37° C. Cells were then treated with 20 μM PAC-1, 10 ng/mL TRAIL, or PAC-1 combined with TRAIL and incubated at 37° C for 12 h. Plates were then transferred to a Molecular Devices ImageXpress high-content screening instrument and incubated at 37° C with 5% CO_2. Images were acquired at four sites per well every 30 min until 48 h post-treatment. Imagery was processed using the MetaXpress Multi-wavelength Cell Scoring module and the number of NucView-fluorescent cells (using the FITC channel) were normalized to the number of Hoechst-stained cells (using the DAPI channel).

2.2.5 Western blots

Whole-cell protein extracts were prepared by collecting cells and medium from plates then pelleting by centrifugation at 4^{o}C for 5 min at 500 x g. Cells were washed in cold PBS, re-centrifuged, then lysed on ice in RIPA buffer (150 mM NaCl, 50 mM Tris-HCl (pH 8.0), 0.5% sodium deoxycholate, 0.1% SDS, 1% NP-40, 0.1 mg/mL phenylmethylsulfonyl fluoride, and Halt protease inhibitor cocktail (Thermo Fisher)). Lysates were clarified by centrifugation at 4^{o}C for 20 min at 20,000 x g, then assayed for protein (BCA protein assay kit, Thermo Fisher). For western blots, up to 40 µg of protein was resolved by SDS-PAGE (12% (w/v) acrylamide) running at 150 volts for 1 h, then transferred to Immobilon-FL PVDF membranes (EMD Millipore) at 100 volts for 1 h. Protein transfer was confirmed by staining membranes with RevertTM Total Protein Stain and scanned at 700 nm using an Odyssey scanner (Li-COR Biosciences). Membranes were then washed before blocking with Odyssey blocking buffer for 1 h at room temp, and incubating overnight at 4^{o}C with primary antibodies (diluted 1:1000 in blocking buffer with 0.2% Tween). Fluorescent conjugated secondary antibodies were diluted in blocking buffer (1:20000) containing 0.2% Tween and 0.01% SDS, and incubated with the membranes at room temperature for 1 h. Washed membranes were scanned using an Odyssey scanner and the images analyzed using ImageStudio software (Li-COR Biosciences).

2.2.6 Flow cytometry

For each sample to be analysed 2.5 x 10^5 cells were collected in microfuge tubes, centrifuged at 4^{o}C for 5 minutes at 300 x g and then decanted and resuspended in cold FACS buffer (PBS, 1% BSA, 1mM EDTA, 0.1% sodium azide). Cells were then centrifuged at 4^{o}C for 5 minutes at 300 x g and decanted followed by resuspension in 5% human serum and incubation

at RT for 15 minutes. Cells were then washed with FACS buffer and resuspended in 10 µL of antibody at manufacturer's recommended dilution and incubated for 30 minutes on ice in the dark. After incubation 0.5 mL of cold FACS buffer was added to each tube, cells were centrifuged at 4^{o}C for 5 minutes at 300 x g then decanted, resuspended in 0.5 mL cold FACS buffer, vortexed and passed through a cell strainer into Falcon tubes (BD). Flow cytometry was performed on a BD Biosciences Fortessa X-20 and data were analysed using FlowJo version 10.5.3.

2.2.7 Irradiation of cells

15,000 KGN cells were seeded in 48-well plates in medium, incubated overnight and then treated with either medium or PAC-1 and irradiated (or mock) in a Faxitron MultiRad 160 with one dose of 5, 10 or 20 Gy. 72 h after irradiation cells were assayed for viability using methodology described earlier (section 2.2). ANOVA adjusted p value calculations were performed using GraphPad Prism with Tukey's multiple comparison test.

2.2.8 Patient-derived cultures and assays

Patient-derived tumour samples were acquired and assayed by A. Farkkila and M. Pihlajoki (tissues collected with informed consent and in accordance with The Code of Ethics of the World Medical Association (Declaration of Helsinki)). Samples were verified to possess the 402C→G (C134W) mutation in FOXL2 and processed as previously described [101]. Briefly, GCT tissue was minced then dissociated with 0.5% collagenase (Sigma–Aldrich) in DMEM/F12 (without FBS) for 2 h. The resulting cell suspension was filtered through a 140-µm mesh to obtain single cells, washed with PBS, resuspended in DMEM/F12 containing 10% FBS, then

plated. Viability was assessed using the cell proliferation agent WST-1 (Roche), and caspase activity was measured using the Caspase Glo® 3/7 kit (Promega).

2.2.9 Statistical analysis

Unless otherwise indicated, experiments were independently repeated at least 3 times, each time using duplicate or triplicate wells. GraphPad Prism (version 8) was used for statistical analysis of viability data. Drug synergy was calculated using viability data processed by the Matlab software plugin module Combenefit [127]. Statistical significance was calculated using either analysis of variance (ANOVA) or Student's t-test.

2.3 Results

2.3.1 PAC-1 potentiates CASP3-mediated apoptosis.

To confirm that PAC-1 cytotoxic activity was dependent on CASP3, we examined PAC-1 activity in cell lines with a range of CASP3 levels (Figure 2.1). The AGCT model cell line KGN expressed high levels of CASP3, while KGN-shCASP3 cells had significantly reduced CASP3 levels, and the control cell lines, a CASP3-transfected MCF7 line ($MCF7_{CASP3}$) [128] and MCF7 (naturally CASP3-null) expressed even less CASP3. PAC-1 sensitivity of KGN in a dose-response assay was consistent with its high level of CASP3, while the other three cell lines with lower levels of CASP3 were more resistant to PAC-1. At doses >30 µM, PAC-1 is reported to induce ER stress independent of CASP3 [129], which is consistent with our observation that >50% killing was achieved at 40 µM PAC-1 even with CASP3-null MCF7 cells. Overall, the data demonstrate that PAC-1 induces cytotoxicity of the established AGCT cell line KGN, similar to reports for other cancers with elevated CASP3 levels [78].

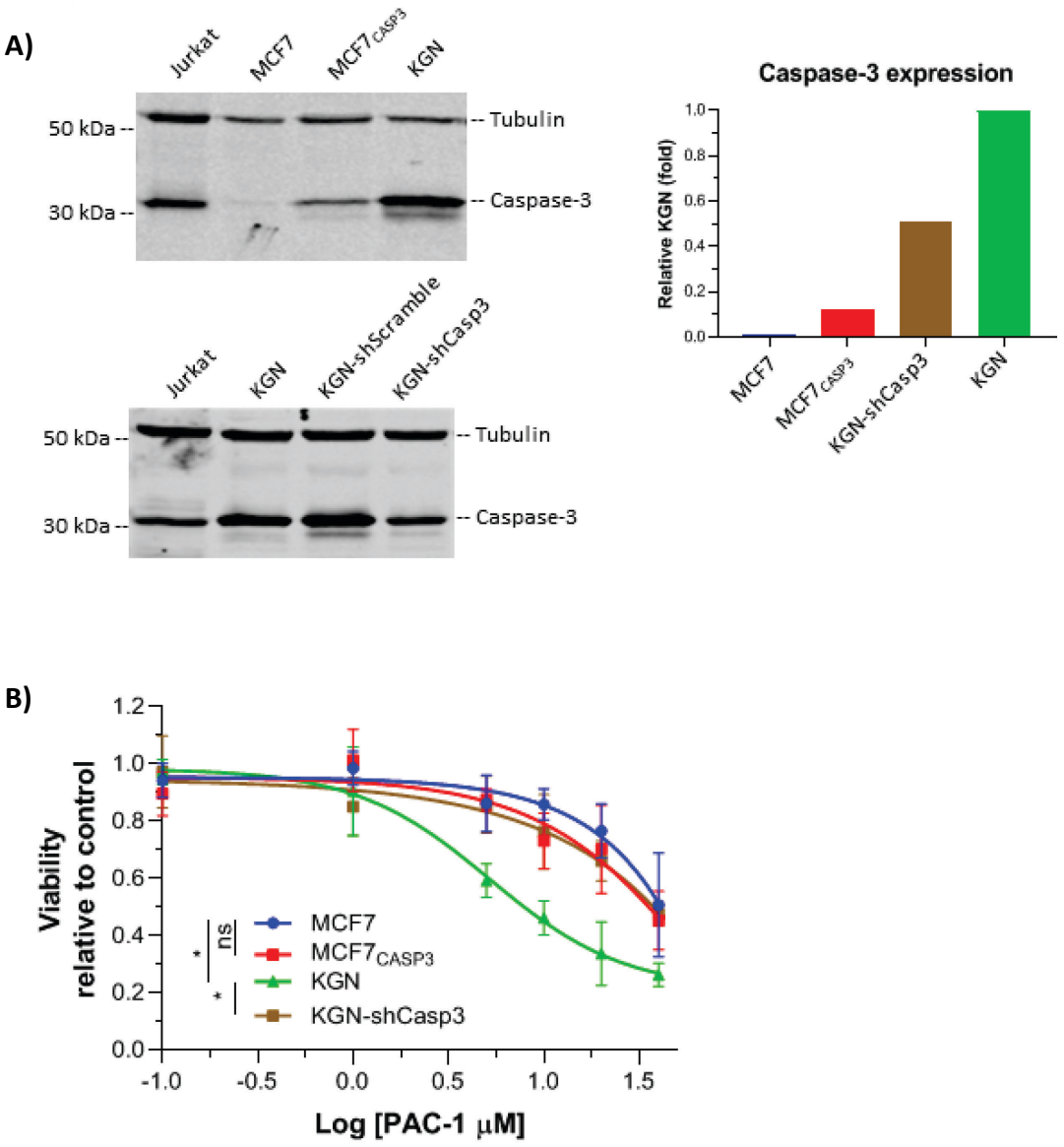

Figure 2.1 – PAC1 toxicity is potentiated by expression of Caspase-3. (A) Left panels: CASP3 expression was detected by Western blot analysis of lysates from untreated CASP3-null MCF7, $MCF7_{CASP3}$ (MCF7 stably transformed with CASP3), KGN, KGN-shScramble and KGN-shCasp3 cells (KGN stably transformed with CASP3 shRNA) with Jurkat cells as a positive control. Right panel: CASP3 expression was quantified, normalizing to tubulin expression for each cell line, and then shown relative to normalized caspase-3 expression in KGN cells. (n = 1 for each western blot). **(B)** MCF7, $MCF7_{CASP3}$, KGN-shCasp3 and KGN cells were treated with PAC-1 (0.1 – 40 μM) then viability determined 48 h later by resazurin metabolic assay. Data are normalised to untreated cells. (Mean +/- SEM for 3 independent experiments)

2.3.2 Granulosa cell tumour cells display sensitivity to CASP3 activating compounds.

We next examined the response of KGN cells to PAC-1 compared to a panel of other apoptosis-inducing agents (Figure 2.2). Conventional chemotherapeutic agents carboplatin (alkylating agent) and gemcitabine (nucleoside analog) interfere with DNA replication, activating the DNA damage response [130] and subsequent apoptosis. TRAIL binds cell death receptors and induces CASP3 activation through both intrinsic and extrinsic apoptotic pathways [114, 155]. Embelin is a SMAC-mimetic that inhibits XIAP, an inhibitor of CASP3 [156-158]. PAC-1 activates apoptosis by direct interaction with CASP3, the point furthest downstream in apoptosis pathways of any of the agents tested here. Clinically relevant drug doses were selected for this study, based on either established dosing guidelines or results from ongoing clinical trials, with viability assessed at 24 and 48 h [131].

The most potent of the drugs tested, based on the dose at which 50% cell death was induced, were PAC-1 and embelin, followed by gemcitabine, with carboplatin and TRAIL failing to reach 50% killing in this assay. Results with gemcitabine and carboplatin are consistent with clinical observations showing poor efficacy of standard chemotherapy in treating AGCT [132, 133]. The lack of response to TRAIL was unexpected, as KGN expresses the TRAIL receptor DR5, although it does not express DR4 (Figure 2.3). Interestingly, the drugs that induced the greatest cytotoxicity act at the most downstream point of apoptosis, where the intrinsic and extrinsic pathways converge. Furthermore, the most potent drugs act proximally to CASP3 which is highly overexpressed in KGN cells (Figure 2.1C). These results suggest that CASP3 activation could be an effective therapeutic strategy for AGCT.

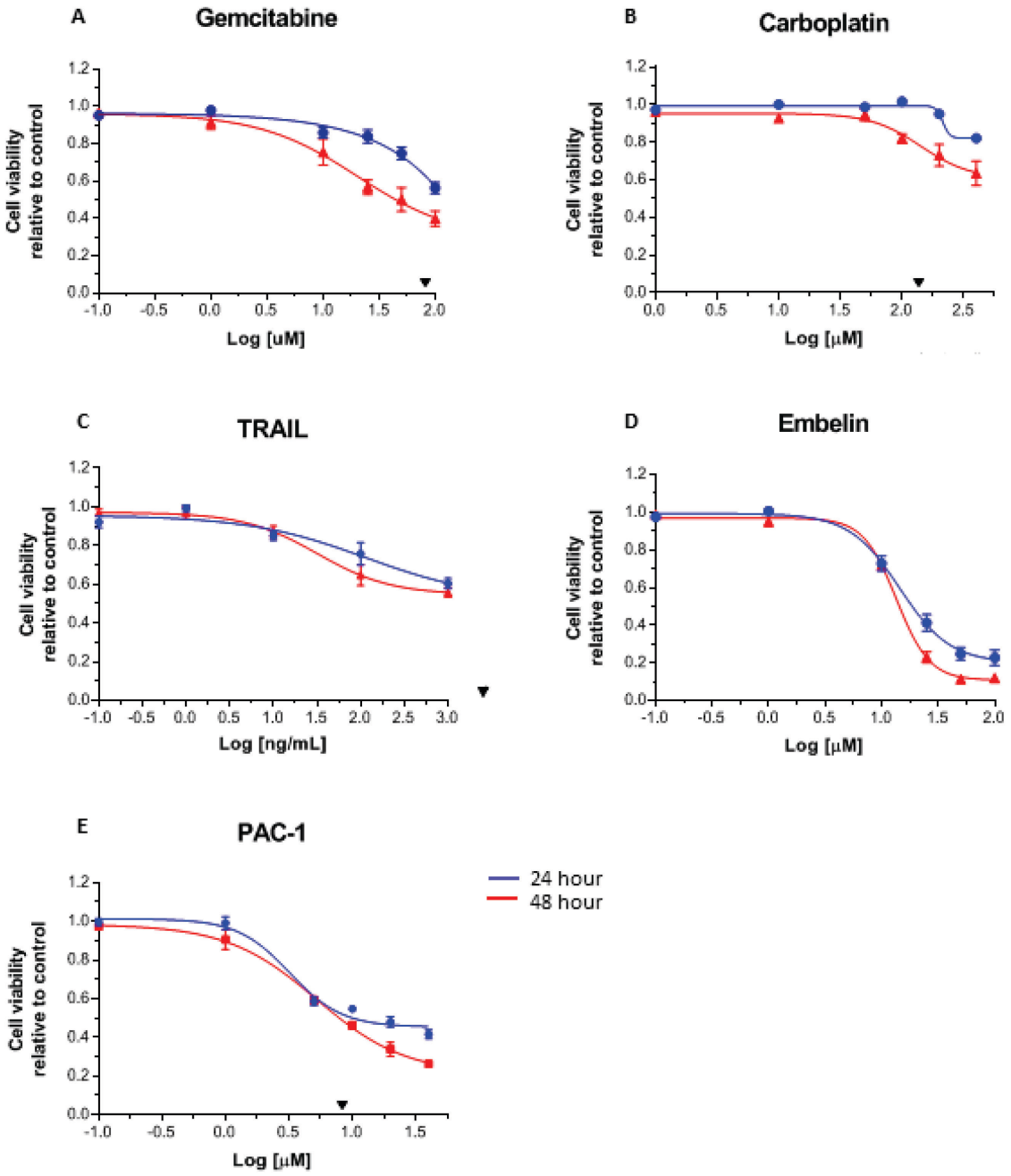

Figure 2.2 – KGN cells are sensitive to caspase-activating compounds compared to other chemotherapy drugs. KGN cells (7000/well) were seeded into 96-well plates containing a range of doses for **(A)** gemcitabine (0.1 – 100 μM), **(B)** carboplatin (1 – 400 μM), **(C)** TRAIL (0.1 – 1000 ng/mL), **(D)** embelin (0.1 – 100 μM), or **(E)** PAC1 (0.1 – 40 μM). After 24 or 48 h viability was determined by resazurin metabolic assay. ▼Indicates peak serum plasma levels reported in literature or from clinical trials [1]. TRAIL (Dulanermin) peak plasma level (80 μg/mL) in phase 1b trial [3]. To our knowledge there have been no human trials with Embelin.

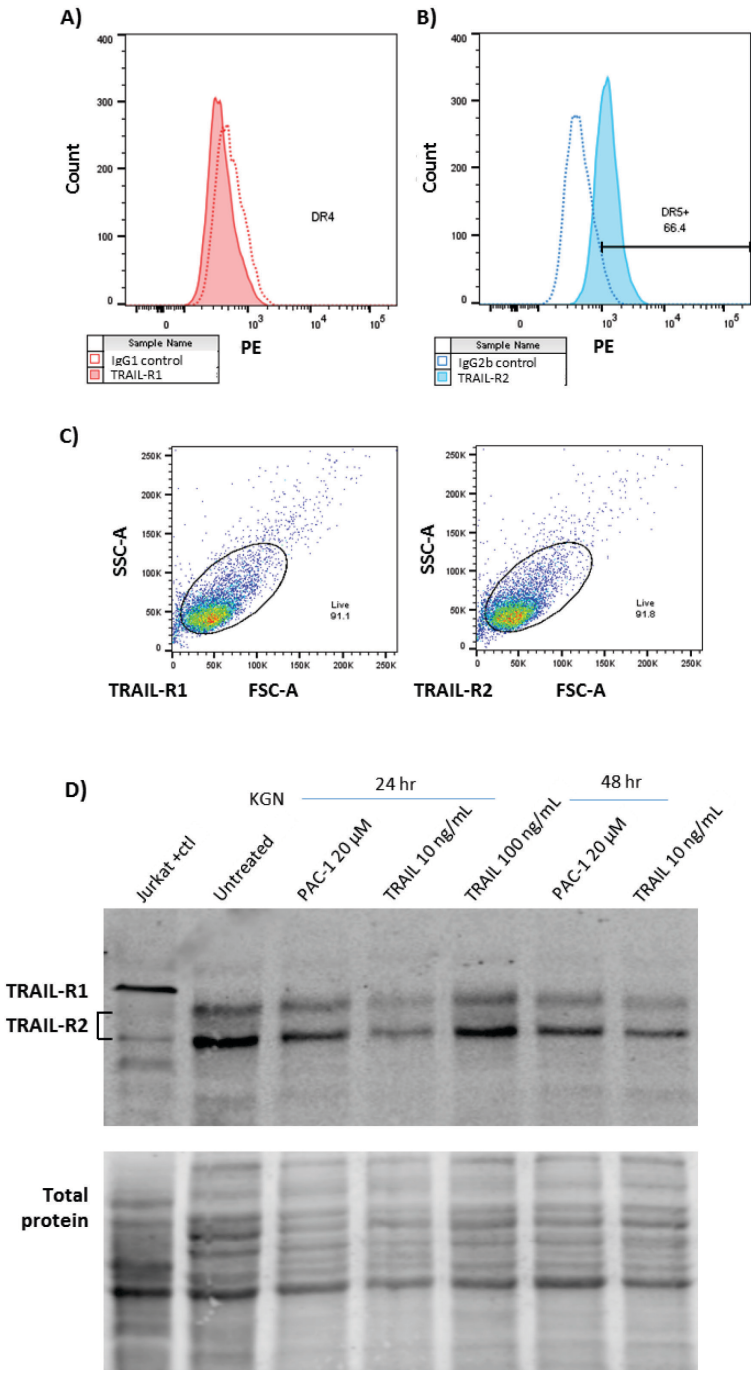

Figure 2.3 - Death receptor expression in KGN cells. (A, B, C) Flow cytometry analysis of untreated KGN cells. **(A)** DR4 expression level compared to isotype control; **(B)** DR5 expression level compared to isotype control; **(C)** Gating strategy used to select populations to be analysed. **(D)** Western blot analysis of TRAIL-R1 (DR4) and TRAIL-R2 (DR5) in KGN cells treated as indicated. Total protein probed using Revert™ Total Protein Stain.

2.3.3 PAC-1 displays no or low synergy with carboplatin, gemcitabine or embelin, but strong synergy with TRAIL in killing KGN cells

PAC-1 has been shown to display synergistic killing with standard chemotherapy drugs in several cancers [79, 134]. PAC-1 synergy in GCT was tested by assessing viability of KGN cells treated with PAC-1 in combination with gemcitabine, carboplatin or embelin. Drug interaction was calculated using both the Loewe and Bliss reference models. The Bliss model uses a probabilistic approach assuming that the two drugs respond independently: suitable for compounds that target different pathways. The Loewe model compares the dose-response of the individual compounds to the combination, assessing deviations from additivity: most applicable when drugs have a similar mode of action on the same pathway or target [135, 136].

We observed that gemcitabine, carboplatin and embelin were not highly effective at boosting KGN killing when used in combination with PAC-1 (Figure 2.4). Gemcitabine combined with PAC-1 induced moderate loss in viability with low to moderate synergy (Loewe analysis) or very little synergy (Bliss analysis). Carboplatin, which induced low to moderate cytotoxicity in combination with PAC-1, showed low or no synergy. Embelin, although cytotoxic on its own and in combination with PAC-1, displayed a weakly antagonistic interaction, illustrating that strong cytotoxicity and strong synergy do not necessarily correlate.

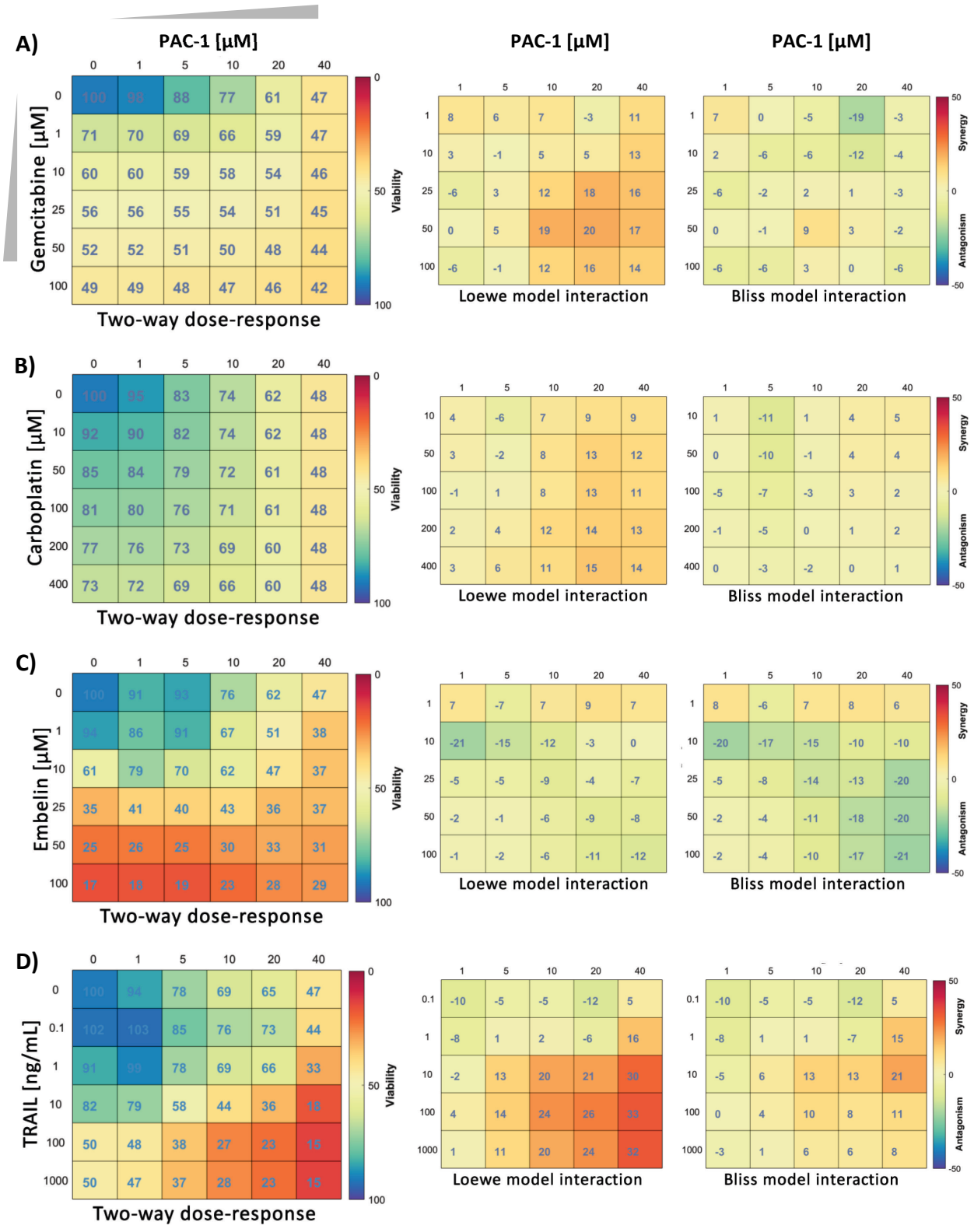
A)
PAC-1 [µM]
Gemcitabine [µM]
Two-way dose-response
Viability
Loewe model interaction
Bliss model interaction
Synergy
Antagonism
B)
Carboplatin [µM]
C)
Embelin [µM]
D)
TRAIL [ng/mL]

Figure 2.4 - PAC-1 is more synergistic with TRAIL than with gemcitabine, carboplatin or embelin in KGN cells. Two-way dose-response assays were set up with 5000 KGN cells/well in 96-well plates. Wells were treated for 48 h with PAC-1 doses from 0 – 40 μM combined with **(A)** gemcitabine (0 – 100 μM); **(B)** carboplatin (0 – 400 μM); **(C)** embelin (0 – 100 μM); or **(D)** TRAIL 0 – 1000 ng/mL. Viability was determined by resazurin metabolic assay (left panels, % viability indicated by color gradient). Drug interaction was calculated by Matlab module Combenefit using both the Loewe (centre panels) and Bliss (right panels) reference models [5]. (n = 3 independent experiments)

As a single agent, we did not observe high levels of KGN killing following TRAIL treatment (Figure 2.2C). Reports that combination with other agents can sensitize cancers to TRAIL [138-140], stimulated us to investigate TRAIL in combination with PAC-1. Two-way dose-response assays combining TRAIL and PAC-1 in KGN cells (Figure 2.4D) showed an increase in loss of viability and strong synergy with the combination. Observing the distribution of z-index scores in two-way dose-response data (Figure 2.5) we selected the relatively low dose of TRAIL 10 ng/mL combined with PAC-1 20 µM for further investigation in single-dose assays. (We calculated an EC_{50} for PAC-1 of 17 µM when used with TRAIL at 10 ng/mL). Interestingly we observed a trend of increased effectiveness of PAC-1 in combination with irradiation (Figure 2.6), which might be expected given the ability of ionizing radiation to activate Caspase-3 as a DNA damage response [137]. This supports reported effectiveness of PAC-1 combined with temozolomide and radiation using *in vivo* glioma models in rodents and dogs [124].

A)

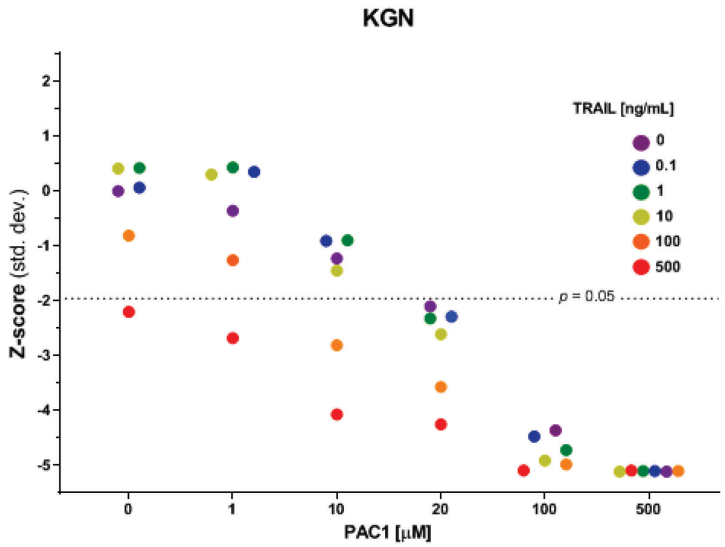

B)

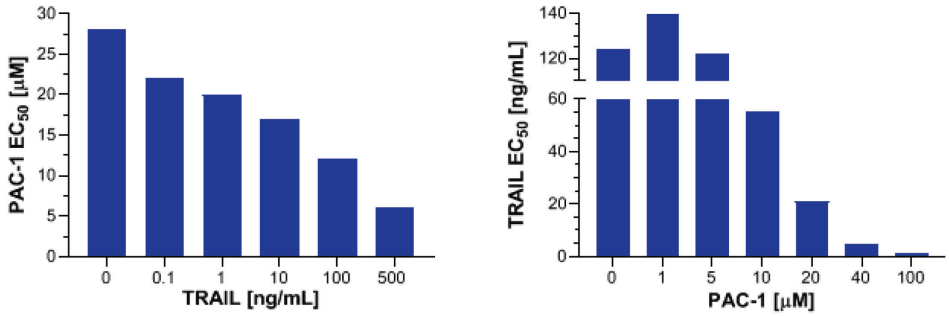

Figure 2.5 - PAC-1 and TRAIL synergy results in mutual lowering of EC_{50} values. (A) 5000 cells/well in 96-well plates were treated in a two-way dose response assay with PAC-1 (0 – 500 μM) and TRAIL (0 – 500 ng/mL). After 48 h viability was measured using a resazurin metabolic assay. Z-scores were calculated from viability data using the equation $Z = (X_o - \mu) / \sigma$ where X_o is the observed response in relative fluorescence units (RFU); μ is the mean RFU for untreated control wells, and σ is the standard deviation of untreated wells. A Z-score of >1.98 or < -1.98 indicates a significance of $p < 0.05$ [4]. **(B)** Using two-way dose-response data, PAC-1 EC_{50} values were plotted against increasing doses of TRAIL (left panel), and TRAIL EC_{50} values were plotted against increasing doses of PAC-1 (right panel).

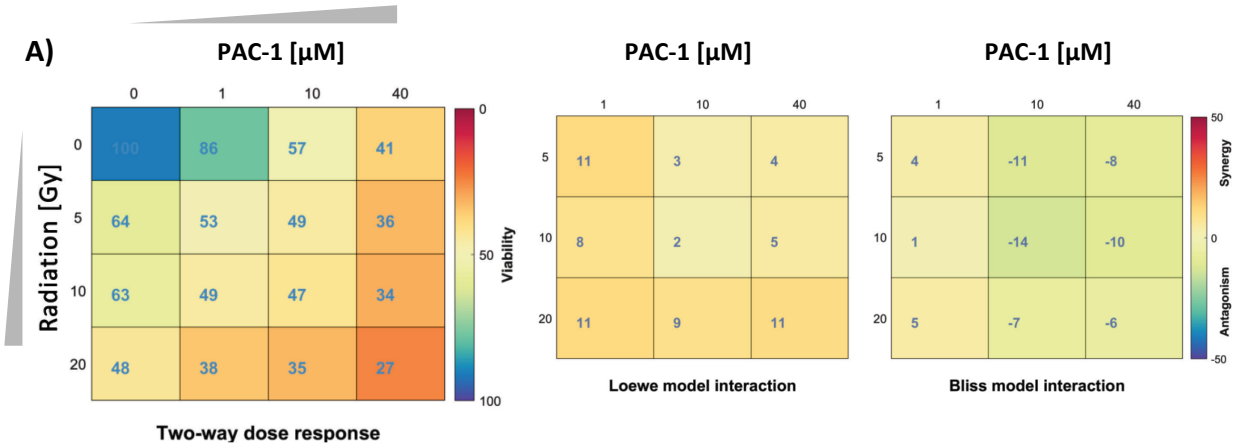

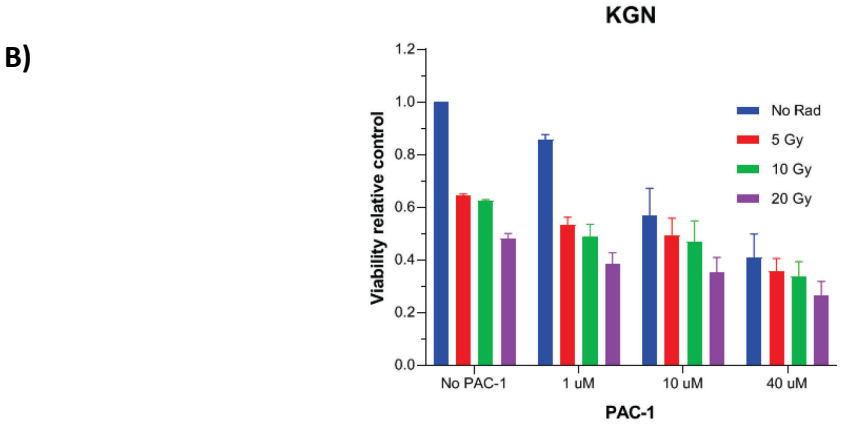

C)

P-values adding PAC-1 to radiation[1]

		PAC-1 [µM]			
		0	1	10	40
Radiation [Gy]	0		0.005	0.0002	<.0001
	5		0.0155	0.0003	<.0001
	10		ns	ns	0.0288
	20		ns	ns	ns

P-values adding radiation to PAC-1[2]

		Radiation [Gy]			
		0	5	10	20
PAC-1 [µM]	0		0.028	<.0001	<.0001
	1		ns	ns	0.0043
	10		0.0345	ns	0.0038
	40		ns	ns	0.0479

[1] – increasing dose of PAC-1 (compared to no PAC-1) at fixed dose of radiation
[2] – increasing dose of radiation (compared to no radiation) at fixed dose of PAC-1

Figure 2.6 - PAC-1 may sensitize KGN cells to radiotherapy. KGN cells were treated with PAC-1 or left untreated, then immediately irradiated at the indicated doses. **(A)** Viability was determined by resazurin metabolic assay 72 h after irradiation. Viability was normalised to untreated control (normalized viability values indicated in the color scale). **(B)** Viability data (analysed with GraphPad Prism), show a trend of increased killing with the combination compared to either agent alone, the differences were not significant. **(C)** Adjusted p-values based two-way analysis of variance comparing addition of PAC-1 to radiation (left) and addition of radiation to PAC-1. (n=3)

2.3.4 Combining TRAIL with PAC-1 rapidly induces CASP3 activity in KGN.

The kinetics of PAC-1-TRAIL induction of CASP3 activity in KGN cells was tracked over time using high-content imaging (Molecular Devices ImageXpress) (Figure 2.7A). PAC-1 (20 μM) generated a moderate level of caspase activity by 48 h, similar to results of the PAC-1-induced loss of viability assay (Figure 2.2E). TRAIL alone (10 ng/mL) was less active than PAC-1 in both cytotoxicity (Figure 2.2C) and CASP3 activation. However the combination of PAC-1 and TRAIL rapidly and dramatically amplified caspase activity reaching over 80% of cells by 24 h (Figure 2.7B). This is consistent with our proposal that PAC-1 primes CASP3 molecules for activation, which then enhances TRAIL-induced death signaling for execution of caspase-mediated apoptosis.

A)

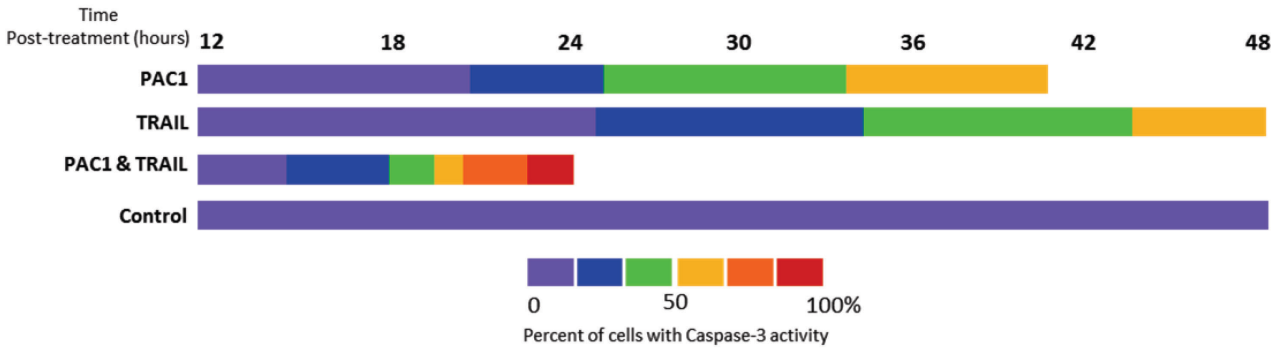

B)

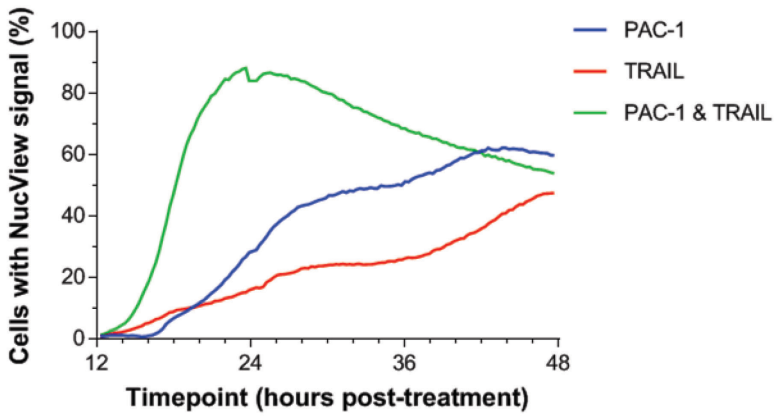

Figure 2.7 - Combining PAC-1 with TRAIL induces rapid activation of caspase-3 in KGN cells. **(A)** KGN cells (5000/well) were treated with either 20 µM PAC-1, 10 ng/mL TRAIL, or 20 µM PAC-1 combined with 10 ng/mL TRAIL. Cells were then stained with Hoechst 33342 and NucView-488 Caspase-3 substrate and monitored over 48 h for caspase-3 cleavage (Molecular Devices ImageXpress high-content imaging). Imagery was then processed using the MetaXpress Multi-wavelength Cell Scoring module and the number of NucView-fluorescent cells was determined relative to the total number of Hoechst-stained cells (percentages are color-coded as indicated in the scale). Length of bars indicates time to reach maximal NucView-fluorescence. Data shown are representative of multiple analyses of caspase-3 activity. **(B)** Quantification of data from (A).

2.3.5 Combination of TRAIL with PAC-1 is less toxic in normal cells.

Most toxicity in patients is the result of off-target effects of drugs on normal tissues. We investigated the impact of PAC-1 and TRAIL on a human dermal fibroblast cell line (F202) as a surrogate for normal non-cancerous cells. A two-way dose-response viability assay demonstrated that F202 cells were much less sensitive to the PAC-1/TRAIL combinations than KGN cells even at relatively higher doses of PAC-1 (Figure 2.8A). Similar results were seen in a second fibroblast cell line and a cell line derived from normal human kidney cells (Figure 2.8B).

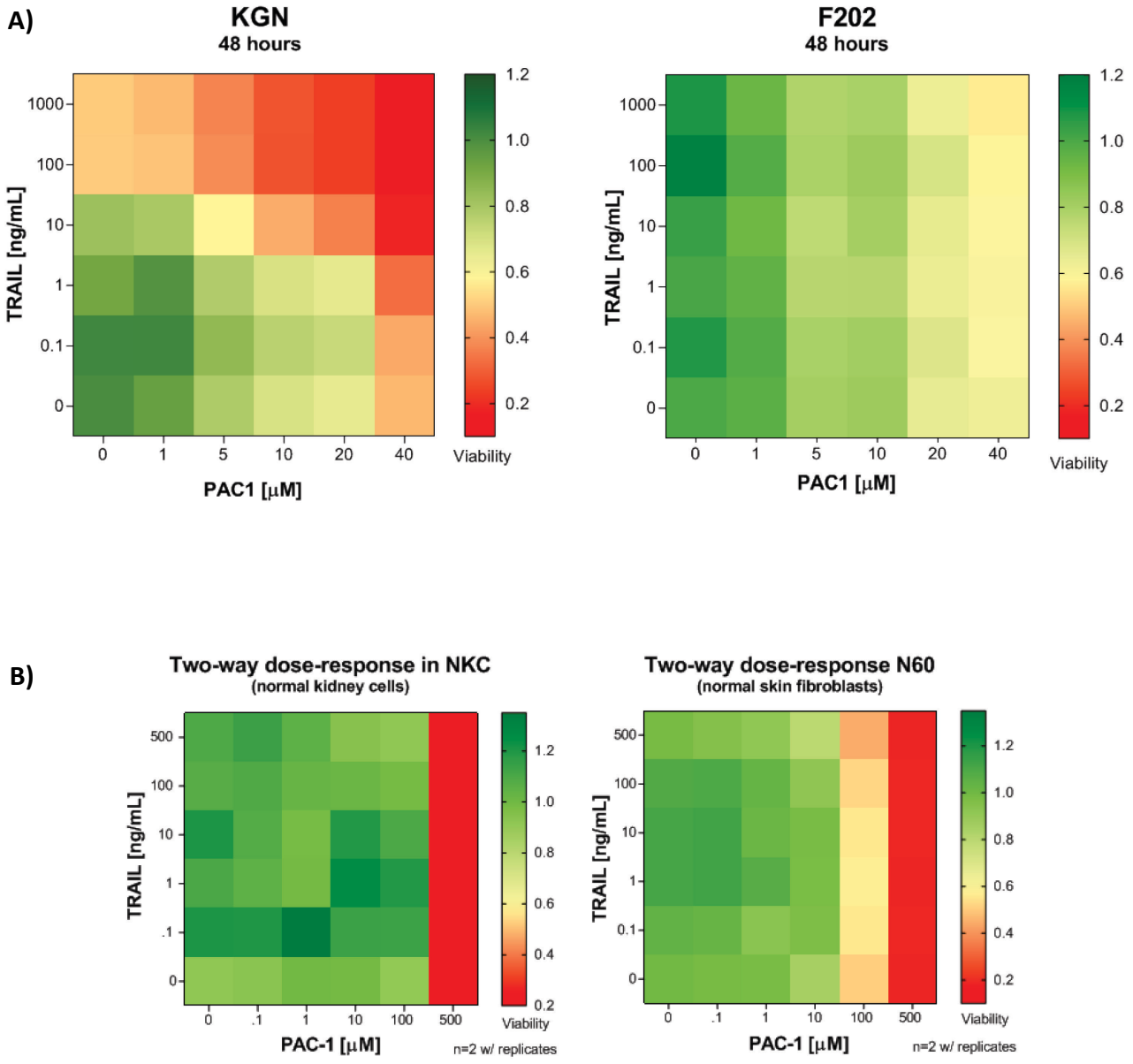

Figure 2.8 – Noncancerous cells are refractory to PAC-1 combined with TRAIL than KGN cells. Two-way dose-response assays were carried out on **(A)** KGN cells and dermal fibroblasts (F202) (5000 cells/well) treated for 48 h with TRAIL (0 – 1000 ng/mL) combined with PAC-1 (0 – 40 µM). **(B)** Normal human kidney cells (NKC) and skin fibroblasts (N60) treated for 48 h with TRAIL (0 – 1000 ng/mL) combined with PAC-1 (0 – 500 µM). Viability was determined by resazurin metabolic assay and normalised to untreated wells (normalized viability values indicated in the color scale). (n = 3 independent experiments)

2.3.6 Combining TRAIL with PAC-1 induces loss of viable cells and increased CASP3 activity in patient-derived granulosa cell tumour cells

The potential clinical utility of PAC-1/TRAIL combination treatment was investigated *in vitro* using patient-derived explants from primary and recurrent GCT. Our *in vitro* work with KGN suggested that maximal CASP3 activity was induced after ~24 h treatment with PAC-1 so for this experiment TRAIL was added to PAC-1 treated cells halfway through the 48 h cell viability assay (Figure 2.9). In cultures of both primary and recurrent disease, the combination of PAC-1 followed by TRAIL resulted in increased CASP3 activation and loss of cell viability relative to single agents and to untreated controls. There was significant increase in CASP3 activity with primary and recurrent disease treated with TRAIL or TRAIL after PAC-1 ($p<0.05$). Interestingly, it appeared that recurrent disease had greater activation of CASP3 than primary disease, with at least similar, if not more, induced cell killing.

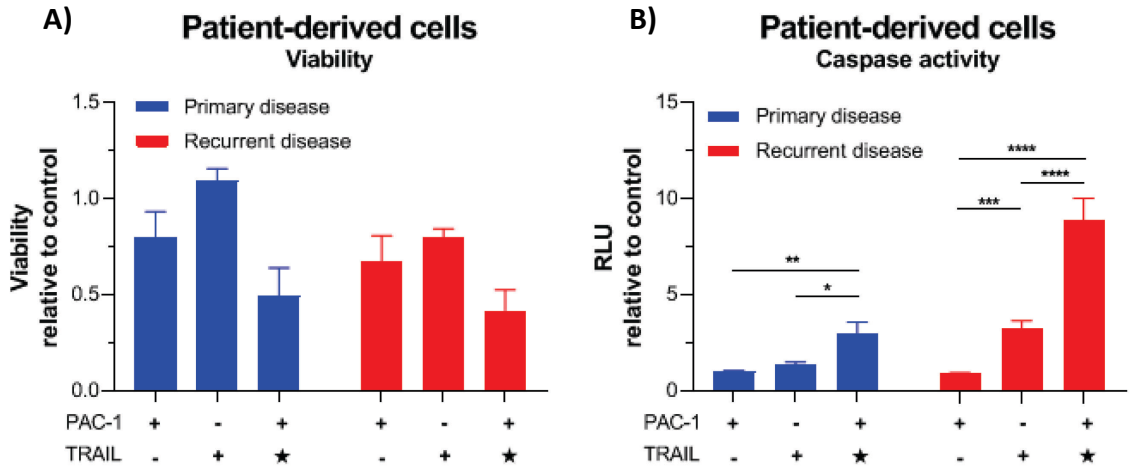

Figure 2.9- PAC-1 combined with TRAIL reduces viability and increases Caspase-3 activity in cultured patient-derived GCT cells. Patient-derived GCT cells were cultured for 5 days then treated with 20 µM PAC-1, 10 ng/mL TRAIL, or 20 µM PAC-1 followed 24 h later with 10 ng/mL TRAIL. **(A)** Viability as measured by WST-1 viability assay 48 h after initiation of PAC-1 treatment. **(B)** Caspase-3 activity measured with Caspase-Glo® 3/7, 48 h after initiation of PAC-1 treatment. Graph represents analysis of two primary tumour samples and two recurrent tumour samples. Star (★) indicates that TRAIL was added 24 h after PAC-1 treatment. Bars represent mean response +/- SEM. Significance tested by two-way ANOVA (* $p<0.05$; ** $p<0.01$; *** $p<0.001$; **** $p<0.0001$). Data was collected by A. Farkkila and M. Pihlajoki (University of Helsinki).

2.4 Discussion

Granulosa cell tumour (GCT) is a rare, sex-cord stromal neoplasm that has been the subject of few clinical trials owing partly to the difficulty in recruiting enough participants (e.g. NCT02101684). GCT is considered a hormonally-responsive tumour, but trials using agents interacting with the ovarian steroidogenesis pathway have had inconclusive results [141]. Chemotherapy, in general, is ineffective for GCT [39, 44, 45, 133] and the lack of effective treatment options contributes to the ~80% mortality among women who suffer relapse [11, 142]. Research on new therapies for AGCT is challenging due to the paucity of research tools: only one established cell line (KGN), and lack of animal tumour models carrying the phenotypical FOXL2^{C134W} mutation. The situation is more dire for research on JGCT as no established cell line exists (COV434 was recently reclassified as small cell carcinoma of the ovary hypercalcemic type (SCCOHT) [55]).

We sought to investigate a different approach, using apoptosis inducers to target GCT. We found that the pro-CASP3 activator PAC-1 was cytotoxic to KGN cells, and this activity was at least partly CASP3-dependent. KGN cells are also sensitive to embelin, a SMAC-mimetic that inhibits the endogenous CASP3 inhibitor XIAP; but are less sensitive to other apoptosis-inducing agents including carboplatin, gemcitabine, and TRAIL. KGN appears therefore to be more sensitive to single agents that influence CASP3 directly than to agents that act upstream in apoptosis signaling pathways.

To examine potential benefit from drug combination, we paired PAC-1 with each of the other agents. The combination of TRAIL and PAC-1 was the only combination that displayed

strong synergy and was very effective at reducing viability of KGN cells. Normal cells were much less sensitive to PAC-1/TRAIL combination in agreement with published reports on the safety of PAC-1 and TRAIL individually.

Using clinically relevant doses of PAC-1 and TRAIL, we established the kinetics of CASP3 activation. We observed a dramatically rapid increase in CASP3 activity with the combination compared to response of either agent alone. This is consistent with PAC-1 - TRAIL synergy as discussed in section 2.3.3. We propose that as a single agent, PAC-1 prepares CASP3 for activation in KGN cells but does not induce immediate auto-cleavage, while TRAIL as a single agent activates death signals that are impeded by Zn-mediated inhibition of CASP3. In combination, we propose that PAC-1 primes CASP3 to a ready-state, then TRAIL sends the signal that sparks CASP3 activity resulting in cell death.

We examined the effect of these apoptosis inducers on patient-derived explants of primary and recurrent GCT tumours as an *in vitro* indicator of clinical relevance. The results were consistent with the KGN-based assays in terms of the superiority of PAC-1/TRAIL combination and suggested that recurrent disease might be more susceptible than primary disease, although only CASP3 activity showed statistical significance.

TRAIL is a well-documented agent and is often efficacious in drug combination *in vitro*, although it has been less promising in clinical trials [90] due to a short half-life, ineffective dosing at the tumour site, and TRAIL resistance. Even so, during a phase I clinical trial of a monoclonal antibody targeting DR5, an early-cohort patient with GCT was one of only a few patients showing some response to treatment [143] and circulating TRAIL is reportedly reduced

in patients with large GCTs and correlated inversely with tumour size suggesting TRAIL may represent a therapeutic target [100]. We have found that it is possible to dramatically increase the ability of TRAIL to induce apoptosis in GCT by combining with PAC-1, which primes CASP3 for activation by TRAIL-induced death signaling (Figure 2.8). This could be a strategy for overcoming reported limitations in the clinical use of TRAIL.

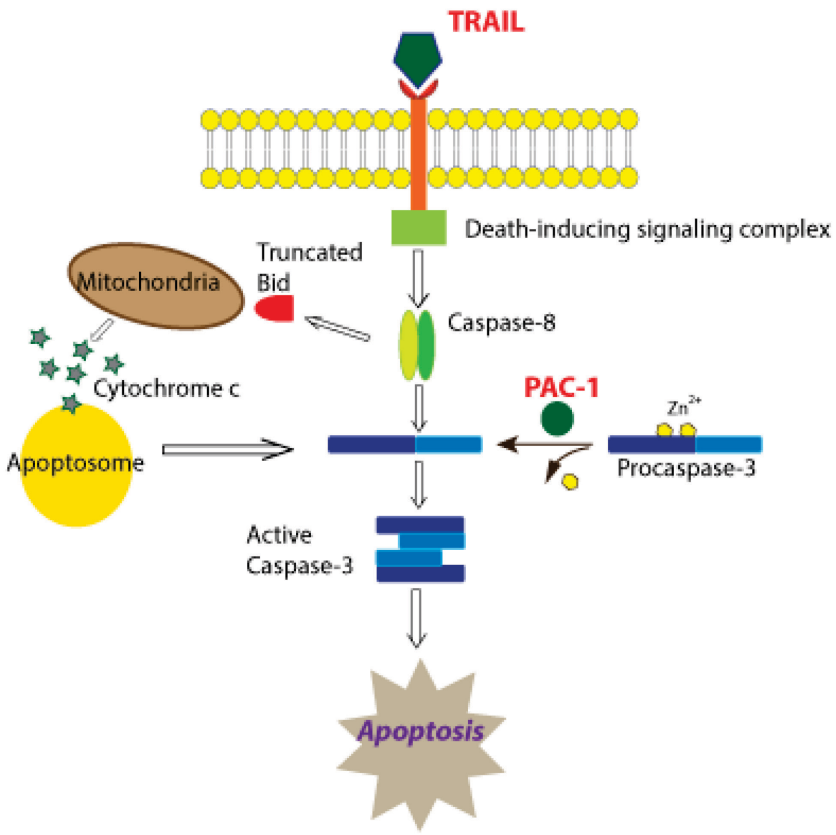

Figure 2.10 - PAC-1 combined with TRAIL leads to increased levels of apoptosis. Based on data presented in this paper, we propose that PAC-1 and TRAIL synergistically function to increase apoptosis through removal of inhibitory Zn^{2+} ions resulting in primed caspase-3 molecules, combined with TRAIL-induced death-signaling that drives final activation of caspase-3 via the extrinsic and/or intrinsic apoptotic pathway.

CHAPTER 3. TRAIL-EXPRESSING ONCOLYTIC VACV AS TREATMENT FOR GRANULOSA CELL TUMOUR

PREFACE

This chapter is an original work by Powel Crosley.

Contributions:

I designed and performed experiments (except where noted), analyzed the data, and prepared the manuscript. Dr. Ryan Noyce assisted in design of the vaccinia shuttle vector plasmid and performance of next generation sequencing of VACV^{TRAIL}. Dr. Kyle Potts performed the experiment shown in Fig 3.5, and provided guidance in experimental design, data interpretation, and manuscript preparation.

3.1 Introduction

Vaccinia virus (VACV) possesses many key attributes necessary for an ideal viral backbone to be used in oncolytic viral gene therapy. These include a short lifecycle, rapid cell-to-cell spread, strong lytic ability, a large cargo capacity, and well-defined molecular biology. It has previously been shown that VACV tumour selectivity is increased by the deletion of the viral J2R gene that encodes thymidine kinase (TK), making the virus dependent on cellular TK that is up-regulated in proliferating cancer cells [147, 148, 159, 160]. It has also been shown that additional disruption of the genes encoding viral ribonucleotide reductase (RR) increases the safety profile of VACV without negatively impacting viral replication in cancer cells [145, 147, 161, 162].

Granulosa cells are susceptible to TRAIL-induced apoptosis as part of normal follicular atresia, and GCT is reported to have an inverse correlation between TRAIL expression and tumour size suggesting a potential for TRAIL as a therapeutic [124]. While TRAIL has exhibited great potential as a cancer therapeutic, *in vitro*, it has consistently failed to display strong efficacy *in vivo*. Reasons for the lack of clinical effectiveness are varied, but include: inadequate delivery methods; a short half-life; and inherent or acquired resistance to TRAIL therapy [121, 163]. Several studies to date have attempted to improve TRAIL effectiveness by combining it with another agent [3, 116, 164-166], while others have investigated use of viral vectors to deliver a TRAIL gene to tumour cells [167-172]. Here we report on the development of a recombinant VACV expressing TRAIL (VACV^{TRAIL}) that generates effective levels of soluble TRAIL during the viral replication cycle. In addition we show that VACV^{TRAIL} combines with PAC-1 to effectively control GCT *in vitro*.

3.2 Materials and methods

3.2.1 Cell lines and reagents

The human cell lines KGN (GCT), F202 and N60 (normal fibroblasts) were cultured as described in section 2.2.1. African green monkey kidney cell line BSC-40 (ATCC® CRL-2761™) was grown in minimal essential medium (MEM) supplemented with 5% FBS. All cells were cultured at 37°C in 5% CO_2. All lines were routinely tested for and found free of mycoplasma either by Hoechst 33342 staining (Thermo Fisher Scientific) and fluorescence imaging, or using the Mycoplasma PCR Detection Kit (Applied Biological Materials, Inc.). Mycophenolic acid (MPA), xanthine, and hypoxanthine (Sigma-Aldrich) were generously provided by Dr. David Evans. FastDigest restriction enzymes *Eco*31I (#FD0293), *Not*I (#FD0593), XhoI (#FD0694), *Bam*HI (#FD0054), and *Xag*I (#FD1304) were purchased from Thermo Fisher Scientific. QIAquick gel extraction kit, and HiSpeed DNA purification kit were purchased from Qiagen.

3.2.2 VACV deletion mutants and generation of recombinant VACV^{TRAIL}

All recombinant viruses used in this study were derived from the VACV Western Reserve strain, and are shown in Figure 3.1. VACV ΔF4L^{nm} virus deleted in the F4L locus, VACV ΔF4LΔJ2R virus disrupted in the F4L locus by *gusA* and *neo* and in the J2R locus by *lacZ* and *mCherry*, and VACV ΔF4L^{nm} ΔJ2R virus deleted in the F4L locus and disrupted in the J2R locus with yellow fluorescent protein (VACV^{YFP}) were generously provided by Dr. David Evans (University of Alberta). Virus stocks were prepared using BSC-40 cells that were infected at a multiplicity of infection (MOI) of 0.03 plaque-forming units (pfu)/cell and incubated 72 h at 37°C with 5% CO_2. Cells were then harvested with a cell scraper and medium plus cells were collected into centrifuge bottles and centrifuged at 2000 x g for 10 minutes. Supernatant was decanted and

pellets were resuspended in 10 mM Tris pH 8.0 and transferred to a dounce homogenizer and dounced 20x with the tight pestle. Virus was then transferred to a 50 mL conical tube and centrifuged at 1100 x g for 10 min. Supernatant was then drawn off and aliquoted to be stored at -80^{o}C. Virus titre was determined by standard plaque assay using 10-fold serially diluted virus plated in duplicate wells of 6-well plates on BSC-40 cells. Infected cells were cultured for 2 days, then fixed and stained with crystal violet. Plaque counts were determined from wells containing 30 – 300 plaques.

The TRAIL gene used to generate VACV^{TRAIL} was human-codon-optimized using OptimumGene™ Codon Optimization Analysis then synthesized by Genscript. This sequence was inserted at Genscript into the pSC67 plasmid vector between the *Not*I and *Xho*I restriction sites, generating pPOX-B17F11-SS-Fur-ILZ-TRAIL. This plasmid DNA was expanded using One Shot™ Stbl3™ chemically competent *E. coli* (Thermo Fisher). 50 ng of plasmid DNA was digested with FastDigest restriction enzymes (Thermo Fisher): *Eco*31I to confirm linear size of the plasmid (6240 bp); *Bam*HI – *Xga*I to check insert orientation; and *Not*I – *Xho*I to verify TRAIL sequence insertion.

Recombinant VACV^{TRAIL} was generated by rescuing the J2R-flanked insert encoding TRAIL and YFP/gpt from pPOX-B17F11-SS-Fur-ILZ-TRAIL into the J2R locus of VACV ΔF4L^{nm} through homologous recombination as described previously [2]. Briefly, BSC-40 cells were grown to confluence and infected for 1 h with VACV ΔF4L^{nm} at a MOI of 2 PFU/cell. Inoculum was then aspirated from the cells and replaced with 4 mL OPTI-MEM and placed back in the incubator. Two h post-infection, infected BSC-40 cells were transfected with 2 μg linearized TRAIL-

encoding shuttle plasmid DNA using Lipofectamine 2000 (Thermo Fisher) as per manufacturer's instructions. Cells were cultured for 48 h at 37^{o}C, then the cells/virus were harvested by scraping into media followed by transfer to 15 mL conical tubes and three rounds of freeze-thaw to release virus from cells.

Recombinant virus from the infected cell lysate was isolated by two rounds of drug treatment (MPA: 25 μg/mL of mycophenolic acid plus 250 μg/mL xanthine, and 15 μg/mL hypoxanthine in liquid culture medium). Serially-diluted virus was used to inoculate a 6-well plate of BSC-40 cells and a companion set of three 60 mm dishes of BSC-40 cells. After 1 h incubation at 37^{o}C, inoculum was aspirated and replaced with MEM containing MPA. One set of wells in the 6-well plate received MEM without MPA. Cells were left to incubate 48 h at 37^{o}C, then the 6-well plate was stained with crystal violet to determine virus titre and corresponding 60 mm dishes were harvested by scraping and freeze-thaw as described earlier. Following drug selection there were three rounds of selection under 0.85% agar (the first containing MPA and then two rounds without MPA). BSC-40 cells were seeded in 100 mm plates and incubated at 37^{o}C until 80% confluent. Cells were then infected with 10-fold serial dilutions of virus and incubated 1 h at 37^{o}C. Inoculum was then aspirated and replaced by agar mixed with MEM, then incubated for 2 – 4 days at 37^{o}C. Once large, single plaques were identifiable multiple clones were picked and placed in separate microfuge tubes with PBS and freeze-thawed 3x to release virus. This step was repeated two more times. PCR was used to confirm the purity of all the recombinant VACV clones using primers

5’- AACTATAGAAGTTAAACTGTGAATGTC -3’ and 5’- TTTACAATGCGTGTAAGTTG - 3’ to amplify the F4L locus and primers 5’-TATTCAGTTGATAATCGGCCCCATGTTT- 3’ and 5’-GAGTCGATGTAACACTTTCTACACACCG-3’ to amplify the J2R locus. PCR products were then run in a 0.8% agarose gel for 1.25 h and visualized using a Hewlett-Packard Alpha Imager with default UV gel imaging parameters.

3.2.3 Virus infection and growth curves

For multistep growth curves, cells were seeded into 60 mm plates, then the next day, medium was removed by aspiration and cells were inoculated with VACV diluted in PBS and incubated 1 h at 37^{o}C. After incubation, either fresh culture medium or medium plus 20 µM PAC-1 was added. For the 0 h time point, plates were aspirated and then fresh medium was added; VACV inoculum was added and cells were then immediately harvested and subjected to three rounds of freeze-thaw. For other time points, infected cells were scraped into the culture medium, drawn off into 15 mL Eppendorf conical tubes and subjected to three rounds of freeze-thaw. Virus titre was determined by plaque assay where 6-well plates of confluent BSC-40 cells were aspirated then inoculated with 10-fold serially diluted virus in duplicate wells and incubated for 1 h at 37^{o}C. After 1 h medium was added to the wells and infected cells were cultured for 2 days, then fixed and stained with crystal violet. Titers were calculated from wells containing 30-300 plaques.

3.2.4 Purification of VACV^{TRAIL}

Prior to sequencing of VACV^{TRAIL} the virus was sucrose purified to remove contaminants such as cellular particles. Thawed virus was resuspended in 5.5 mL of cold Tris pH 9.0 + 2 mM $MgCl_2$ + 50 U/mL benzonase, then transferred to a 7 mL dounce homogenizer and dounced 20x.

Inoculum was then transferred to 50 mL conical tube and centrifuged at 1500 x g for 10 min at 4^{o}C. Supernatant was then transferred to a new tube and stored on ice. The pellet was resuspended in Tris as above, dounced 20x and inoculum was transferred to a 50 mL conical tube and centrifuged as above. Supernatants were pooled and incubated 30 min at 37^{o}C, then centrifuged at 1500 x g for 10 min. 19 mL 36% sucrose in 10 mM Tris pH 9.0 was added to a 38 mL Oakridge tube and overlaid with 19 mL of virus (10 mM Tris pH 9.0 + $MgCl_2$ was used to bring virus volume up to 19 mL). Tubes were then centrifuged at 26500 x g for 90 min. Sucrose was aspirated and the pellet was resuspended in 10 mM Tris pH 8.0, aliquoted and stored at -80^{o}C. Illumina Next Generation *de novo* sequencing mapped purified VACV^{TRAIL} to VACV WT and confirmed correct location of the insert (data not shown).

3.2.5 Cytotoxicity assays

Cells were seeded in 48-well plates (KGN: 15000 cells/well; F202: 10000 cells/well) and incubated overnight. Wells were then aspirated and cells were inoculated in replicate wells with VACV diluted in PBS to the indicated MOI and incubated for 1 h at 37^{o}C before medium or medium plus PAC-1 20 µM was added back into the wells. Mock infections consisted of incubation with PBS alone followed by adding medium alone. After being incubated for 2 days, 44 µM resazurin (Sigma-Aldrich) was added to the wells and plates were further incubated 3 – 4 h at 37˚C. Fluorescence was read using a FLUOstar plate reader (BMG LabTech) with 544 nm excitation/590 nm emission filters. Relative fluorescent unit (RFU) readings for treated wells were normalised to the average RFU for mock-infected cells.

3.2.6 Generation of TRAIL supernatant

BSC-40 or KGN cells were seeded in 150 mm plates and grown to ~70% confluence. Cells were then inoculated with either VACV^{TRAIL} or VACV^{YFP} in medium at MOI 1.0 PFU/cell and incubated at 37^{o}C for 48 h. Medium was collected, passed twice through 0.22 µm filters and then UV-inactivated (x2) using a Stratalinker® UV crosslinker at 0.999 J/cm^2. Virus inactivation was confirmed by plaque assay, following which TRAIL concentration in supernatant from KGN cells was measured with a human TRAIL AlphaLisa Detection Kit (PerkinElmer, AL3089C/F), while supernatant from BSC-40 cells was measured with a colorimetric human TRAIL ELISA (RayBiotech, ELH-TRAIL). Supernatant was stored at -80^{o}C until use.

Remaining cells in the plates were scraped into 14 mL Eppendorf conical tubes, washed with PBS and then lysed using RIPA buffer (150 mM NaCl, 10 mM Tris, pH 7.2, 0.1% SDS, 1.0% Triton X-100, 1% Deoxycholate, 5 mM EDTA) with 1 mM phenylmethylsulfonyl fluoride and 1x protease cocktail (Sigma Cat P7626). Lysate was assayed for protein (BCA protein assay kit, Thermo Fisher). TRAIL protein expression was confirmed by western blot with anti-human TRAIL antibody (Cedarlane, CLDB040) using methods described in section 2.2.6.

3.2.7 TRAIL supernatant cytotoxicity

5000 KGN cells were seeded in 96-well plates and incubated overnight. Cells were then incubated with 50 µM caspase inhibitor (R & D Systems, z-DEVD-FMK (FMK004), z-IETD-FMK (FMK007), z-VAD-FMK (FMK001)), or normal medium for 1 h at 37^{o}C before being treated with PAC-1 at 20 µM, VACV^{TRAIL} supernatant at 10 ng/mL (estimate based on ELISA), PAC-1 plus VACV^{TRAIL} supernatant, or mock-treated (medium only). 48 h after treatment, viability was assessed by resazurin metabolic activity assay as described in section 2.2.3.

3.3 Results

3.3.1 Generation of a recombinant TRAIL-expressing vaccinia virus (VACV^{TRAIL})

Gene therapy offers the potential for high local dosing and long-term expression of a therapeutic protein. VACV has been shown to be an excellent vector for delivering gene therapy safely, and can be designed with selectivity for tumour cells [145, 146, 173]. To extend the results of our work described in chapter 2, we designed a synthetic gene for expression of a secretable trimeric form of human TRAIL in order to avoid some of the issues previously cited as limiting TRAIL effectiveness in clinical trials. The engineered TRAIL gene encodes the signal peptide sequence for human-Fibrillin1 [174], a Furin cleavage site, and a modified yeast GCN4-pII isoleucine motif (Figure 3.2) (RMKQIEDKIEEILSKIYHIENEIARIKKLIGER [159, 175]) linked to the extracellular domain of TRAIL (aa 114-281). This synthetic TRAIL gene was inserted into a VACV shuttle vector (pSC67) downstream of a synthetic early/late poxvirus promoter, and upstream of a YFP/gpt expression cassette already present in pSC67 (Figure 3.1). The resulting plasmid (pPOX-B17F11-SS-Fur-ILZ-TRAIL) was digested with restriction enzymes to ensure correct insertion and orientation of the gene (Figure 3.3).

Recombinant VACV^{TRAIL} was rescued by homologous recombination into the J2R locus of VACV ΔF4L^{nm} followed by drug selection and plaque purification. DNA from independently isolated plaques was then PCR-amplified with F4 and J2 primers to verify the site of gene insertion (Figure 3.4). Crude stocks for four VACV^{TRAIL} isolates were generated in BSC-40 cells, then titred by standard plaque assay.

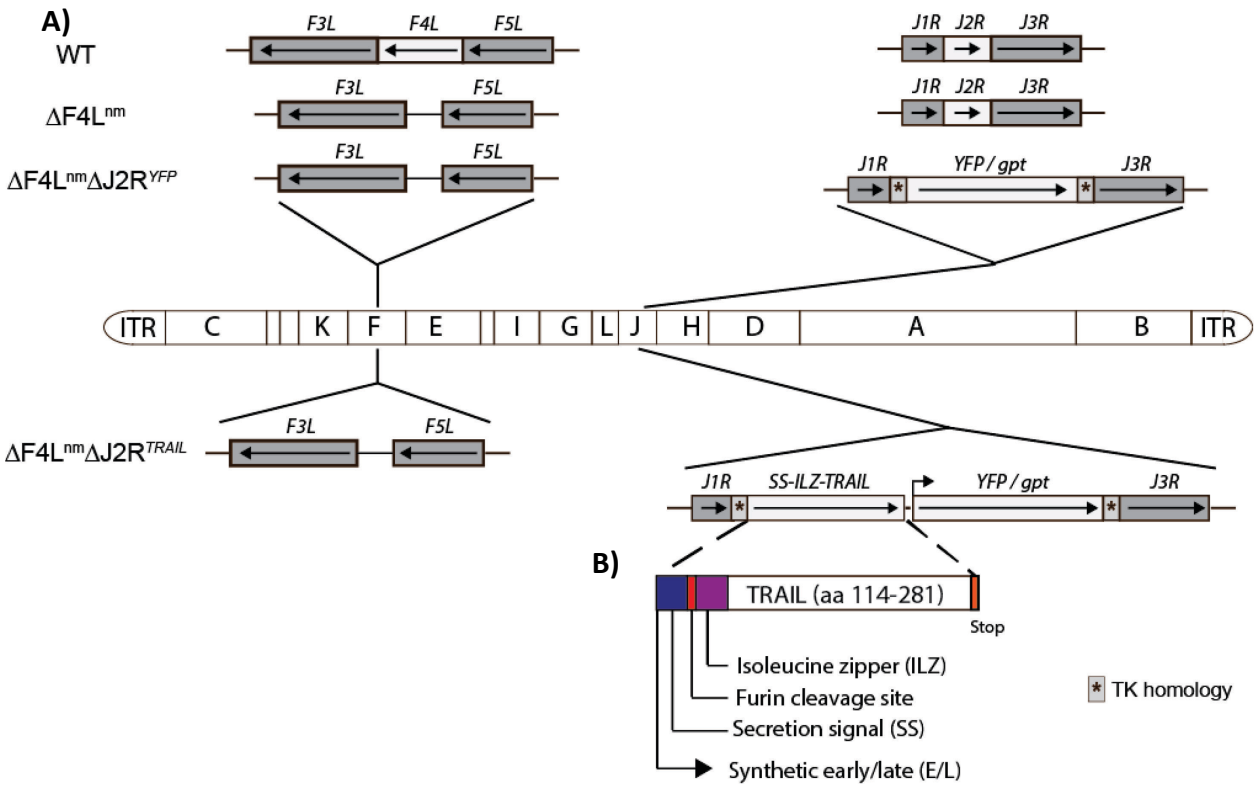

Figure 3.1 - Genomic maps of VACV constructs. (A) Viruses used in this project were generated from the VACV Western Reserve strain. Viral thymidine kinase (TK) is encoded by the J2R gene. The small subunit (R2) of viral ribonucleotide reductase is encoded by the F4L gene. nm, no marker; YFP, yellow fluorescent protein; gpt, xanthine phosphoribosyltransferase gene; ITR, inverted terminal repeat; *, viral thymidine kinase homology region; and WT, wild-type. Letters A-L (M, N, and O not shown) indicate HindIII restriction fragments of the viral genome in order of largest to smallest. **(B)** Design of the synthetic gene for expression of secretable TRAIL. Diagram modified from [2].

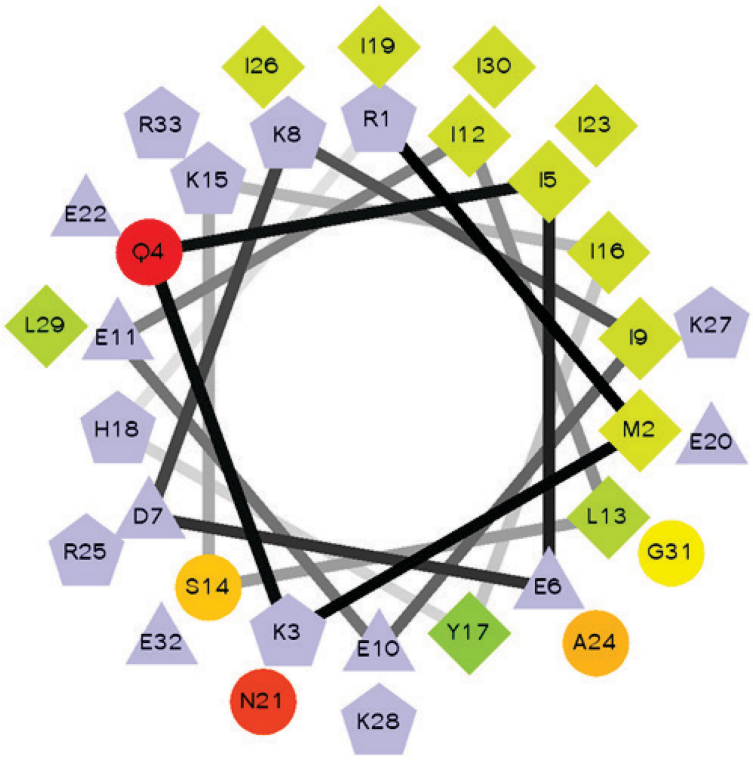

Figure 3.2 - Isoleucine zipper monomer sequence results in formation of a helical wheel coil. Hydrophobic residues are diamonds; negatively-charged residues are triangles; positively-charged residues are pentagons; hydrophilic residues are circles. Green indicates the most hydrophobicity while red indicates the most hydrophilicity. Helical wheel projection was generated online using Helical Wheel Projections: rzlab.ucr.edu/scripts/wheel/wheel.cgi with sequence: RMKQIEDKIEEILSKIYHIENEIARIKKLIGER.

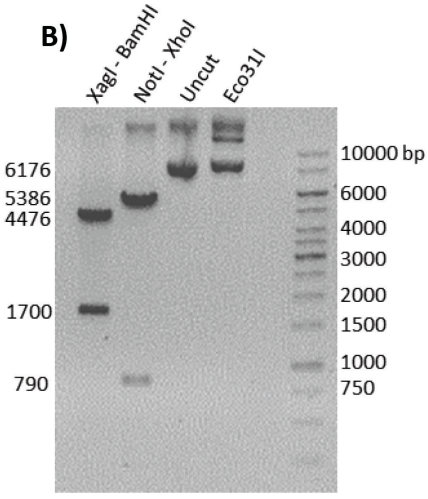

Figure 3.3 – Restriction analysis of pPOX-B17F11-SS-Fur-ILZ-TRAIL plasmid DNA confirms proper insertion of TRAIL cassette. (A) Design of plasmid pPOX-B17F11-SS-Fur-ILZ-TRAIL with restriction enzymes and key regions. **(B)** 50 ng of plasmid DNA was digested with FastDigest restriction enzymes (Thermo Fisher): *Eco*31I to confirm linear size of the plasmid (6176 bp); *Xag*I – *Bam*HI to check insert orientation (1700 & 5386 bp); and *Not*I – *Xho*I to verify TRAIL insert size (790 bp). Plasmid map generated by SnapGene Viewer version 4.3.10.

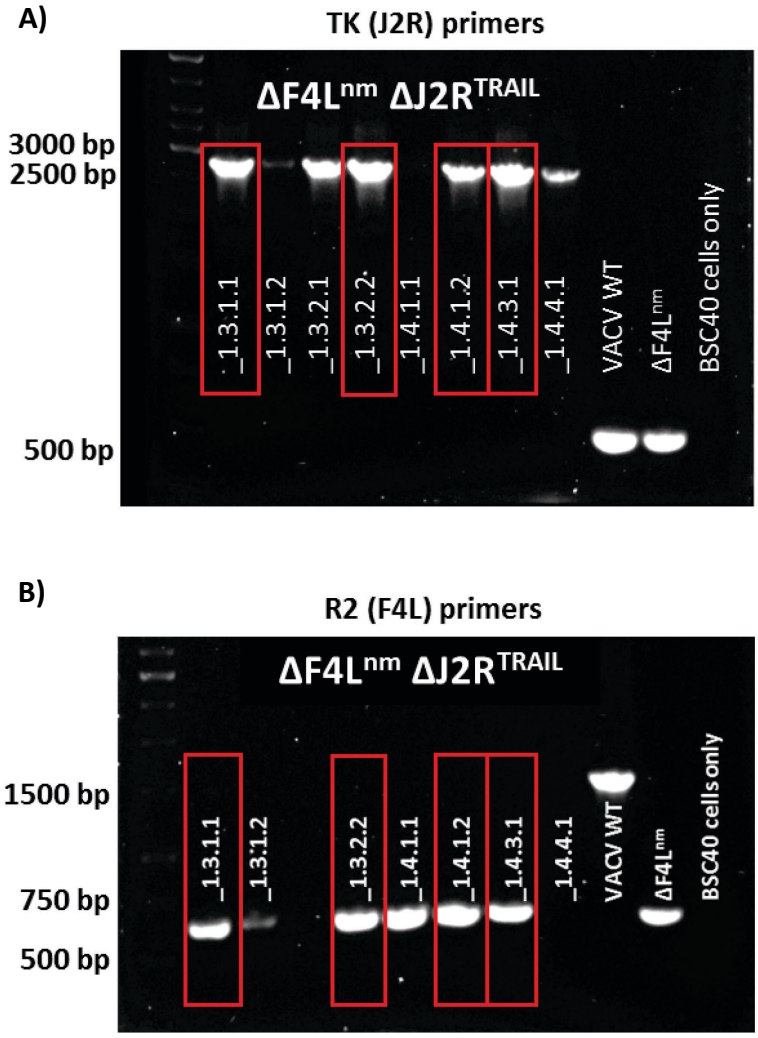

Figure 3.4 – PCR analysis indicates correct insertion of TRAIL and YPF/gpt cassettes into the J2R locus in VACV^{TRAIL}**. (A)** Primers for TK (J2R) reveal insertion of the expected size for the TRAIL-YFP/gpt DNA sequence (2767 bp VACV^{TRAIL}, 516 bp WT). **(B)** Primers upstream and downstream of R2 (F4L) confirm maintenance of gene deletion in recombinant virus (1527 bp WT, 658 bp ΔF4L^{nm}). Plaques highlighted in red were selected for further expansion.

3.3.2 Recombinant TRAIL-expressing VACV mutant replicates effectively and is cytotoxic in KGN cells.

Previous work in our lab had shown that KGN were capable of supporting robust replication by a panel of VACV strains and subject to virus-mediated toxicity in a dose-dependent manner (data by K. Potts, Figure 3.5). To determine whether GCT would support VACV^{TRAIL} replication we conducted multistep growth assays using four clones of VACV^{TRAIL} and compared them to the VACV ΔF4LΔJ2R double mutant used during other research by our lab (Figure 3.6A) [145]. KGN supported robust replication by all tested VACV^{TRAIL} strains so next we wanted to assess the impact of PAC-1 on virus replication. We repeated growth assays in KGN cells with one selected clone (VACV^{TRAIL} 1.3.2.2, hereafter referred to as VACV^{TRAIL}) both with and without co-administration of 20 µM PAC-1, and compared that to the growth of VACV^{YFP} (non-TRAIL expressing VACV ΔF4L^{nm}ΔJ2R expressing YFP) with and without PAC-1. Patterns of virus replication were similar between VACV^{TRAIL} and VACV^{YFP}, although the addition of PAC-1 dramatically reduced replication of both viruses over the 72 h growth period (Figure 3.6B).

A)

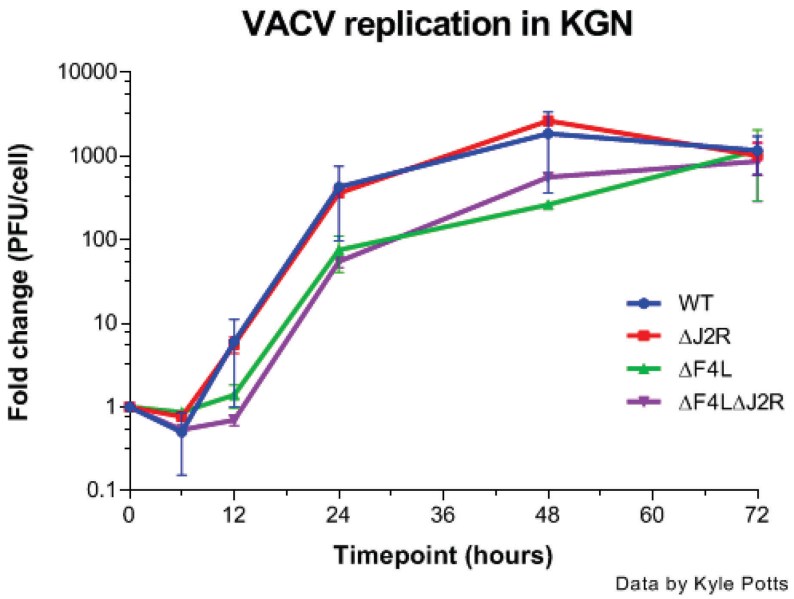

B)

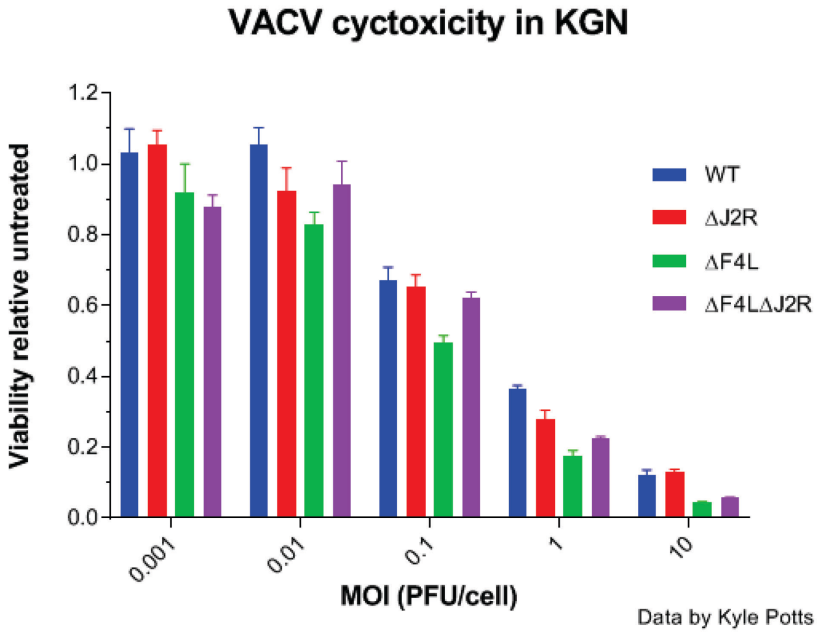

Figure 3.5 VACV efficiently replicates and is cytotoxic in KGN cells. (A) KGN cells were seeded in 60 mm plates and incubated overnight. Plates were aspirated and inoculated with one of the indicated VACV viruses at MOI 0.03 for a growth assay. **(B)** 48-well plates were seeded with 15000 KGN cells/well, incubated overnight then inoculated with the indicated VACV viruses using 10-fold serial dilutions in PBS. After 1 h medium was added to the wells and incubated for 72 h. Viability was then determined by resazurin metabolic activity assay.

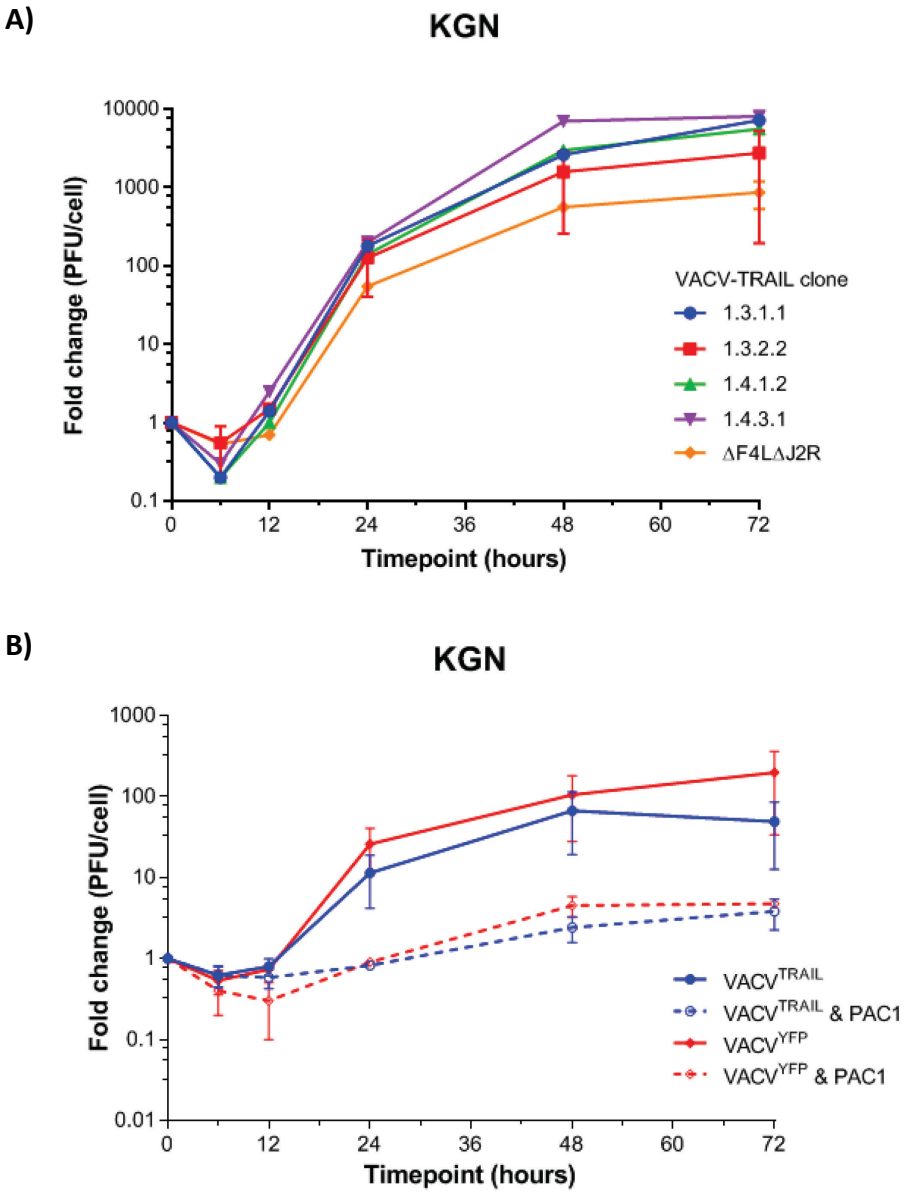

Figure 3.6 – PAC-1 attenuates VACV replication in KGN cells. (A) 60 mm plates were seeded with KGN cells, incubated overnight at 37°C and inoculated with indicated VACV clones or control virus VACV ΔF4LΔJ2R at MOI 0.03 and incubated 1 h at 37°C. Medium was then added to the plates and virus was collected at indicated time points. **(B)** 60 mm plates were seeded with KGN cells, incubated overnight and infected with VACV^{TRAIL} clone 1.3.2.2 or control virus VACV^{YFP} at MOI 0.03 for 1 h after which either normal medium or medium plus 20 µM PAC-1 was added to the plates. Cells were then incubated at 37°C for the times indicated, and virus titres determined as described in Materials and Methods.

Next we looked at the cytotoxicity of VACV^{TRAIL} in KGN (Figure 3.7). After 48 h metabolic assays showed significantly more cytotoxicity in cells infected by VACV^{TRAIL} compared to VACV^{YFP}. Importantly, toxicity of both viruses was increased by adding PAC-1 even though PAC-1 had been previously shown to reduce virus replication. The significant difference between VACV^{TRAIL} and VACV^{YFP} suggests that indeed TRAIL was being secreted from infected cells and PAC-1 priming of CASP3 was reflected in the increased toxicity observed with VACV^{TRAIL} and PAC-1 combination versus VACV^{TRAIL} alone.

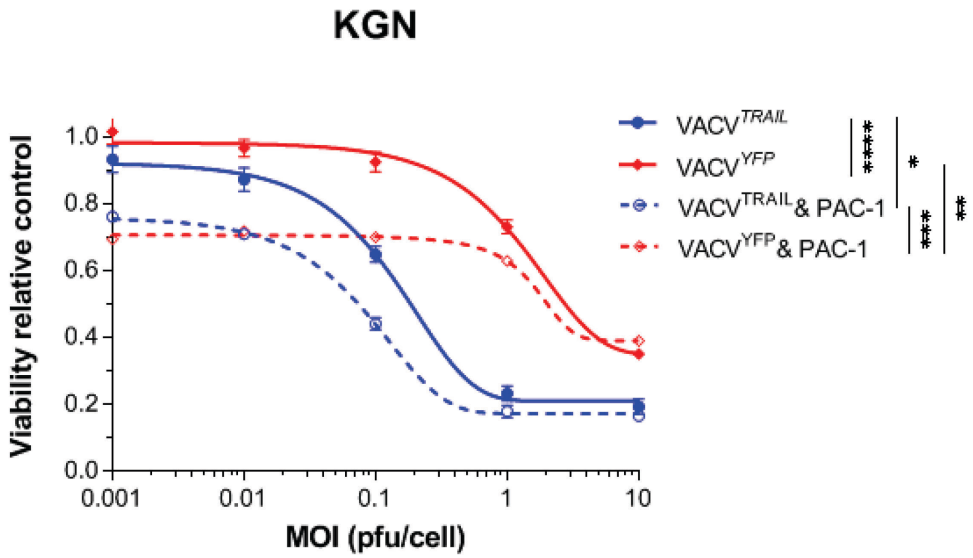

Figure 3.7 – PAC-1 potentiates cytotoxicity of VACV^{TRAIL} **in KGN cells.** 15000 cells were seeded in 48-well plates overnight after which wells were aspirated and cells inoculated with VACV at indicated MOI and incubated at 37°C for 1 h. After 1 h medium or medium plus 20 µM PAC-1 was added to the wells and incubated for 48 h. Viability was then determined by resazurin metabolic activity assay. Significance was calculated comparing area under the curve using GraphPad Prism ver. 8. (Paired t-tests of the data result in $p > 0.05$ for VACV^{YFP}/VACV^{YFP} & PAC-1 and VACV^{TRAIL} & PAC-1/VACV^{YFP} & PAC-1.)

3.3.3 VACV^{TRAIL} *secretes functional TRAIL*

The difference in cytotoxicity between VACV^{TRAIL} and VAC^{YFP}–infected cells suggested that TRAIL was being secreted by infected cells. In order to determine the amount of TRAIL secreted, and measure its effectiveness as an agent, supernatant was collected from BSC-40 cells infected with four VACV^{TRAIL} clones. Levels of TRAIL in the supernatant were determined using an anti-TRAIL colorimetric ELISA (Figure 3.8A). At 48 h post-infection of the propagating cell line BSC40, VACV^{TRAIL} clones generated ~80 ng/mL of TRAIL while TRAIL in VACV^{YFP} supernatant was at or below detection limits. We then selected the VACV^{TRAIL} clone that generated the most TRAIL (1.3.2.2) for use in follow-on assays and tested expression of VACV-encoded TRAIL in infected KGN cells (Figure 3.8B). Again, 48 h post-infection the supernatant was collected, filtered twice, UV-inactivated, and verified as virus-free using a plaque assay. This virus-free supernatant was then assayed for TRAIL using a Perkin Elmer AlphaLisa TRAIL detection kit. KGN was found to generate detectable, and significant, levels of TRAIL when infected with VACV^{TRAIL}. KGN infected with VACV^{YFP} showed no trace of TRAIL in the supernatant. Differences between levels of TRAIL detected in BSC-40 and KGN cells are most likely explained by several factors: BSC-40 cells are much smaller than KGN cells resulting in an order of magnitude difference in both cell number and therefore pfu used to inoculate the same size dish (150 mm); while cells were incubated in 20 mL of media, slight variations in volume will affect detected concentrations; and the assay of BSC-40 supernatant was done with a colorimetric-based ELISA with multiple wash/handling steps whereas the KGN assay was done with a no-wash AlphaLISA assay designed for high-throughput and high-sensitivity.

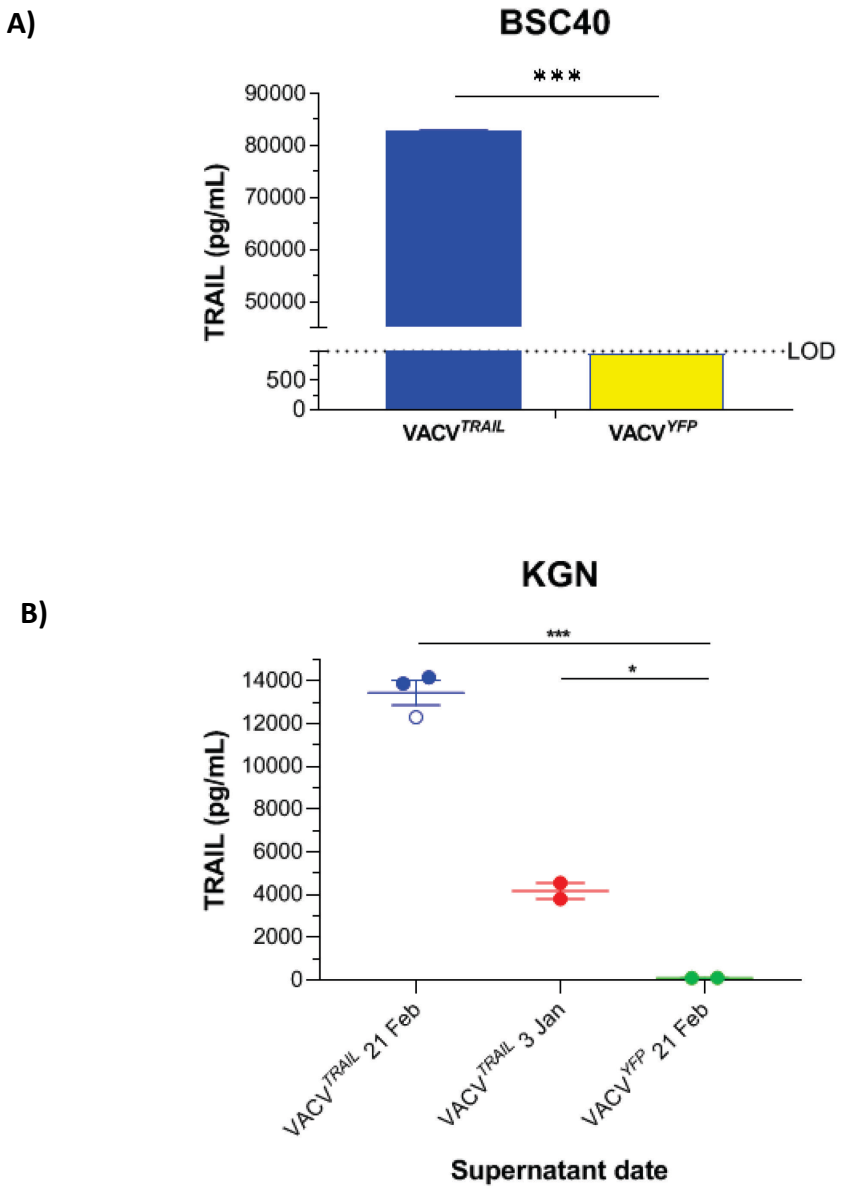

Figure 3.8 – BSC-40 and KGN cells infected with VACV^{TRAIL} **secrete detectable levels of soluble TRAIL. (A)** BSC-40 cells were grown in 150 mm plates to ~70% confluence and then infected with one of the VACV^{TRAIL} clones. At 48 h supernatant was drawn off, filtered and UV-inactivated before measuring TRAIL by colorimetric ELISA (RayBiotech #ELH-TRAIL). **(B)** KGN cells were grown as in (A) and infected with VACV^{TRAIL} (clone 1.3.2.2) or VACV^{YFP}. After 48 h supernatant was drawn off, filtered and UV-inactivated before being assayed by AlphaLisa TRAIL detection kit (Perkin-Elmer, #AL3089C). Significance determined by one-way ANOVA corrected by Sidak's multiple comparison test. Open circle in (B) identifies result for supernatant sample that was diluted 2-fold in medium to verify assay sensitivity. Different dates in (B) represent separate supernatant collection dates. LOD: Limit of detection

Assays of supernatant detected concentrations of TRAIL that had already been secreted, but we also wanted to see if TRAIL was still being expressed by cells 48 h after initial infection. To do that we washed cells remaining in the dish after medium was decanted and then generated protein lysate for western blot detection of human TRAIL (Figure 3.9).

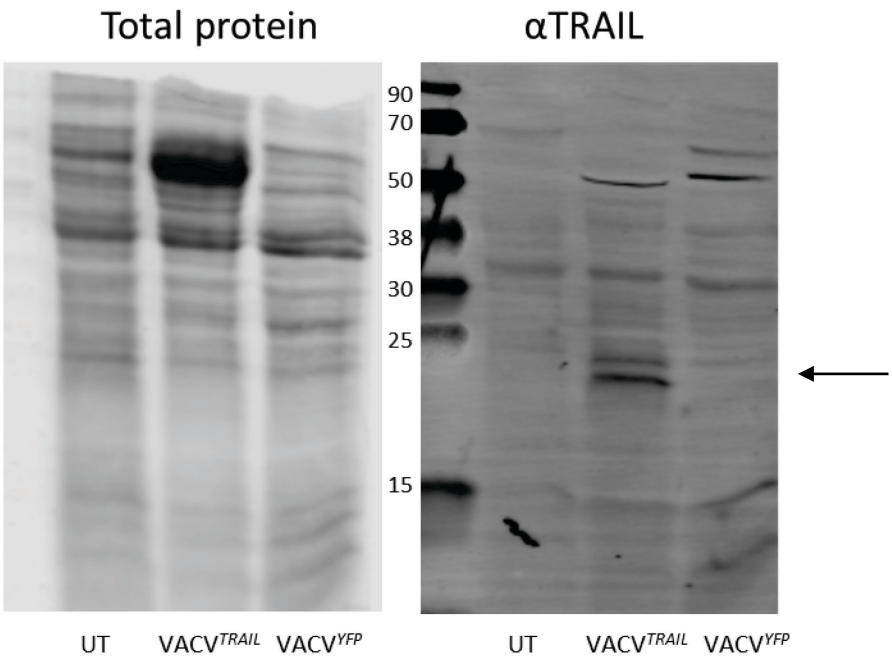

Figure 3.9 - KGN cells infected with VACV^{TRAIL} **express soluble TRAIL.** Lysates from infected KGN cells were probed with anti-TRAIL antibody. Detected band (arrow) is the correct size for the modified monomer of TRAIL extracellular domain (~24 kDa). Total protein probed using Revert^{TM} Total Protein Stain.

The cells that had been infected with VACV^{TRAIL} showed detection of a band ~24 kDa, which correlates with reports on the size of extracellular TRAIL. Neither the mock-infected KGN, nor the VACV^{YFP}-infected cells showed expression of TRAIL, supporting the determination that the soluble TRAIL detected was being produced by our virus-encoded gene, rather than the endogenous cellular TRAIL gene.

3.3.4 Secreted TRAIL is an active agent in VACV^{TRAIL} *toxicity.*

To verify that the TRAIL detected in the supernatant was active soluble TRAIL, we repeated *in vitro* cytotoxicity assays similar to those in chapter 2 using 20 µM PAC-1 and supernatant containing ~10 ng/mL TRAIL from VACV^{TRAIL} infection. KGN cells were treated with PAC-1 and supernatant for 48 h, at which time a metabolic activity assay was conducted. In addition, some wells were pre-incubated for 1 h with either 50 µM z-DEVD-FMK (a CASP 3 inhibitor) or 50 µM z-IETD-FMK (a CASP8 inhibitor) before drug was added to the well.

Figure 3.10 displays that with PAC-1 alone, CASP3 inhibition (DEVD-FMK) reduced the toxicity of PAC-1 in KGN cells whereas inhibition of CASP8 (IETD-FMK) did not. When VACV^{TRAIL} supernatant alone was used on cells it was effective at controlling KGN and significantly more effective than VACV^{YFP} supernatant alone. Furthermore, while CASP3 inhibition strongly reduced toxicity of VACV^{TRAIL} supernatant, CASP8 inhibition almost totally protected KGN from TRAIL supernatant toxicity. VACV^{YFP} supernatant showed no toxicity to KGN cells. Finally, when PAC-1 was combined with supernatant, VACV^{TRAIL} was effective in combination whereas VACV^{YFP} was no better than PAC-1 alone. Inhibition of CASP3 gave some small amount of protection from PAC-1 combined with VACV^{TRAIL} supernatant, and CASP8 inhibition provided

somewhat more although as described in chapter 2, the combination of PAC-1 and TRAIL was more effective than either agent alone.

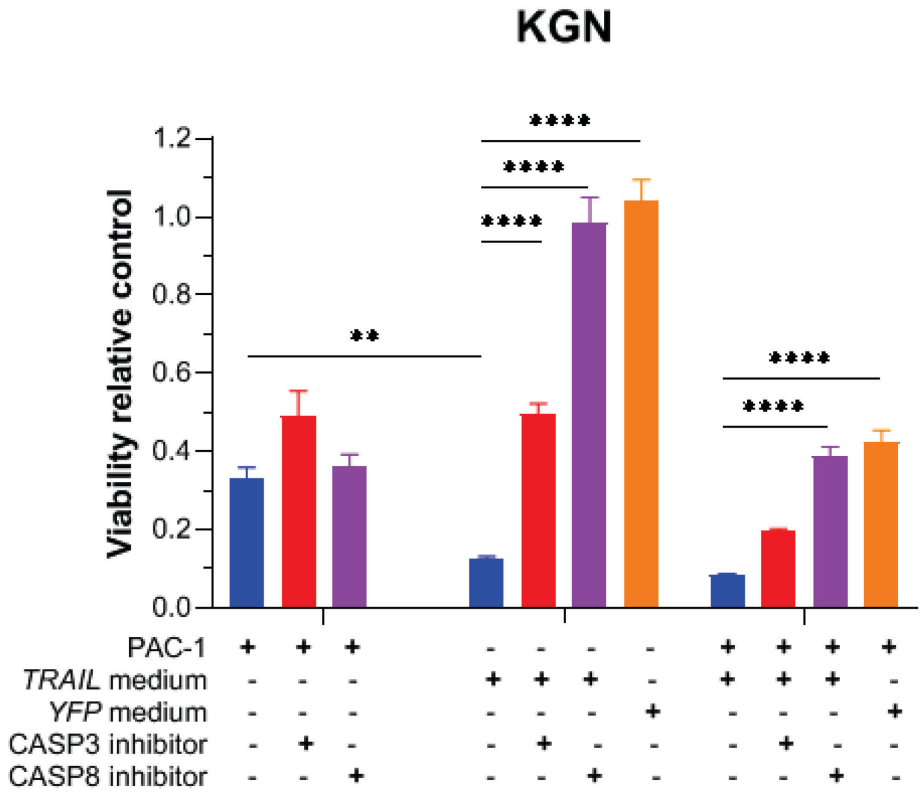

Figure 3.10 - Soluble TRAIL generated by VACV^{TRAIL} **-infected cells has cytotoxic activity both alone and in combination with PAC-1 to control KGN.** Virus-free supernatant was used with and without 20 µM PAC-1 on KGN cells in 96-well plates replicating earlier cytotoxicity assays. Supernatant was from either VACV^{TRAIL}-infected cells (~10 ng/mL concentration) or VACV^{YFP}-infected cells (no TRAIL detected). Some wells were pre-incubated with 50 µM z-DEVD-FMK (CASP3 inhibitor) or 50 µM z-IETD-FMK (CASP8 inhibitor). 48 h after PAC-1/supernatant treatment, a metabolic activity assay was conducted, RFU values were normalised to untreated cells.

3.4 Discussion

TRAIL has been known to be a tumour-selective, apoptosis-inducing protein since its initial discovery in 1995 [176]. While many studies have shown soluble TRAIL to have great effect *in vitro*, that success has not translated to the clinic where several limitations have appeared including: a short half-life ; ready clearance by the body; and the resulting difficulty in achieving therapeutic dosing at tumour sites [177]. One avenue for attempting to increase effectiveness is through gene therapy where the TRAIL gene would be delivered directly to the tumour cell. Multiple vectors have been described including mesenchymal stromal cells, adenovirus and poxvirus encoding TRAIL [117, 120, 167, 168]. Kim, *et al.*, reported on the superiority of a soluble, isoleucine zipper (ILZ)-stabilized trimeric TRAIL (stTRAIL) molecule delivered by a replication-incompetent adenovirus vector when compared to full-length TRAIL, also delivered by an adenovirus vector. They found that stTRAIL had more tumour-suppressor activity (as measured by CASP3 activity) and that expression of stTRAIL persisted for more than 4 days [120]. It should be noted that these results were achieved following infection with a MOI of up to 100 pfu/cell, a dose that may not be achievable in the clinic.

Ziauddin, *et al.*, used an oncolytic vaccinia virus vector to construct a recombinant VACV that delivered membrane-associated TRAIL, and combined that with oxaliplatin. They reported significant improvement in survival of mouse models implanted with colorectal carcinomatosis when treated with the recombinant VACV and oxaliplatin, although they do not elucidate a possible mechanism for oxaliplatin interaction with TRAIL [167]. Yuan, *et al.*, generated mesenchymal stromal cells (MSC) expressing full-length TRAIL that they found significantly more effective at inducing apoptosis than MSC expressing ILZ-stabilized soluble TRAIL [117].

We pursued developing an alternative means of delivering TRAIL by inserting a synthetic soluble TRAIL gene into the genome of an oncolytic vaccinia virus, which itself has shown high selectivity for cancer cells with an excellent safety profile *in vivo*. The TRAIL gene included a synthetic viral promoter that would be active from early to late in the VACV life cycle providing robust expression of TRAIL. To that we attached sequences encoding the secretion signal peptide for human Fibrillin-1, which is reportedly expressed to high levels in KGN and ovarian follicles [178]. A Furin cleavage site was added to remove the signal peptide and activate the TRAIL molecule [179], and an ILZ motif to induce trimerization of secreted monomeric TRAIL molecules. This would minimize dependence on a Zn^{2+} ion for stable trimerization of TRAIL in the presence of PAC-1. To that we fused coding sequences for the extracellular domain of TRAIL, amino acids 114-281. After rescuing VACV^{TRAIL} we verified that two key genes for viral DNA replication (F4L and J2R) had been deleted (in the case of F4L) or disrupted (by inserting our TRAIL construct in to the J2R locus).

Next we evaluated the ability of VACV^{TRAIL} clones to replicate in GCT cell line KGN, and assessed the growth of a selected VACV^{TRAIL} to replicate in the presence of PAC-1. We found that all tested clones of VACV^{TRAIL} efficiently replicated in KGN but we also saw that replication was markedly diminished in KGN when treated with 20 μM PAC-1. This reduced virus replication, however, did not negatively impact the cytotoxicity of VACV^{TRAIL}, as we saw that VACV^{TRAIL}-infected cells treated with PAC-1 were significantly less viable than cells treated with virus alone, and VACV^{TRAIL} was significantly more cytotoxic than non-TRAIL-expressing VACV.

Finally, we wanted to confirm that functional TRAIL is secreted by VACV^{TRAIL} -infected cells. We saw that in both BSC-40 cells and KGN cells, infection with VACV^{TRAIL} for 48 h resulted in robust generation and secretion of human TRAIL. We also found that virus-free supernatant of VACV^{TRAIL} -infected cells was cytotoxic to KGN cells both alone and in combination with PAC-1. The toxicity of supernatant alone was stronger than we observed in earlier assays with rhTRAIL (Figures 2.2D and 3.10), but could reflect the fact that other cytokines may also be expressed as the result of infection by VACV^{TRAIL}. Again, the synergy between PAC-1 and TRAIL was reflected by the fact that inhibition of CASP8 (the initiator caspase in the extrinsic apoptotic pathway) was able to eliminate any toxicity from combining PAC-1 and TRAIL beyond the effect of PAC-1 alone.

What we show here is that VACV^{TRAIL} combined with PAC-1 constitutes an effective treatment alternative, *in vitro*, for GCT. We propose that this combination would generate a three-pronged attack on GCT through activation of CASP3, localized delivery of clinically relevant levels of TRAIL, and the additional induction of killing by oncolysis in cells that may harbor TRAIL resistance.

CHAPTER 4. ESTABLISHMENT OF XENOGRAFT MODELS FOR GRANULOSA CELL TUMOUR

PREFACE

This chapter is an original work by Powel Crosley except section 4.3.3 which is part of a paper submitted for publication in the manuscript: H. Chen, P. Crosley, A.K. Azad, N. Gupta, N. Gokul, Z. Xu, M. Weinfeld, L. Postovit, S.A. Pangas, M.M. Hitt, Y. Fu; RUNX3 promotes the tumourigenic phenotype in KGN, a human granulosa cell tumour-derived cell line; Int J Mol Sci, 20 (2019).

Contributions:

I designed and performed experiments, analyzed the data, and prepared the figures for this chapter. Kate Agopsowicz assisted in animal experiments. Dr. YangXin Fu and Jiesi Zhou transformed KGN cells with Runx3 and empty vector constructs; Huachen Chen performed western blots of lysate recovered from recovered tissue samples, probing for Runx3.

4.1 Introduction

Animal models have an important role in the process of discovering new drug candidates, validating their target(s) and method(s) of action, and gaining an appreciation for how the agent(s) work within a complex biological system [180]. Testing done *in vitro*, or analysis run *in silico* provides much of the information on which early progress is made in researching new cancer therapies, but no *in vitro* model is going to fully encapsulate simultaneous effects on the nervous system, as an example, by a drug that may be targeting ovarian cancer [181]. Probably the most widely-used animal model is the xenograft model where human cells or tissue are implanted into immunocompromised animals, typically mice. A primary limitation of xenograft models of human disease, however, is that they will not provide a robust understanding for how a human with the disease will react to treatment because the animals have compromised immune systems [182]. In contrast, animal diseases that model diseases in humans are sometimes available, and these likely would be immunocompetent, but they will almost surely be different from human disease in some aspect such as important biomarkers, or a genetic alteration required to artificially stimulate the disease [181]. Even so, moving a therapy from bench to bedside will almost always depend on having demonstrated a capability and efficacy *in vivo* that supports the findings developed *in vitro* or *in silico*.

We report here on attempts to establish a xenograft animal model of human GCT utilizing two models of immune compromised mice and KGN-based tumour cells in order to have a disease model that carries the characteristic FOXL2^{C134W} mutation found in adult GCT. NIH-III *nude* mice were developed at the U.S. National Institutes for Health (NIH). In addition to the *nude* gene, which results in the absence of thymus and T-cell function, this mouse has two

other mutations: *Btk*^{xid}, X-linked immunodeficiency (xid) which affects maturation of B-lymphocytes; and *Lyst*^{bg} (beige) which results in defective natural killer (NK) cells. Both xid and beige are important in regulating the function of the immune system. Another mouse strain used in xenograft models is called Nod-*scid* gamma (NSG). These mice carry two mutations on the NOD/ShiLtJ genetic background: severe combined immune deficiency (*scid*) and a complete null allele of the IL2 receptor common gamma chain (*IL2rg*^{null}).

Unlike many cancers, there is no established protocol for inducing xenograft GCT tumours in mice, and the few cases that report having done so were limited to having established very small lesions that would not be dependable as a model for evaluating treatment success [63-66].

4.2 Materials and methods

4.2.1 Cell lines and reagents

The human GCT cell line, KGN, and derivatives of the KGN cell line, were cultured as described in section 2.2.1.

4.2.2 Animal care and housing

All studies reported were conducted with the approval of the University of Alberta Health Sciences Animal Care and Use Committee in accordance with guidelines from the Canadian Council for Animal Care. Animals were housed with access to food and water *ad libitum* in ventilated cages (3 mice per cage) in a biosafety level 2 containment suite at the University of Alberta Health Sciences Laboratory Animal Services Facility.

4.2.3 In vivo KGN tumour model

Female NIH-III mice (Charles River Laboratories) were 6 weeks old and at least 18 g in weight at the time of KGN cell implantation. Mice were anesthetized with 2% isoflurane after

which six (6) mice were injected subcutaneously in one flank with 0.1 mL of 5 x 10^6 KGN tumour cells in PBS and six (6) mice received intraperitoneal injections of 1 x 10^7 tumour cells in 0.2 mL of PBS. Mice were weighed and flank tumour sites were palpated for signs of tumour twice per week.

4.2.4 Construction of KGN-luc cell line

A lentivirus vector for expression of luciferase was generated by packaging pLenti-CMV-puro-luc (Addgene w168-1) as described by Campeau et al. [154] and in section 2.2.2. The day before transduction, KGN cells were seeded in a 6-well plate to be 50% confluent at the time of transduction. Media was aspirated and 6 µg of polybrene (Millipore Sigma) was added to 1 mL lentivirus stock and placed in each well. One well was mock-infected with medium as control. At 48 h post-transduction, puromycin (Thermo Fisher) was added to the medium (final concentration 2.5 µg/mL) for selection of transduced KGN-luc cells. After five (5) days of drug selection, cells were pooled.

4.2.5 In vitro luciferase assay

KGN-luc cells were assayed for detection of luciferase activity per manufacturer's protocol (Promega #E4030). Briefly, a dilution series of KGN-luc cells were seeded in 24-well plates overnight, then washed twice with PBS before being lysed with Promega Reporter Lysis Buffer (#E3971) by two freeze-thaw cycles. Lysates were scraped into 1.5 mL microfuge tubes, spun at 12,000 x g for 2 minutes at 4^{o}C then supernatants were transferred to fresh microfuge tubes. Using 96-well white opaque plates 20 µL of each lysate was added to duplicate wells. A BMG FLUOstar Omega plate reader injected Promega Luciferase Assay Reagent (#E151A) and measured luciferase activity. Mock transduced KGN cells were used as negative control.

4.2.6 In vivo KGN-luc tumour model

Female NSG mice were 7 weeks old and at least 20 g in weight at the time of KGN-luc cell implantation. Thirty-one (31) 150 mm plates of KGN-luc (p 11) were harvested for implantation. Mice were anesthetized with 2% isoflurane after which three (3) mice were injected s.c. in the right flank, three (3) mice were injected i.p., with both models receiving 50 µL of cell suspension containing 1 x 10^7 tumour cells in PBS with 50% Matrigel (Corning). In addition, three (3) mice were injected intraperitoneally using 50 µL of cell suspension containing 1 x 10^7 tumour cells in PBS without Matrigel. For monitoring, mice were weighed under anesthesia and then injected with 10 µL of 15 mg/mL luciferin per gram of weight and imaged with the IVIS Spectrum imaging system (Perkin Elmer) weekly until the bioluminescent signal fell to background levels, after which imaging was carried out biweekly to minimize stress to the animals.

4.2.7 In vivo advanced passage KGN-luc tumour model

Advanced passage cells were prepared for implantation into mice by harvesting sixty (60) 150 mm plates of KGN-luc cells (passage 86). Female NSG mice were 7 weeks old and at least 20 g in weight at the time of cell implantation. Mice were anesthetized with 2% isoflurane after which three (3) mice were injected s.c. in the right flank and three (3) mice were injected i.p., both models receiving 0.5 mL of cell suspension (5 x 10^7 tumour cells in PBS containing 50% Matrigel (Corning)). Post-implantation, an aliquot of remaining cells in Matrigel was placed in tissue culture to confirm viability of cells that had been implanted. Monitoring of mice was conducted by weighing them under anesthesia and then injecting 10 µL of 15 mg/mL luciferin per gram of weight for bioluminescence imaging with the IVIS Spectrum imaging system (Perkin

Elmer). This occurred weekly until the bioluminescent signal fell to background levels, after which imaging was carried out biweekly to minimize stress to the animals.

4.2.8 KGN-Runx3 tumour model

Flag-tagged KGN-Vector (empty vector) and KGN-Runx3 cells were generously provided by Dr. YangXin Fu (University of Alberta). Both cell lines were tested for, and found free of, mycoplasma using the Mycoplasma PCR Detection Kit (Applied Biological Materials, Inc.). Female NSG mice were 7 weeks old and at least 24 g at the time of initial injection. For this experiment cells were injected twice in the same location, two weeks apart. Forty (40) 150 mm plates each of KGN-Vector and KGN-Runx3 were harvested for implantation into mice at each timepoint. At each timepoint, mice were anesthetized with 2% isoflurane after which six (6) mice were injected s.c. with 0.25 mL of cell suspension containing 2 x 10^7 tumour cells in PBS with 50% Matrigel (Corning). The left flank was injected with KGN-Vector cells and the right flank was injected with KGN-Runx3. Post-implantation, an aliquot of remaining cells in Matrigel was placed in tissue culture to confirm viability of cells that had been implanted. Mice were weighed and palpated weekly for signs of tumour growth.

4.2.9 Generation of KGN-RUNX3F1 cell lines

Following termination of the KGN-Runx3 animal experiment, mice were dissected and four (4) mice were found to have small (~4 mm diameter) lesions at the spot where KGN-Runx3 cells had been implanted s.c.. No lesions were seen on the flank injected with KGN-Vector cells. Tissue excised from the lesions was washed 3x in PBS supplemented with 200 U/mL penicillin, 200 U/mL streptomycin, and 0.50 µg/mL Fungizone®, then digested overnight at 37^{o}C with constant rocking in a buffer made up of 10 mM HEPES pH 7.4, 2% BSA, 10 µg/mL insulin, 300

U/mL collagenase, 100 U/mL hyaluronidase, and DMEM/F12. Following digestion the mixture was passed through a cell strainer and 500 µL was seeded into triplicate wells of a 24-well plate and incubated at 37^{o}C overnight, after which digestion buffer was aspirated and replaced with normal DMEM/F12 medium. When one of the triplicate wells for each mouse became 80% confluent all three replicates for that mouse were trypsinized and pooled into 100 mm dishes for normal tissue culture of putative KGN-RUNX3F1 cells.

4.2.10 KGN-RUNX3F1 RNA isolation and quantitative reverse transcription PCR (qRT-PCR)

RNA isolation and qRT-PCR were performed in the Fu lab as described previously [183]. Briefly, total cellular RNA was extracted by using TRIzol® (Invitrogen) according to the manufacturer's instructions and treated with DNase to remove DNA contamination. cDNA was synthesized using the superscript II reverse transcriptase in the presence of random primers and RNaseOUT™ recombinant ribonuclease inhibitor (Invitrogen) according to the manufacturer's instructions. qRT-PCR was carried out using the Mastercycler® ep realplex real-time PCR system (Eppendorf). The reaction mixture consisted of 1 µl of cDNA, 1 µl of 10 µM primers, and 10 µl of SYBR® Select Master Mix (Applied Biosystems) in a total volume of 20 µl. Primer sequences are shown in Table 4.1.

Table 4.1 - Primer sequences for isolation of qRT-PCR [183]

Gene	Forward primer	Reverse primer
RUNX3	TGGCAGGCAATGACGAGAACTACT	TGAACACAGTGATGGTCAGGGTGA
GAPDH	GGACCTGACCTGCCGTCTAGAA	GGTGTCGCTGTTGAAGTCAGAG

4.3 Results

4.3.1 Preliminary attempt establishing KGN tumour model in NIH III mice

Previous work in our lab had attempted to replicate one of the few reports on establishing KGN xenograft models in mice. That report stated that 5 x 10^6 subcutaneously (s.c.) injected KGN cells generated bowel metastases, but no primary tumour, within 16 weeks [63]. In our experiment, we injected 5 x 10^6 KGN cells s.c. into the flank of six (6) female NIH III mice. We chose the NIH III mouse model because they are more immunodeficient than the Balb/$c^{nu-/nu-}$ mice used in the published study, which we thought would increase the chance of a successful xenograft. In addition, we injected another cohort of three (3) mice with 1 x 10^7 cells intraperitoneally (i.p.) in an attempt to develop a model of peritoneal recurrence. At 93 days post-injection, with no sign of disease by palpation of the s.c. injection site, the mice were euthanized. Postmortem pathology confirmed none of the s.c. or i.p. injected KGN cells had established a tumour (postmortem report #15-170 by P. N. Nation DVM).

4.3.2 KGN-luc tumour model in NSG mice

In order to facilitate surveillance of tumour development *in vivo*, KGN cells were transformed with firefly luciferase, which we named KGN-luc (Figure 4.1), for bioluminescence monitoring of tumour growth using the IVIS Spectrum imaging system. We also assessed the comparative sensitivity of KGN-luc and KGN to PAC-1 in a limited dose-response assay (Figure 4.2) and found the transformation with luciferase did not alter sensitivity to PAC-1. Two *in vivo* experiments were ultimately carried out with these cells.

In the first experiment, female NSG mice were injected either s.c. or i.p. with 1 x 10^7 KGN-luc cells. Six (6) mice (3 i.p. and 3 s.c.) were injected with cell suspension containing 50%

Matrigel to try and provide an initially supportive environment for successful grafting of the KGN-luc cells. Three (3) additional mice were injected i.p. with cell suspension lacking Matrigel to see if Matrigel did affect tumour development. Beginning 19 days post-injection, mice were periodically imaged with the IVIS Spectrum imaging system to monitor any tumour development. Initially, bioluminescent signal fell by about 50% (Figure 4.3) until around day 47, at which time the signal seemed to strengthen. At or around day 105, however, it became obvious that the signal had plateaued or was again slowly degrading back towards the day 47 level. At day 206 with no physical indication of palpable disease in the s.c.-injected mice, and no indication of tumour growth by imaging, the mice were euthanized and the mouse that had displayed the strongest signal (s.c.-injected) was dissected (Figure 4.4). A localized bioluminescent signal was detected under the skin, but no macroscopic disease was evident and when the tissue sample was dissociated and cultured no adherent cells were detected.

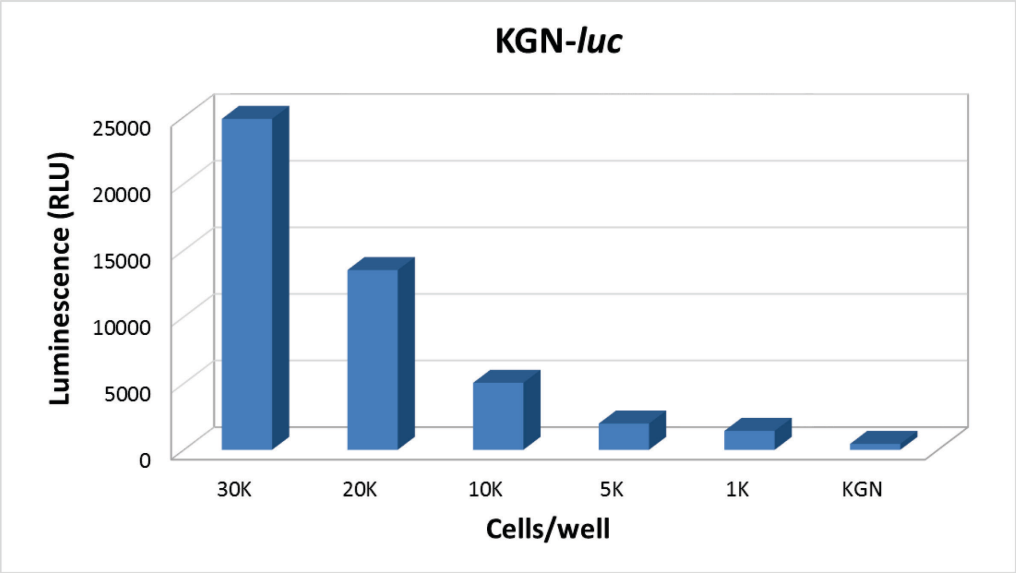

Figure 4.1 - KGN cells transduced with a firefly luciferase gene showed cell-number dependent expression of luciferase. Indicated number of KGN-luc cells were seeded in 24-well plates overnight then washed, lysed with reporter lysis buffer and lysate was then assayed for luciferase activity with BMG FLUOstar Omega plate reader. Non-transduced KGN served as control.

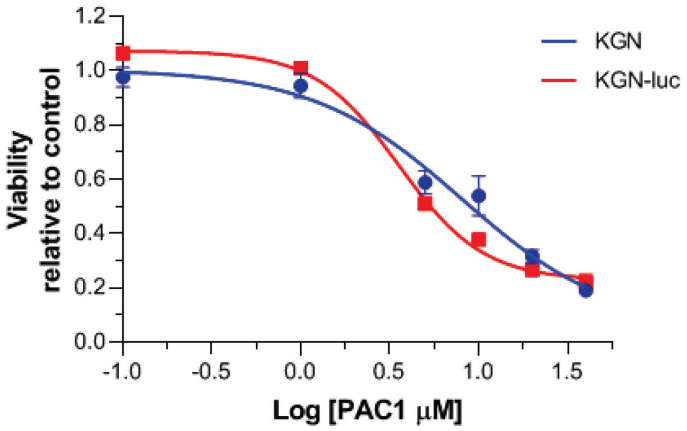

Figure 4.2 - KGN and KGN-luc are equally sensitive to PAC-1. 5000 cells of KGN or KGN-luc were seeded into 96-well plates with PAC-1 at indicated doses. After 48 h viability was determined by resazurin metabolic assay.

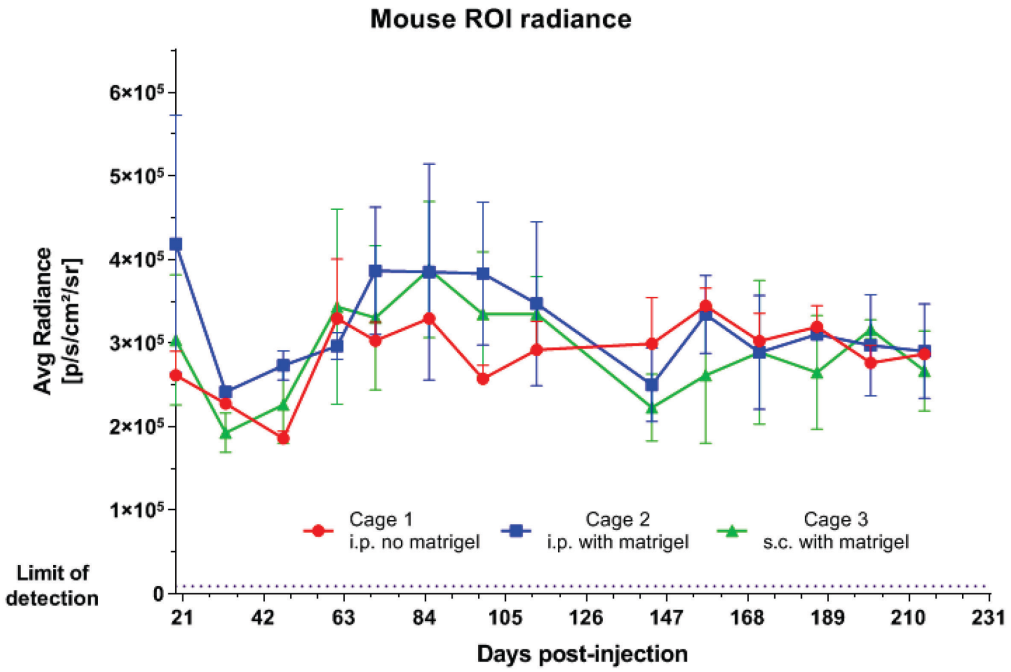

Figure 4.3 - Bioluminescent signal from KGN-luc rebounded slightly from day 47 - day 85 then slowly degraded. Mice were regularly monitored using an IVIS Spectrum imager. Mice were injected with 10 µL 15 mg/mL luciferase per gram of weight and imaged over a 20-minute period. Values represent average peak radiance per cage +/- SEM.

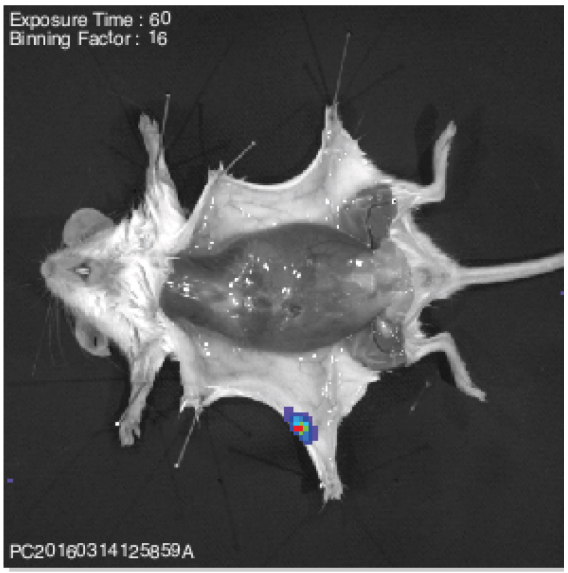

Figure 4.4 - Localized bioluminescent signal did not reveal macroscopic disease. A subcutaneously-injected mouse displaying the strongest signal on day 206 was dissected to determine whether a tumour nodule had actually developed.

It was reported by Imai, *et al.*, that advanced passage KGN cells were more aggressive than early passage KGN [64]. Furthermore, they reported that both early (p7) and advanced passage (p58) cells injected s.c. generated metastatic tumours in the bowel of BALB/c $^{Foxn1/Foxn1}$ nude mice. The advanced passage cells were reported to develop metastatic tumours faster than early passage cells, with more nodules, but the size of nodules in each model were similar. There was no mention of primary tumour development. For the second experiment we generated advanced passage (p 86) KGN-luc cells. We observed, qualitatively, that advanced passage KGN-luc cells did proliferate more quickly *in vitro* than low passage cells. Low passage ($p < 20$) KGN-luc cells generally required 6-8 days to become confluent following a 1:8 split during tissue culture, whereas advanced passage (> p 70) cells became confluent 3 -4 days following a 1:8 split.

With advanced passage KGN-luc cells, six (6) female NSG mice were injected either s.c. (3 mice) or i.p. (3 mice) with 5×10^7 KGN-luc cells in PBS with 50% Matrigel. Imaging was carried out weekly until day 36, after which imaging was reduced to biweekly due to the flat-lining of signal at or near background levels. Unlike the initial animal experiment involving KGN-luc, there was no recovery of bioluminescent signal at or around 47 days, and lack of any indication of tumour growth, by palpation of s.c.-injected mice and imaging (Figures 4.5 and 4.6), led to the mice being euthanized at day 106 and dissected. No macroscopic disease was detected in either i.p. or s.c. injected mice, and nothing unusual was seen in the bowels of dissected mice. Unlike the findings reported by Imai, *et al.*, we did not see the faster

proliferation, *in vitro*, of advanced passage KGN-luc translate into more aggressive tumour cells *in vivo*.

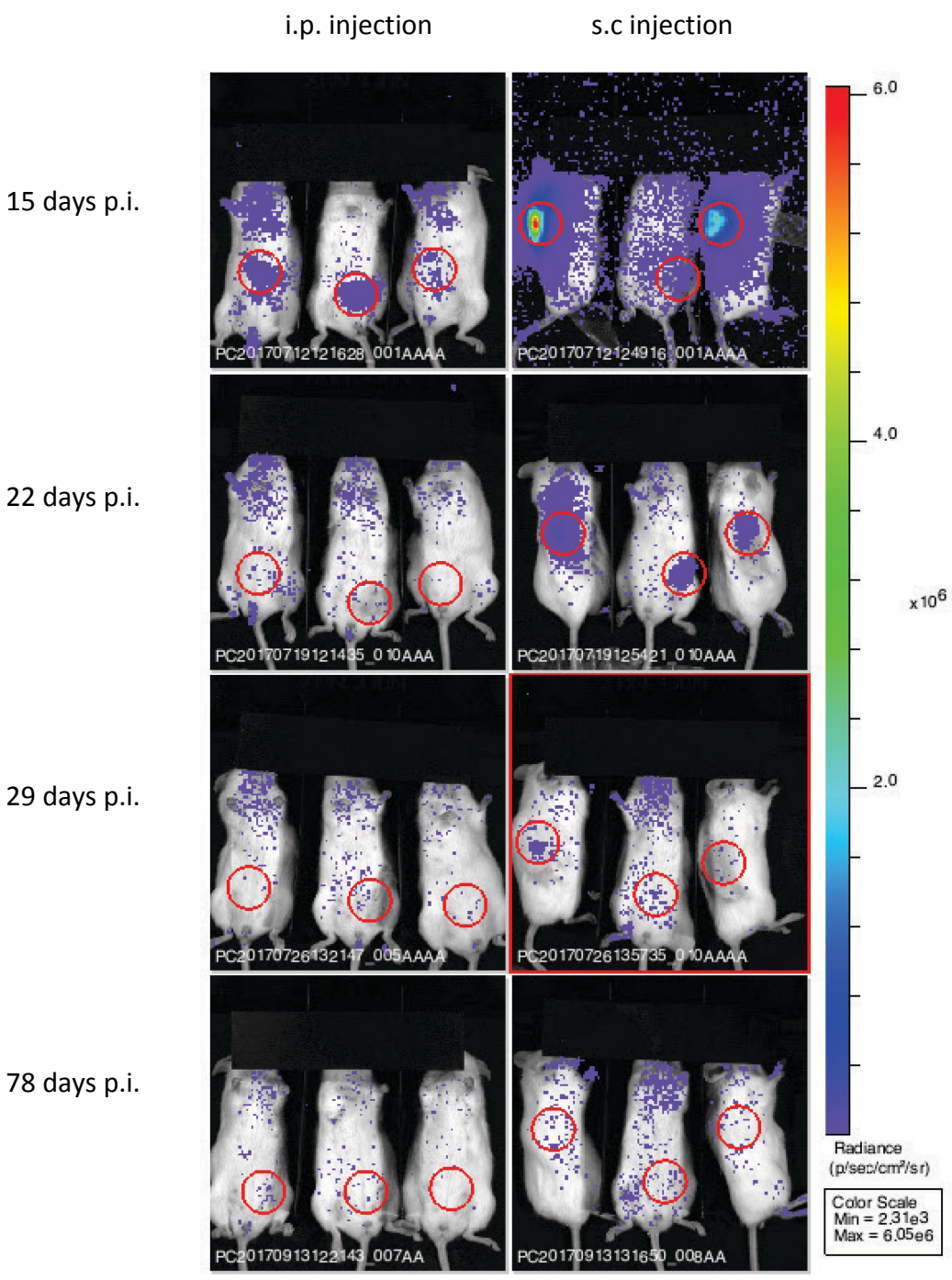

Figure 4.5 – Advanced passage KGN-luc tumour model failed to develop in NSG mice. 5 x 10^7 KGN-luc cells in matrigel were injected into female NSG mice (three mice i.p. and three mice s.c.) and monitored by IVIS imaging over 106 days. Images show the loss in luciferase signal over the study period. Radiance measured as photons/sec/cm^2/steradian. The regions of interest (ROI) are circled in red.

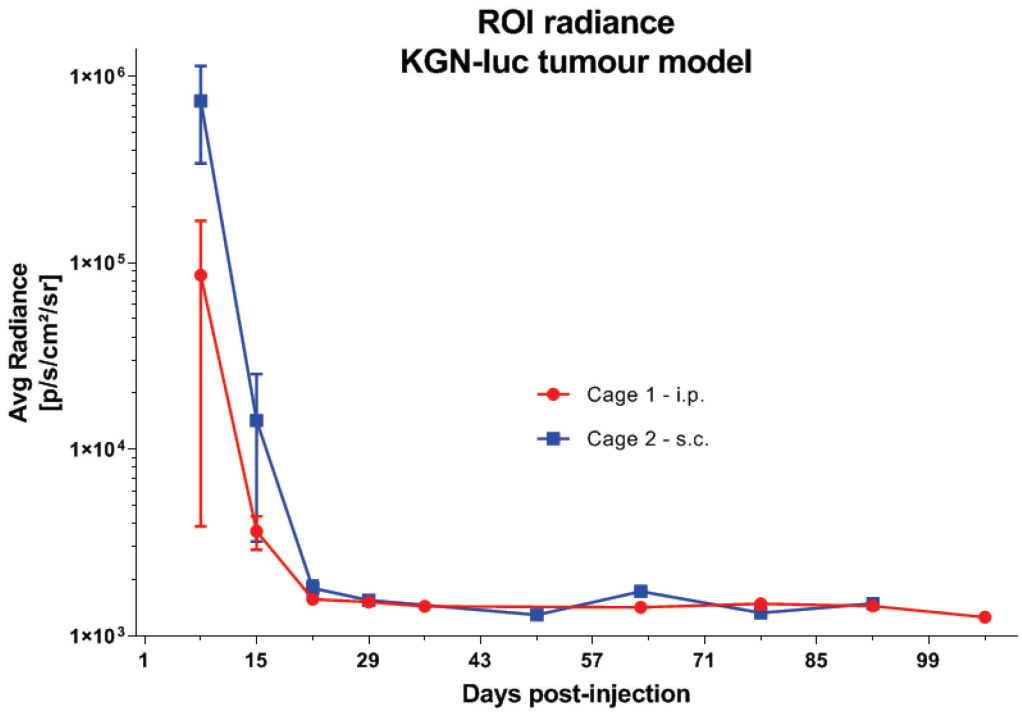

Figure 4.6 - Signal from implanted advanced passage KGN-luc cells deteriorated rapidly following injection into mice. Quantification of bioluminescent signal measured by IVIS imaging. Regions of interest are defined in Figure 4.2.

4.3.3 KGN-Runx3 tumour model in NSG mice

Runt-related transcription factor RUNX3 is present in normal granulosa cells of mice and regulates folliculogenesis and steroidogenesis [184, 185]. It was found to be highly expressed in an ovarian stromal cell tumour (COV434), but is absent in the GCT cell line KGN [183]. One study showed RUNX3 is silenced in KGN cells due to promoter methylation [186]. Re-expression of RUNX3 promotes cell proliferation, anchorage-independent growth, and motility in KGN cells *in vitro* so we wanted to see whether RUNX3 overexpression could increase proliferation of KGN cells in vivo [183].

To determine whether RUNX3 promotes formation of KGN tumours in a mouse xenograft model, we injected KGN-Vector and KGN-Runx3 cells s.c. in the flanks of female NSG mice and monitored tumour formation twice a week by palpation for 185 days. Interestingly, four out of six injections of KGN-Runx3 cells, but none of the six KGN-Vector injections, formed small tumours (Figure 4.7). We then dissociated tumours into single cells and expanded them in culture. Cells from all four tumours proliferated well in culture and displayed the same morphology as regular KGN cells. Huachen Chen (in the lab of Dr. YangXin Fu, University of Alberta) confirmed that these tumour-derived cells were indeed KGN-Runx3 cells by the expression of RUNX3-FLAG as determined by Western blotting using a RUNX3 specific antibody or an anti-FLAG antibody (Figure 4.7C), as well as by qRT-PCR using primers specific to human RUNX3 (Table 4.2) [183]. These results suggest that expression of RUNX3 increases the capacity of KGN cells to form tumours in mice.

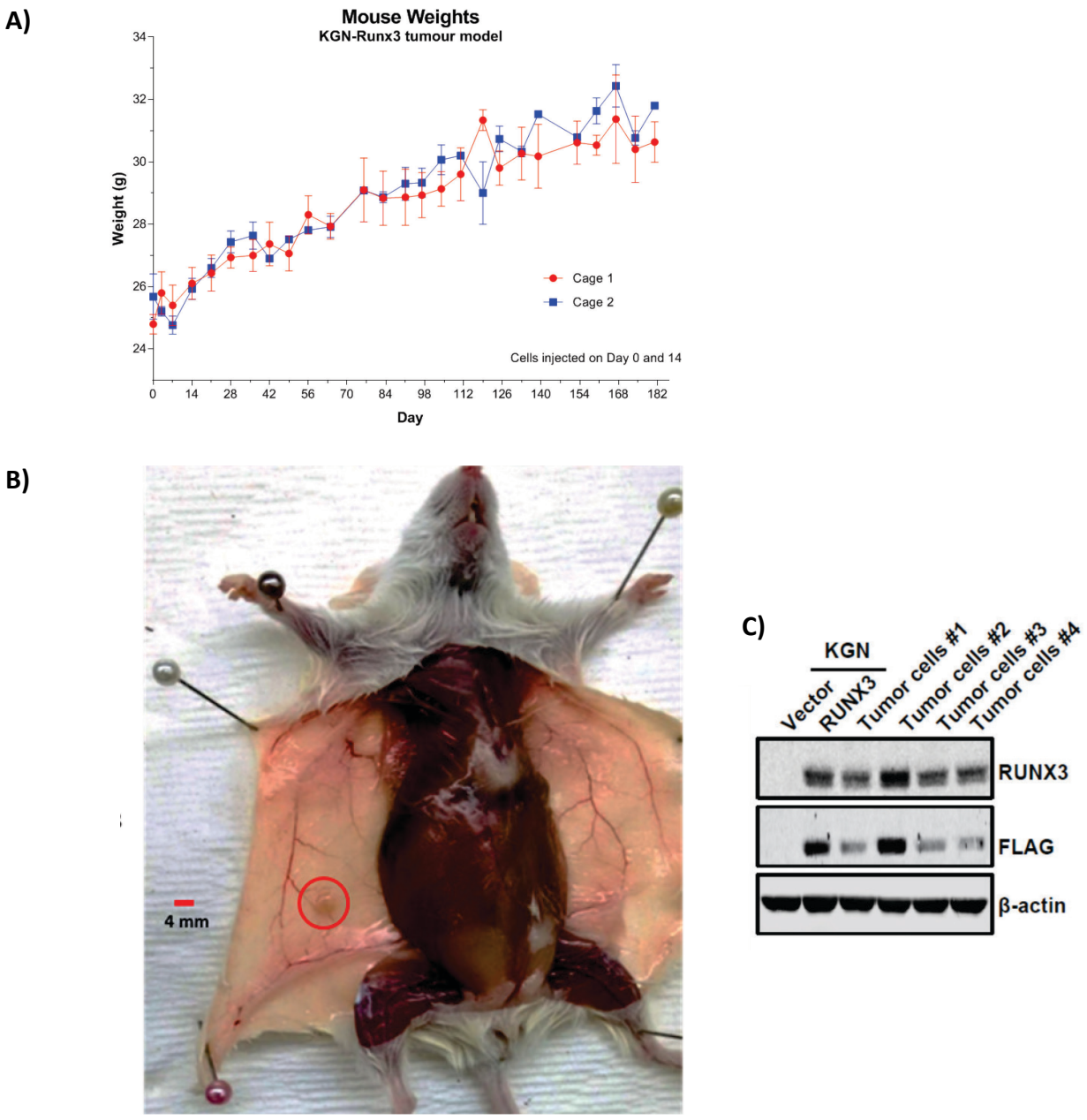

Figure 4.7 - KGN-Runx3-transformed cells generate small lesions in female NSG mice. (A) Distribution of mouse weights during the study period. **(B)** Representative image of mouse showing establishment of localized lesion at the site of KGN-Runx3 s.c. injections. Four of six mice had lesions on the Runx3 flank while none had lesions on the contralateral KGN-Vector-injected flank. **(C)** Western blot shows dissociated tissue from harvested tumours display both human Runx3 and Flag expression.

Table 4.2 - RUNX3 is strongly expressed in cultured tumour cells recovered from KGN-RUNX3 tumour model.

Cells	Fold-change in RUNX3 expression relative to KGN-Vector cells (empty vector)
KGN-Vector cells	1.0
KGN-RUNX3 cells	19619
KGN-RUNX3 tumour cells	22693

4.4 Discussion

Animal models are an essential component of cancer research as both the U.S. Food and Drug Administration (FDA) and Health Canada require animal tests before allowing human use of new drugs [187]. The purpose of these models is not just to assess the effectiveness of a proposed therapeutic, but also to gain insight into other areas of concern such as route of administration, potential reaction at the site of administration, and pharmacokinetics of a new agent. Appropriate model selection should be based on relevance of the model to the reality of human disease.

While there are at least 10 spontaneous or genetically-engineered tumour models for GCT, none of them are known to carry the FOXL2^{C134W} signature mutation found in AGCT [153]. Because the FOXL2 mutation is so prevalent in AGCT, and continues to be present in recurrent disease, we wanted to establish a xenograft animal model for testing our VACV^{TRAIL}/PAC-1 combination therapy that was based on KGN cells, which are known to carry the FOXL2 mutation. An early attempt by our lab to implant KGN cells in female NIH III mice had not been successful (Table 4.3).

Table 4.3 - Summary of animal experiments

Cell line	Mouse strain	Cells injected	Injection site	Result	Endpoint
KGN [a]	NIH-III	5 x 10^6	s.c. & i.p. no matrigel	No tumours	93 days
KGN-*luc* [a]	NSG	1 x 10^7	s.c. & i.p. +/- matrigel	No tumours	214 days
KGN-*luc* [b]	NSG	5 x 10^7	s.c. & i.p. +/- matrigel	No tumours	106 days
KGN-*Runx3* or KGN-empty vector [c, d]	NSG	2 x 10^7 (x2)	s.c. + matrigel	4 of 6 *Runx3* mice had small tumours	185 days
Notes:	a – Experiment conducted prior to start of Masters project b – The cells were advanced passage (p 86) c – KGN-*Runx3* and empty vector cells were injected into opposite flanks d – cells were injected twice, 14 days apart				

In order to facilitate *in vivo* monitoring of tumour development, we transformed KGN cells with firefly luciferase (KGN-luc) to enable bioluminescence imaging of the animals. For our initial experiment we injected female NSG mice, which are more immune-compromised than NIH III mice, with what we thought was a large number (1 x 10^7) of KGN-luc cells both i.p. and s.c. with Matrigel; and i.p. into a small cohort of mice without Matrigel. The KGN-luc did allow us to monitor the mice with bioluminescence imaging, but at endpoint no tumour was detected in any mice even though the s.c. mice showed a localized bioluminescent signal. For the next experiment, we injected a larger number (5 x 10^7) of late passage KGN-luc cells in Matrigel either i.p. or s.c. into female NSG mice. The late passage cells had a significantly higher growth rate than the KGN cells we had used in the previous experiment. We hypothesized that the higher cell count and faster growth rate combined with an initial supporting matrix of Matrigel would give KGN-luc cells the best opportunity to survive and then proliferate. We found that

while initial bioluminescent signal was strong and localized, it dissipated and fell to near background levels within 60 days. At 106 days post-injection the mice were euthanized and no macroscopic disease was detectable in either the i.p. or s.c. cohorts.

Next we made an attempt to increase the chance of *in vivo* KGN proliferation using cells we received from Dr. YangXin Fu, who had transformed KGN cells with runt-related transcription factor RUNX3 (KGN-Runx3) or an empty vector (KGN-Vector) RUNX3 is known to be oncogenic in ovarian cancer but is silenced in KGN cells [183]. Using female NSG mice, we injected 2 x 10^7 KGN-Runx3 cells in Matrigel into one flank and an equal number of KGN-Vector cells in Matrigel into the contralateral flank. Two weeks later we repeated the injections into the same location similar to the procedure used in another published study [66]. Our thought was that the initial injection would condition the local environment and increase the chances of establishing a tumour when the second injection of cells was made. After 180 days there was no sign of disease by palpation and the mice were euthanized. We found, however, that 4 of 6 mice had flat, small (4 mm diameter) lesions on the side injected with KGN-Runx3 and none of the KGN-Vector-injected sites had lesions. We dissociated tissue from the sites and cultivated them through five passages. Their gross morphology was similar to KGN, and both western blot and qRT-PCR assessment of the cells confirmed expression of human RUNX3. These cells (KGN-RUNX3F1) could serve as the starting point to attempt serial passaging in mice in order to boost their tumourigenicity.

CHAPTER 5. DISCUSSION AND FUTURE DIRECTIONS

5.1 Summary and key findings

Ovarian cancer, in general, is the fifth-leading cause of death among women [188]. Granulosa cell tumour (GCT) is a rare, sex-cord stromal cell ovarian cancer that is generally categorized as low malignant potential, but is known for late recurrence. Women who do relapse will die of disease 80% of the time [16]. This thesis has investigated the novel combination of a small-molecule activator of CASP3 (PAC-1) with an apoptosis-inducing ligand (TRAIL) as a potential therapy for GCT. CASP3 is the primary effector of apoptosis and begins proteolytic cleavage of substrates once it is activated. TRAIL is a transmembrane protein that acts as a ligand for DR4 and DR5, which induce the extrinsic apoptotic pathway ending with CASP3 activation. We tested the hypothesis that treating GCT with PAC-1 would 'prime' CASP3 for death signaling induced by administration of TRAIL, resulting in increased killing of GCT cells. Furthermore, this project examined whether a recombinant, oncolytic vaccinia virus that encodes TRAIL could successfully operate as gene therapy in order to overcome some of the documented inefficiencies in the clinical use of TRAIL. We have made significant contributions to preclinical research on treatment of GCT including the first report of using oncolytic virus for GCT, and in the use of oncolytic VACV as a vector for gene therapy.

5.1.1 Combination of PAC-1 with TRAIL for treatment of GCT

We sought to investigate a different approach in the treatment of GCT by using PAC-1 as a sensitising agent in combination with TRAIL to induce apoptosis. Initially we wanted to see whether PAC-1, itself, could be an effective agent in GCT. Using different cell lines with differing levels of CASP3 expression we found that loss of viability in the presence of PAC-1 did tend to

increase with increasing levels of CASP3. With respect to other apoptosis-inducing agents, we found GCT model cell line KGN less sensitive to carboplatin, gemcitabine, and TRAIL, but very sensitive to embelin. Embelin is a SMAC-mimetic that inhibits XIAP, which in turn is an inhibitor of CASP3 [156-158]. KGN appears therefore to be more sensitive to single agents that have direct interaction with CASP3 than to agents that depend on inducing CASP3-driven apoptosis through signaling pathways.

To look at potential benefit from drug combination we paired PAC-1 with each of the other agents and calculated a measure of drug synergy for each combination. While overall loss of viability was not striking when combining PAC-1 with carboplatin or gemcitabine, the combined effect did display weak synergy. Embelin, on the other hand, was effective at reducing viability with PAC-1 but the combination shows an antagonistic relationship for reasons that don't seem obvious. TRAIL displayed a strong synergistic relationship with PAC-1 and the combination was very effective at reducing viability of KGN cells. We also found that normal cells were much less sensitive to PAC-1/TRAIL combination in keeping with published reports on the safety of PAC-1 and TRAIL individually. The PAC-1/TRAIL synergy allowed us to select a low dose of TRAIL (10 ng/mL) to combine with a clinically relevant dose of PAC-1 (20 μM) for more detailed assessment.

First we looked to understand the kinetics of combining PAC-1 and TRAIL through time-course measurement of CASP3 activation. Caspase activation is required to initiate apoptosis and we knew from endpoint measurements that low-dose TRAIL with PAC-1 was effective, but what was dramatic was how rapid the increase in CASP3 activity was compared to agents alone.

It confirmed the synergy that exists between PAC-1 and TRAIL and offers interesting scenarios as to what might be happening. As single agents PAC-1 and TRAIL are less effective at directly activating CASP3 enzymatic activity. Perhaps PAC-1 prepares CASP3 for activation but is not inducing immediate auto-cleavage, and TRAIL is inducing death signals but CASP3 is inhibited by either Zn^{2+} ions or XIAP. In combination, we hypothesize that as PAC-1 primes CASP3 to a ready-state, TRAIL sends the signal to spark CASP3 activity.

With the lack of animal models expressing the FOXL2^{C134W} mutation we looked at using patient-derived tissue as an indicator of clinical relevance. Using a similar dose level with PAC-1 and TRAIL we treated four patient samples (two primary and two recurrent disease). Our *in vitro* work with KGN suggested that it may take ~24 h for PAC-1 to start having optimal effect, so for this experiment the TRAIL was added 24 h after PAC-1. The results were consistent with the KGN-based assays in terms of the superiority of PAC-1/TRAIL combination and suggested that recurrent disease may be as, or more, susceptible as primary disease, although only CASP3 activity showed statistical significance. The possibility that recurrent disease may be more sensitive to PAC-1/TRAIL is intriguing because it is recurrent disease that represents the challenge for women diagnosed with GCT.

TRAIL is a well-documented agent and is often used in drug combinations *in vitro*, although it has been less than effective in clinical trials [114] due to inherent or developed resistance to TRAIL, a short half-life, and ineffective dosing at the tumour site. Even so, during a phase I clinical trial of a monoclonal antibody targeting death receptor 5, an early-cohort patient with GCT was one of only a few patients showing some response to treatment [189] and

circulating TRAIL has been found to be reduced in patients with large GCTs and correlates inversely with tumour size suggesting TRAIL may represent a therapeutic target [124]. We have found that it is possible to dramatically increase the ability of TRAIL to induce apoptosis in GCT by sensitising the cells with PAC-1, which we propose is priming CASP3 for activation by TRAIL-induced death signaling. This could be a strategy for overcoming reported limitations in the clinical use of TRAIL because this result is achieved at very low dose levels, far below what has been used in clinic.

5.1.2 TRAIL-expressing VACV as a gene therapy vector

VACV possesses many key attributes necessary for an ideal viral backbone to be used in oncolytic viral gene therapy. These include a short lifecycle, rapid cell-to-cell spread, strong lytic ability, a large cargo capacity, and well-defined molecular biology. It has previously been shown that VACV tumour selectivity is increased by the deletion of the viral J2R gene that encodes thymidine kinase (TK), making the virus dependent on the cellular TK that is up-regulated in proliferating cancer cells [147, 148, 159, 160]. It has also been shown that additional disruption of viral ribonucleotide reductase (RR) increases the safety profile of VACV without negatively impacting viral replication in cancer cells [145, 147, 161, 162]. TRAIL has been known to be a tumour-selective, apoptotic-inducing compound since its initial discovery in 1995 [176]. While many studies have shown soluble TRAIL to have great effect *in vitro*, that success has not translated to the clinic where several limitations have appeared including a short half-life and ready clearance by the body, resulting in difficulty achieving therapeutic dosing at tumour sites [177]. One avenue for attempting to increase effectiveness is through gene therapy where the TRAIL gene would be delivered directly to the tumour cell. Multiple vectors have been

proposed as means for delivering TRAIL to the site of tumours [117, 120, 167, 168]. Each study reports some measure of success against the particular cancer they were treating, although each has its own limitations, also. For example, Ziauddin, *et al.*, reported successful combination of a full-length TRAIL-expressing poxvirus with oxaliplatin, but did not identify or propose what the mechanism might be that sensitizes oxaliplatin-treated cells to TRAIL [167]. Kim, *et al.*, meanwhile, proposed a replication-deficient adenovirus to deliver secretable TRAIL, but with a potential requirement for 100 pfu/cell it may not be directly translatable to the clinic [120].

We pursued developing an alternative means of delivering TRAIL by encoding a synthetic gene for secretion of soluble TRAIL into the genome of an oncolytic vaccinia virus, which our lab has shown through other research has high selectivity for cancer cells and has an excellent safety profile *in vivo* [145]. Our unique design combined the extracellular domain of human TRAIL with an isoleucine zipper, a Furin cleavage site, the promoter for human Fibrillin-1, and a synthetic viral early/late promoter. We called this recombinant virus VACV^{TRAIL} and we proposed that in light of our results showing synergy between rhTRAIL and PAC-1 *in vitro*, we would expect to see beneficial effect from the combination of VACV^{TRAIL} with PAC-1.

We evaluated the ability of VACV^{TRAIL} to replicate in, and reduce viability of, KGN cells, and compared that to results using VACV^{TRAIL} in the presence of PAC-1. We found that VACV^{TRAIL} replication was moderated in the presence of PAC-1, but loss of viability by KGN cells was enhanced by the combination. This may be due to apoptotic activity induced by expression of TRAIL from infected cells overcoming a reduced replication rate. Thus, the reduction in virus

replication does not have a negative impact on the ability of VACV^{TRAIL} to kill tumour cells when combined with PAC-1.

Finally, we wanted to confirm that TRAIL is being secreted by VACV^{TRAIL}-infected cells, and that it is an active cytotoxic agent. We collected supernatant from infected KGN cells, measured TRAIL concentrations with an AlphaLISA assay, and then used the supernatant in cytotoxicity assays combined with PAC-1. The synergy between PAC-1 and secreted TRAIL was significant and inhibition of CASP8 (the initiator caspase in the extrinsic apoptotic pathway) was able to eliminate any cytotoxicity from PAC-1/TRAIL combination beyond the effect of PAC-1 alone, which confirmed that the secreted TRAIL is inducing the extrinsic apoptotic pathway.

5.1.3 Establishment of a xenograft model for GCT

While there are at least 10 spontaneous or genetically-engineered tumour models for GCT, none of them are known to carry the FOXL2^{C134W} signature mutation found in AGCT [153]. Because the FOXL2 mutation is so prevalent in AGCT, and continues to be present in recurrent disease [41], we wanted to establish a xenograft animal model for testing our VACV^{TRAIL}/PAC-1 combination therapy using KGN or KGN-derived cells, which are known to carry the FOXL2 mutation. An earlier attempt by our lab to implant KGN cells in female NIH III mice had not been successful.

In order to facilitate monitoring of tumour development, we transformed KGN cells with firefly luciferase (KGN-luc) to enable bioluminescent imaging of the animals, and utilized them for a pair of animal experiments. At first we injected 1 x 10^7 KGN-luc cells into mice combined with an initial supporting matrix of Matrigel to give the cells the best opportunity to survive and proliferate. The bioluminescent signal from IVIS imaging initially dipped before showing a brief

rebound, but after 214 days p.i. we could not detect any s.c. tumour development even though IVIS imaging showed localized bioluminescence in at least one animal. We saw no evidence of disease when that animal was dissected, leading us to hypothesize that perhaps at least some of the KGN-luc cells were still viable but dormant or senescent. We further postulated that a higher number of initially-injected cells would increase the possibility of a successful graft so for the second experiment we injected female NSG mice with 5 x 10^7 KGN-luc cells with Matrigel. We found that while initial bioluminescent signal was strong and localized as in the first experiment, it dissipated rapidly and fell to near background levels within 60 days. At 106 days p.i. the mice were euthanized and no macroscopic disease was detectable in either the i.p. or s.c. cohorts.

Next we made an attempt to increase the chance of *in vivo* KGN proliferation using cells we received from Dr. YangXin Fu, who had transformed KGN cells with runt-related transcription factor RUNX3 (KGN-Runx3) or an empty vector (KGN-Vector). Using female NSG mice, we injected 2 x 10^7 KGN-Runx3 cells in Matrigel into one flank and an equal number of KGN-Vector cells in Matrigel into the contralateral flank. Two weeks later we repeated the injections into the same location. Our thought was that the initial injection would condition the local environment and increase the chances of establishing a tumour when the second injection of cells was made, but after 180 days there was no sign of disease by palpation and the mice were euthanized. We found, however, that 4 of 6 mice had flat, small (4 mm diameter) lesions on the side injected with KGN-Runx3 and none of the KGN-Vector-injected sites had lesions. While small (~32 mm^3), these lesions were actually larger than those reported by Kim, *et al.*,

who had used a similar strategy for implanting KGN cells into Balb/c nude mice [66]. We dissociated tissue from the lesions categorized this resulting cell line as KGN-RUNX3F1.

While the length of time required to establish a tumour of that size is currently not ideal from the standpoint of testing potential therapeutics, the establishment of a human GCT CDX in this mouse model does show that it is possible and provides a baseline for continuing to develop the platform. We continue to look at possibilities for increasing KGN's proliferation rate *in vivo*.

5.2 Future directions

5.2.1 Establish a xenograft animal model for testing VACV^{TRAIL} combined with PAC-1

While a xenograft model of GCT has not been wholly successful so far, we continue to look for ways to improve the chances for a KGN CDX model to proliferate *in vivo* because it would present us with an opportunity to assess how FOXL2^{C134W}-mutant GCT responds to VACV^{TRAIL} and PAC-1. One possibility is to attempt serial passage of KGN-RUNX3F1 in mice. If tumours develop following implantation, they would subsequently be implanted into new cohorts of mice in an attempt to serially increase their aggressiveness. It is reported that PDX models of cancer develop increased aggressiveness when maintained by serial passage in immunocompromised mice with no change in gene expression profile [190]. We would hope that KGN-RUNX3F1 would see a concomitant increase in aggressiveness through serial passaging in mice.

A second approach we are considering is establishing a KGN-based cell line that overexpresses Activin A. Clinical experience has shown that overexpression of Activin A is linked with worse prognosis in several cancers [191] and activin expression is known to enhance

ovarian follicle development. In fact, GCT has been shown to have a high activin A to inhibin A ratio, while the FOXL2^{C134W} mutation is thought to suppress follistatin leading to the loss of activin antagonism, and increased cell proliferation [191, 192]. We propose to transduce KGN cells to overexpress activin A and try to establish a CDX model in a fashion similar to what was used to generate KGN-RUNX3F1 cells.

5.2.2 Generate a genetically-modified syngeneic model of GCT

Thirdly, we will need to assess the effectiveness of VACV^{TRAIL} and PAC-1 in immunocompetent mice, both from the perspective of treatment efficacy and determining how the immune system might respond to VACV^{TRAIL} infection. We know from other research in our lab that VACV ΔF4LΔJ2R is both effective and tolerated in multiple immunocompetent animal models [145] and we would fully expect that VACV^{TRAIL} would mirror that performance profile. We plan to test VACV^{TRAIL} using an oocyte-driven PIK3CA* mouse model that generates bilateral GCT [153, 193]. This model also overexpresses activin A, supporting the points raised above about activin overexpression and development of GCT. This immunocompetent model will allow us to investigate how the virus holds up following administration, and whether we are able to induce a tumour-specific immune response in vivo.

5.3 Conclusions

Even though it is rare, GCT strikes 1,000s of young girls and women world-wide every year and ~40% of them will relapse. Current therapies are not effective enough in controlling recurrent disease which means there is a need for innovative treatments that will not also bring a burden of off-target toxicity. PAC-1 is a novel small-molecule compound that has shown itself to be effective in the treatment of several cancers both *in vitro* and *in vivo*, is currently in

clinical trials, and has shown very little toxicity, to date. To the best of our knowledge, this thesis represents the first report combining PAC-1 with TRAIL as a therapeutic strategy, and the first report combining oncolytic vaccinia virus gene therapy with PAC-1. We have shown that GCT is vulnerable to agents that act proximal to CASP3 in apoptotic pathways and that drug synergy between PAC-1 and TRAIL allows for treatment of disease at lower doses of each compound than might otherwise be required in-clinic. We also showed that a recombinant oncolytic vaccinia virus can be effective in use as a gene therapy vector and deliver TRAIL directly to tumour cells at therapeutic dose levels, *in vitro*. Finally, we have shown that GCT model cell line KGN can be altered through transfection with RUNX3, which acts as an oncogene in ovarian cancer, to improve proliferation of KGN cells *in vivo*, although there is still much work to be carried out to fully establish this as an animal model for treatment of GCT. The novel combination of two compounds that have individually displayed low toxicity in clinical trials, with oncolysis by VACV, which also has an established safety record, appears very effective *in vitro* against a disease that currently has few effective alternatives for women who relapse. This represents a potential solution that is strongly worthy of further preclinical development with no reason that it could not be expanded to look at being used for many cancers.

References

[1] D.R. Liston, M. Davis, Clinically Relevant Concentrations of Anticancer Drugs: A Guide for Nonclinical Studies, Clin Cancer Res, 23 (2017) 3489-3498.

[2] D.B. Gammon, B. Gowrishankar, S. Duraffour, G. Andrei, C. Upton, D.H. Evans, Vaccinia virus-encoded ribonucleotide reductase subunits are differentially required for replication and pathogenesis, PLoS Pathog, 6 (2010) e1000984.

[3] J.C. Soria, E. Smit, D. Khayat, B. Besse, X. Yang, C.P. Hsu, D. Reese, J. Wiezorek, F. Blackhall, Phase 1b study of dulanermin (recombinant human Apo2L/TRAIL) in combination with paclitaxel, carboplatin, and bevacizumab in patients with advanced non-squamous non-small-cell lung cancer, J Clin Oncol, 28 (2010) 1527-1533.

[4] A. Birmingham, L.M. Selfors, T. Forster, D. Wrobel, C.J. Kennedy, E. Shanks, J. Santoyo-Lopez, D.J. Dunican, A. Long, D. Kelleher, Q. Smith, R.L. Beijersbergen, P. Ghazal, C.E. Shamu, Statistical methods for analysis of high-throughput RNA interference screens, Nat Methods, 6 (2009) 569-575.

[5] G.Y. Di Veroli, C. Fornari, D. Wang, S. Mollard, J.L. Bramhall, F.M. Richards, D.I. Jodrell, Combenefit: an interactive platform for the analysis and visualization of drug combinations, Bioinformatics, 32 (2016) 2866-2868.

[6] Canadaian Cancer Society, Ovarian cancer statistics, 2018.

[7] S. Jamieson, P.J. Fuller, Molecular pathogenesis of granulosa cell tumors of the ovary, Endocrine reviews, 33 (2012) 109-144.

[8] S.T. Schumer, S.A. Cannistra, Granulosa cell tumor of the ovary, J Clin Oncol, 21 (2003) 1180-1189.

[9] C.V. Rokitansky, Uber abnormalitiaten des corpus luteum, Allg Wien Med Z, (1859) 253-258.

[10] S. Bryk, A. Farkkila, R. Butzow, A. Leminen, M. Heikinheimo, M. Anttonen, A. Riska, L. Unkila-Kallio, Clinical characteristics and survival of patients with an adult-type ovarian granulosa cell tumor: a 56-year single-center experience, Int J Gynecol Cancer, 25 (2015) 33-41.

[11] G. Ohel, H. Kaneti, J.G. Schenker, Granulosa cell tumors in Israel: a study of 172 cases, Gynecol Oncol, 15 (1983) 278-286.

[12] L. Unkila-Kallio, A. Leminen, A. Tiitinen, O. Ylikorkala, Nationwide data on falling incidence of ovarian granulosa cell tumours concomitant with increasing use of ovulation inducers, Hum Reprod, 13 (1998) 2828-2830.

[13] E. Bjorkholm, C. Silfversward, Granulosa- and theca-cell tumors. Incidence and occurrence of second primary tumors, Acta Radiol Oncol, 19 (1980) 161-167.

[14] N. Kalfa, R.A. Veitia, B.A. Benayoun, B. Boizet-Bonhoure, C. Sultan, The new molecular biology of granulosa cell tumors of the ovary, Genome Med, 1 (2009) 81.

[15] A. Koul, S. Malander, N. Loman, T. Pejovic, S. Heim, R. Willen, O. Johannsson, H. Olsson, M. Ridderheim, A.A. Borg, BRCA1 and BRCA2 mutations in ovarian cancer: Covariation with specific cytogenetic features, Int J Gynecol Cancer, 10 (2000) 289-295.

[16] S. Jamieson, P.J. Fuller, Management of granulosa cell tumour of the ovary, Curr Opin Oncol, 20 (2008) 560-564.

[17] M.A. Edson, A.K. Nagaraja, M.M. Matzuk, The mammalian ovary from genesis to revelation, Endocrine reviews, 30 (2009) 624-712.

[18] K.A. Schultz, A.K. Harris, D.T. Schneider, R.H. Young, J. Brown, D.M. Gershenson, L.P. Dehner, D.A. Hill, Y.H. Messinger, A.L. Frazier, Ovarian Sex Cord-Stromal Tumors, J Oncol Pract, 12 (2016) 940-946.

[19] M.K. Wilson, P. Fong, S. Mesnage, K. Chrystal, A. Shelling, K. Payne, H. Mackay, L. Wang, S. Laframboise, M. Rouzbahman, W. Levin, A.M. Oza, Stage I granulosa cell tumours: A management conundrum? Results of long-term follow up, Gynecol Oncol, 138 (2015) 285-291.

[20] A.J. Jacobs, G. Deppe, C.J. Cohen, Combination chemotherapy of ovarian granulosa cell tumor with cis-platinum and doxorubicin, Gynecologic oncology, 14 (1982) 294-297.

[21] J.T. Stenwig, J.T. Hazekamp, J.B. Beecham, Granulosa cell tumors of the ovary. A clinicopathological study of 118 cases with long-term follow-up, Gynecol Oncol, 7 (1979) 136-152.

[22] H.D. Sun, H. Lin, M.S. Jao, K.L. Wang, W.S. Liou, Y.C. Hung, Y.C. Chiang, C.H. Lu, H.C. Lai, M.H. Yu, A long-term follow-up study of 176 cases with adult-type ovarian granulosa cell tumors, Gynecol Oncol, 124 (2012) 244-249.

[23] A. Hammer, F.F. Lauszus, A.C. Petersen, Ovarian granulosa cell tumor and increased risk of breast cancer, Acta Obstet Gynecol Scand, 92 (2013) 1422-1425.

[24] B.-S. Huang, H.-D. Sun, Y.-M. Hsu, W.-H. Chang, H.-C. Horng, M.-S. Yen, K.-C. Chao, S.-L. Edmond Hsieh, P.-H. Wang, Clinical presentation and outcome of adult-type granulosa cell tumors: A retrospective study of 30 patients in a single institute, Journal of the Chinese Medical Association, 77 (2014) 21-25.

[25] S.L.P. Regan, P.G. Knight, J.L. Yovich, Y. Leung, F. Arfuso, A. Dharmarajan, Granulosa Cell Apoptosis in the Ovarian Follicle-A Changing View, Front Endocrinol (Lausanne), 9 (2018) 61.

[26] N. Colombo, G. Parma, V. Zanagnolo, A. Insinga, Management of ovarian stromal cell tumors, J Clin Oncol, 25 (2007) 2944-2951.

[27] P.H. Wang, H.D. Sun, H. Lin, K.L. Wang, W.S. Liou, Y.C. Hung, Y.C. Chiang, C.H. Lu, H.C. Lai, T.C. Chang, G. Taiwanese Gynecologic Oncology, Outcome of patients with recurrent adult-type granulosa cell tumors--a Taiwanese Gynecologic Oncology Group study, Taiwan J Obstet Gynecol, 54 (2015) 253-259.

[28] H. Wu, S.A. Pangas, K.W. Eldin, K.R. Patel, J. Hicks, J.E. Dietrich, R. Venkatramani, Juvenile Granulosa Cell Tumor of the Ovary: A Clinicopathologic Study, J Pediatr Adolesc Gynecol, 30 (2017) 138-143.

[29] G. Calaminus, R. Wessalowski, D. Harms, U. Gobel, Juvenile granulosa cell tumors of the ovary in children and adolescents: results from 33 patients registered in a prospective cooperative study, Gynecol Oncol, 65 (1997) 447-452.

[30] L. Ma, L. Zhang, Y. Zhuang, Y. Ding, J. Chen, A rare case report of ovarian juvenile granulosa cell tumor with massive ascites as the first sign, and review of literature: Case report and review of literature, Medicine (Baltimore), 97 (2018) e10916.

[31] L. Bessiere, A.L. Todeschini, A. Auguste, S. Sarnacki, D. Flatters, B. Legois, C. Sultan, N. Kalfa, L. Galmiche, R.A. Veitia, A Hot-spot of In-frame Duplications Activates the Oncoprotein AKT1 in Juvenile Granulosa Cell Tumors, EBioMedicine, 2 (2015) 421-431.

[32] F. Zangeneh, V.C. Kelley, Granulosa-theca-cell tumor of the ovary in children, Am J Dis Child, 115 (1968) 494-508.

[33] A.M. Dorward, K.L. Shultz, L.G. Horton, R. Li, G.A. Churchill, W.G. Beamer, Distal Chr 4 harbors a genetic locus (Gct1) fundamental for spontaneous ovarian granulosa cell tumorigenesis in a mouse model, Cancer research, 65 (2005) 1259-1264.

[34] C. Zaloudek, H.J. Norris, Granulosa tumors of the ovary in children: a clinical and pathologic study of 32 cases, Am J Surg Pathol, 6 (1982) 503-512.

[35] R.H. Young, G.R. Dickersin, R.E. Scully, Juvenile granulosa cell tumor of the ovary. A clinicopathological analysis of 125 cases, Am J Surg Pathol, 8 (1984) 575-596.

[36] B.A. Benayoun, N. Kalfa, C. Sultan, R.A. Veitia, The forkhead factor FOXL2: a novel tumor suppressor?, Biochim Biophys Acta, 1805 (2010) 1-5.

[37] S.P. Shah, M. Kobel, J. Senz, R.D. Morin, B.A. Clarke, K.C. Wiegand, G. Leung, A. Zayed, E. Mehl, S.E. Kalloger, M. Sun, R. Giuliany, E. Yorida, S. Jones, R. Varhol, K.D. Swenerton, D. Miller, P.B. Clement, C. Crane, J. Madore, D. Provencher, P. Leung, A. DeFazio, J. Khattra, G. Turashvili, Y. Zhao, T. Zeng, J.N. Glover, B. Vanderhyden, C. Zhao, C.A. Parkinson, M. Jimenez-Linan, D.D. Bowtell, A.M. Mes-Masson, J.D. Brenton, S.A. Aparicio, N. Boyd, M.

Hirst, C.B. Gilks, M. Marra, D.G. Huntsman, Mutation of FOXL2 in granulosa-cell tumors of the ovary, N Engl J Med, 360 (2009) 2719-2729.

[38] N. Kalfa, C. Sultan, Juvenile ovarian granulosa cell tumor: a benign or malignant condition?, Gynecol Endocrinol, 25 (2009) 299-302.

[39] F.T. Kuo, I.K. Bentsi-Barnes, G.M. Barlow, M.D. Pisarska, Mutant Forkhead L2 (FOXL2) proteins associated with premature ovarian failure (POF) dimerize with wild-type FOXL2, leading to altered regulation of genes associated with granulosa cell differentiation, Endocrinology, 152 (2011) 3917-3929.

[40] M. Kobel, C.B. Gilks, D.G. Huntsman, Adult-type granulosa cell tumors and FOXL2 mutation, Cancer research, 69 (2009) 9160-9162.

[41] S. Yanagida, M.S. Anglesio, T.M. Nazeran, A. Lum, M. Inoue, Y. Iida, H. Takano, T. Nikaido, A. Okamoto, D.G. Huntsman, Clinical and genetic analysis of recurrent adult-type granulosa cell tumor of the ovary: Persistent preservation of heterozygous c.402C>G FOXL2 mutation, PloS one, 12 (2017) e0178989.

[42] R. Rosario, H. Araki, C.G. Print, A.N. Shelling, The transcriptional targets of mutant FOXL2 in granulosa cell tumours, PloS one, 7 (2012) e46270.

[43] N. Kalfa, P. Philibert, C. Patte, A. Ecochard, P. Duvillard, P. Baldet, F. Jaubert, M. Fellous, C. Sultan, Extinction of FOXL2 expression in aggressive ovarian granulosa cell tumors in children, Fertil Steril, 87 (2007) 896-901.

[44] A. Farkkila, M.K. McConechy, W. Yang, A. Talhouk, Y. Ng, A. Lum, R.D. Morin, K. Bushell, A. Riska, J.N. McAlpine, C.B. Gilks, L. Unkila-Kallio, M. Anttonen, D.G. Huntsman, FOXL2 402C>G Mutation Can Be Identified in the Circulating Tumor DNA of Patients with Adult-Type Granulosa Cell Tumor, J Mol Diagn, 19 (2017) 126-136.

[45] M. Gurumurthy, A. Bryant, S. Shanbhag, Effectiveness of different treatment modalities for the management of adult-onset granulosa cell tumours of the ovary (primary and recurrent), The Cochrane database of systematic reviews, 4 (2014) CD006912.

[46] National Comprehensive Cancer Network (U.S.), The complete library of NCCN clinical practice guidelines in oncology, National Comprehensive Cancer Network, Jenkintown, PA, 2005, pp. 1 computer optical disc.

[47] C. Iavazzo, I.D. Gkegkes, N. Vrachnis, Fertility sparing management and pregnancy in patients with granulosa cell tumour of the ovaries, Journal of obstetrics and gynaecology : the journal of the Institute of Obstetrics and Gynaecology, 35 (2015) 331-335.

[48] N. Rinne, A. Farthing, J. Borley, Fertility sparing surgery in advanced and recurrent granulosa cell tumours of the ovary, Journal of obstetrics and gynaecology : the journal of the Institute of Obstetrics and Gynaecology, 38 (2018) 143-145.

[49] I. Ray-Coquard, P. Morice, D. Lorusso, J. Prat, A. Oaknin, P. Pautier, N. Colombo, E.G. Committee, Non-epithelial ovarian cancer: ESMO Clinical Practice Guidelines for diagnosis, treatment and follow-up, Ann Oncol, 29 (2018) iv1-iv18.

[50] J.L. Meisel, D.M. Hyman, A. Jotwani, Q. Zhou, N.R. Abu-Rustum, A. Iasonos, M.C. Pike, C. Aghajanian, The role of systemic chemotherapy in the management of granulosa cell tumors, Gynecol Oncol, 136 (2015) 505-511.

[51] D. Teoh, R. Freedman, P.T. Soliman, Nearly 30 Years of Treatment for Recurrent Granulosa Cell Tumor of the Ovary: A Case Report and Review of the Literature, Case reports in oncology, 3 (2010) 14-18.

[52] J.K. Wolf, J. Mullen, P.J. Eifel, T.W. Burke, C. Levenback, D.M. Gershenson, Radiation treatment of advanced or recurrent granulosa cell tumor of the ovary, Gynecol Oncol, 73 (1999) 35-41.

[53] J. Hauspy, M.E. Beiner, I. Harley, B. Rosen, J. Murphy, W. Chapman, L.W. Le, A. Fyles, W. Levin, Role of adjuvant radiotherapy in granulosa cell tumors of the ovary, Int J Radiat Oncol Biol Phys, 79 (2011) 770-774.

[54] C. E, R. Samant, M.F. Fung, T. Le, L. Hopkins, M. Senterman, Palliative radiotherapy for recurrent granulosa cell tumor of the ovary: a report of 3 cases with radiological evidence of response, Gynecol Oncol, 102 (2006) 406-410.

[55] B.L. Seagle, P. Ann, S. Butler, S. Shahabi, Ovarian granulosa cell tumor: A National Cancer Database study, Gynecol Oncol, 146 (2017) 285-291.

[56] S. Bryk, E. Pukkala, J.I. Martinsen, L. Unkila-Kallio, L. Tryggvadottir, P. Sparen, K. Kjaerheim, E. Weiderpass, A. Riska, Incidence and occupational variation of ovarian granulosa cell tumours in Finland, Iceland, Norway and Sweden during 1953-2012: a longitudinal cohort study, BJOG, 124 (2017) 143-149.

[57] S. Sakr, E. Abdulfatah, S. Thomas, Z. Al-Wahab, R. Beydoun, R. Morris, R. Ali-Fehmi, S. Bandyopadhyay, Granulosa Cell Tumors: Novel Predictors of Recurrence in Early-stage Patients, Int J Gynecol Pathol, 36 (2017) 240-252.

[58] Y. Nishi, T. Yanase, Y. Mu, K. Oba, I. Ichino, M. Saito, M. Nomura, C. Mukasa, T. Okabe, K. Goto, R. Takayanagi, Y. Kashimura, M. Haji, H. Nawata, Establishment and characterization of a steroidogenic human granulosa-like tumor cell line, KGN, that expresses functional follicle-stimulating hormone receptor, Endocrinology, 142 (2001) 437-445.

[59] S. Jamieson, R. Butzow, N. Andersson, M. Alexiadis, L. Unkila-Kallio, M. Heikinheimo, P.J. Fuller, M. Anttonen, The FOXL2 C134W mutation is characteristic of adult granulosa cell tumors of the ovary, Mod Pathol, 23 (2010) 1477-1485.

[60] Y. Xue, B. Meehan, E. Macdonald, S. Venneti, X.Q.D. Wang, L. Witkowski, P. Jelinic, T. Kong, D. Martinez, G. Morin, M. Firlit, A. Abedini, R.M. Johnson, R. Cencic, J. Patibandla, H. Chen, A.I. Papadakis, A. Auguste, I. de Rink, R.M. Kerkhoven, N. Bertos, W.H. Gotlieb, B.A. Clarke, A. Leary, M. Witcher, M.C. Guiot, J. Pelletier, J. Dostie, M. Park, A.R. Judkins, R. Hass, D.A. Levine, J. Rak, B. Vanderhyden, W.D. Foulkes, S. Huang, CDK4/6 inhibitors target SMARCA4-determined cyclin D1 deficiency in hypercalcemic small cell carcinoma of the ovary, Nat Commun, 10 (2019) 558.

[61] E. Chan-Penebre, K. Armstrong, A. Drew, A.R. Grassian, I. Feldman, S.K. Knutson, K. Kuplast-Barr, M. Roche, J. Campbell, P. Ho, R.A. Copeland, R. Chesworth, J.J. Smith, H. Keilhack, S.A. Ribich, Selective Killing of SMARCA2- and SMARCA4-deficient Small Cell Carcinoma of the Ovary, Hypercalcemic Type Cells by Inhibition of EZH2: In Vitro and In Vivo Preclinical Models, Mol Cancer Ther, 16 (2017) 850-860.

[62] N.I. Fleming, K.C. Knower, K.A. Lazarus, P.J. Fuller, E.R. Simpson, C.D. Clyne, Aromatase is a direct target of FOXL2: C134W in granulosa cell tumors via a single highly conserved binding site in the ovarian specific promoter, PloS one, 5 (2010) e14389.

[63] M. Bilandzic, Y. Wang, N. Ahmed, R.B. Luwor, H.J. Zhu, J.K. Findlay, K.L. Stenvers, Betaglycan blocks metastatic behaviors in human granulosa cell tumors by suppressing NFkappaB-mediated induction of MMP2, Cancer letters, 354 (2014) 107-114.

[64] M. Imai, M. Muraki, K. Takamatsu, H. Saito, M. Seiki, Y. Takahashi, Spontaneous transformation of human granulosa cell tumours into an aggressive phenotype: a metastasis model cell line, BMC Cancer, 8 (2008) 319.

[65] J. Tu, H.H. Cheung, G. Lu, Z. Chen, W.Y. Chan, MicroRNA-10a promotes granulosa cells tumor development via PTEN-AKT/Wnt regulatory axis, Cell Death Dis, 9 (2018) 1076.

[66] J.H. Kim, Y.H. Kim, H.M. Kim, H.O. Park, N.C. Ha, T.H. Kim, M. Park, K. Lee, J. Bae, FOXL2 posttranslational modifications mediated by GSK3beta determine the growth of granulosa cell tumours, Nat Commun, 5 (2014) 2936.

[67] S. Bryk, Epidemiological, clinical, and prognostic factors in adult-type ovarian granulosa cell tumors, Obstetrics and Gynecology, Helsinki, 2017.

[68] G. Mangili, C. Sigismondi, L. Frigerio, M. Candiani, A. Savarese, G. Giorda, R. Lauria, S. Tamberi, S. Greggi, D. Lorusso, Recurrent granulosa cell tumors (GCTs) of the ovary: a MITO-9 retrospective study, Gynecol Oncol, 130 (2013) 38-42.

[69] K. Uygun, A. Aydiner, P. Saip, M. Basaran, F. Tas, Z. Kocak, M. Dincer, E. Topuz, Granulosa cell tumor of the ovary: retrospective analysis of 45 cases, Am J Clin Oncol, 26 (2003) 517-521.

[70] E. Babarovic, I. Franin, M. Klaric, A.M. Ferrari, R. Karnjus-Begonja, S. Eminovic, D.V. Ostojic, D. Vrdoljak-Mozetic, Adult Granulosa Cell Tumors of the Ovary: A Retrospective Study of 36 FIGO Stage I Cases with Emphasis on Prognostic Pathohistological Features, Anal Cell Pathol (Amst), 2018 (2018) 9148124.

[71] D. Hanahan, R.A. Weinberg, The hallmarks of cancer, Cell, 100 (2000) 57-70.

[72] D. Hanahan, R.A. Weinberg, Hallmarks of cancer: the next generation, Cell, 144 (2011) 646-674.

[73] J.F. Kerr, A.H. Wyllie, A.R. Currie, Apoptosis: a basic biological phenomenon with wide-ranging implications in tissue kinetics, Br J Cancer, 26 (1972) 239-257.

[74] G. Jing, J.J. Wang, S.X. Zhang, ER stress and apoptosis: a new mechanism for retinal cell death, Exp Diabetes Res, 2012 (2012) 589589.

[75] S. Elmore, Apoptosis: a review of programmed cell death, Toxicol Pathol, 35 (2007) 495-516.

[76] S. Fulda, K.M. Debatin, Extrinsic versus intrinsic apoptosis pathways in anticancer chemotherapy, Oncogene, 25 (2006) 4798.

[77] R.U. Janicke, M.L. Sprengart, M.R. Wati, A.G. Porter, Caspase-3 is required for DNA fragmentation and morphological changes associated with apoptosis, J Biol Chem, 273 (1998) 9357-9360.

[78] M.L.G. Ramirez, G.S. Salvesen, A primer on caspase mechanisms, Semin Cell Dev Biol, 82 (2018) 79-85.

[79] A.B. Parrish, C.D. Freel, S. Kornbluth, Cellular mechanisms controlling caspase activation and function, Cold Spring Harb Perspect Biol, 5 (2013).

[80] M. Brentnall, L. Rodriguez-Menocal, R.L. De Guevara, E. Cepero, L.H. Boise, Caspase-9, caspase-3 and caspase-7 have distinct roles during intrinsic apoptosis, BMC Cell Biol, 14 (2013) 32.

[81] M. Potokar, I. Milisav, M. Kreft, M. Stenovec, R. Zorec, Apoptosis triggered redistribution of caspase-9 from cytoplasm to mitochondria, FEBS Letters, 544 (2003) 153-159.

[82] M. Donepudi, M.G. Grutter, Structure and zymogen activation of caspases, Biophys Chem, 101-102 (2002) 145-153.

[83] O. Ramuz, D. Isnardon, E. Devilard, E. Charafe-Jauffret, J. Hassoun, F. Birg, L. Xerri, Constitutive nuclear localization and initial cytoplasmic apoptotic activation of endogenous caspase-3 evidenced by confocal microscopy, Int J Exp Pathol, 84 (2003) 75-81.

[84] E.A. Prokhorova, G.S. Kopeina, I.N. Lavrik, B. Zhivotovsky, Apoptosis regulation by subcellular relocation of caspases, Scientific Reports, 8 (2018) 12199.

[85] D.R. McIlwain, T. Berger, T.W. Mak, Caspase functions in cell death and disease, Cold Spring Harb Perspect Biol, 5 (2013) a008656.

[86] K.L. Huber, J.A. Hardy, Mechanism of zinc-mediated inhibition of caspase-9, Protein Sci, 21 (2012) 1056-1065.

[87] S.J. Riedl, M. Renatus, R. Schwarzenbacher, Q. Zhou, C. Sun, S.W. Fesik, R.C. Liddington, G.S. Salvesen, Structural basis for the inhibition of caspase-3 by XIAP, Cell, 104 (2001) 791-800.

[88] Y. Huang, Y.C. Park, R.L. Rich, D. Segal, D.G. Myszka, H. Wu, Structural basis of caspase inhibition by XIAP: differential roles of the linker versus the BIR domain, Cell, 104 (2001) 781-790.

[89] C. Lukacs, C. Belunis, R. Crowther, W. Danho, L. Gao, B. Goggin, C.A. Janson, S. Li, S. Remiszewski, A. Schutt, M.K. Thakur, S.K. Singh, S. Swaminathan, R. Pandey, R. Tyagi, R. Gosu, A.V. Kamath, A. Kuglstatter, The structure of XIAP BIR2: understanding the selectivity of the BIR domains, Acta Crystallogr D Biol Crystallogr, 69 (2013) 1717-1725.

[90] B.P. Eckelman, G.S. Salvesen, The human anti-apoptotic proteins cIAP1 and cIAP2 bind but do not inhibit caspases, J Biol Chem, 281 (2006) 3254-3260.

[91] S. Fulda, Molecular pathways: targeting death receptors and smac mimetics, Clin Cancer Res, 20 (2014) 3915-3920.

[92] F. Todt, Z. Cakir, F. Reichenbach, F. Emschermann, J. Lauterwasser, A. Kaiser, G. Ichim, S.W. Tait, S. Frank, H.F. Langer, F. Edlich, Differential retrotranslocation of mitochondrial Bax and Bak, EMBO J, 34 (2015) 67-80.

[93] N. Sovolyova, S. Healy, A. Samali, S.E. Logue, Stressed to death - mechanisms of ER stress-induced cell death, Biol Chem, 395 (2014) 1-13.

[94] R. Sano, J.C. Reed, ER stress-induced cell death mechanisms, Biochim Biophys Acta, 1833 (2013) 3460-3470.

[95] R. Bravo, V. Parra, D. Gatica, A.E. Rodriguez, N. Torrealba, F. Paredes, Z.V. Wang, A. Zorzano, J.A. Hill, E. Jaimovich, A.F. Quest, S. Lavandero, Endoplasmic reticulum and the unfolded protein response: dynamics and metabolic integration, Int Rev Cell Mol Biol, 301 (2013) 215-290.

[96] N. Morishima, K. Nakanishi, H. Takenouchi, T. Shibata, Y. Yasuhiko, An endoplasmic reticulum stress-specific caspase cascade in apoptosis. Cytochrome c-independent activation of caspase-9 by caspase-12, J Biol Chem, 277 (2002) 34287-34294.

[97] M.A. Miles, C.J. Hawkins, Executioner caspases and CAD are essential for mutagenesis induced by TRAIL or vincristine, Cell Death Dis, 8 (2017) e3062.

[98] B. Feeney, A.C. Clark, Reassembly of active caspase-3 is facilitated by the propeptide, J Biol Chem, 280 (2005) 39772-39785.

[99] K.G. Ponder, L.H. Boise, The prodomain of caspase-3 regulates its own removal and caspase activation, Cell Death Discov, 5 (2019) 56.

[100] K.S. Putt, G.W. Chen, J.M. Pearson, J.S. Sandhorst, M.S. Hoagland, J.T. Kwon, S.K. Hwang, H. Jin, M.I. Churchwell, M.H. Cho, D.R. Doerge, W.G. Helferich, P.J. Hergenrother, Small-molecule activation of procaspase-3 to caspase-3 as a personalized anticancer strategy, Nat Chem Biol, 2 (2006) 543-550.

[101] A.G. Daniel, E.J. Peterson, N.P. Farrell, The bioinorganic chemistry of apoptosis: potential inhibitory zinc binding sites in caspase-3, Angew Chem Int Ed Engl, 53 (2014) 4098-4101.

[102] S.J. Eron, D.J. MacPherson, K.B. Dagbay, J.A. Hardy, Multiple Mechanisms of Zinc-Mediated Inhibition for the Apoptotic Caspases-3, -6, -7, and -8, ACS Chem Biol, 13 (2018) 1279-1290.

[103] R.C. Botham, H.S. Roth, A.P. Book, P.J. Roady, T.M. Fan, P.J. Hergenrother, Small-Molecule Procaspase-3 Activation Sensitizes Cancer to Treatment with Diverse Chemotherapeutics, ACS Cent Sci, 2 (2016) 545-559.

[104] Q.P. Peterson, D.R. Goode, D.C. West, K.N. Ramsey, J.J. Lee, P.J. Hergenrother, PAC-1 activates procaspase-3 in vitro through relief of zinc-mediated inhibition, J Mol Biol, 388 (2009) 144-158.

[105] H.S. Roth, R.C. Botham, S.C. Schmid, T.M. Fan, L. Dirikolu, P.J. Hergenrother, Removal of Metabolic Liabilities Enables Development of Derivatives of Procaspase-Activating Compound 1 (PAC-1) with Improved Pharmacokinetics, J Med Chem, 58 (2015) 4046-4065.

[106] Q.P. Peterson, D.C. Hsu, C.J. Novotny, D.C. West, D. Kim, J.M. Schmit, L. Dirikolu, P.J. Hergenrother, T.M. Fan, Discovery and canine preclinical assessment of a nontoxic procaspase-3-activating compound, Cancer research, 70 (2010) 7232-7241.

[107] M. MacFarlane, TRAIL-induced signalling and apoptosis, Toxicology letters, 139 (2003) 89-97.

[108] Z. Mahmood, Y. Shukla, Death receptors: targets for cancer therapy, Experimental cell research, 316 (2010) 887-899.

[109] A. Ashkenazi, V.M. Dixit, Apoptosis control by death and decoy receptors, Curr Opin Cell Biol, 11 (1999) 255-260.

[110] S.K. Kelley, A. Ashkenazi, Targeting death receptors in cancer with Apo2L/TRAIL, Current opinion in pharmacology, 4 (2004) 333-339.

[111] D. de Miguel, J. Lemke, A. Anel, H. Walczak, L. Martinez-Lostao, Onto better TRAILs for cancer treatment, Cell Death Differ, 23 (2016) 733-747.

[112] A. Ashkenazi, R.C. Pai, S. Fong, S. Leung, D.A. Lawrence, S.A. Marsters, C. Blackie, L. Chang, A.E. McMurtrey, A. Hebert, L. DeForge, I.L. Koumenis, D. Lewis, L. Harris, J. Bussiere, H. Koeppen, Z. Shahrokh, R.H. Schwall, Safety and antitumor activity of recombinant soluble Apo2 ligand, The Journal of clinical investigation, 104 (1999) 155-162.

[113] R.S. Herbst, S.G. Eckhardt, R. Kurzrock, S. Ebbinghaus, P.J. O'Dwyer, M.S. Gordon, W. Novotny, M.A. Goldwasser, T.M. Tohnya, B.L. Lum, A. Ashkenazi, A.M. Jubb, D.S. Mendelson, Phase I dose-escalation study of recombinant human Apo2L/TRAIL, a dual proapoptotic receptor agonist, in patients with advanced cancer, J Clin Oncol, 28 (2010) 2839-2846.

[114] J. Lemke, S. von Karstedt, J. Zinngrebe, H. Walczak, Getting TRAIL back on track for cancer therapy, Cell Death Differ, 21 (2014) 1350-1364.

[115] P.M. Holland, Death receptor agonist therapies for cancer, which is the right TRAIL?, Cytokine Growth Factor Rev, 25 (2014) 185-193.

[116] A. Mohr, T. Chu, N.G. Brooke, M.R. Zwacka, MSC.sTRAIL Has Better Efficacy than MSC.FL-TRAIL and in Combination with AKTi Blocks Pro-Metastatic Cytokine Production in Prostate Cancer Cells, Cancers, 11 (2019).

[117] Z. Yuan, K.K. Kolluri, E.K. Sage, K.H. Gowers, S.M. Janes, Mesenchymal stromal cell delivery of full-length tumor necrosis factor-related apoptosis-inducing ligand is superior to soluble type for cancer therapy, Cytotherapy, (2015).

[118] C. Voelkel-Johnson, D.L. King, J.S. Norris, Resistance of prostate cancer cells to soluble TNF-related apoptosis-inducing ligand (TRAIL/Apo2L) can be overcome by doxorubicin or adenoviral delivery of full-length TRAIL, Cancer Gene Ther, 9 (2002) 164-172.

[119] C.Y. Cheah, D. Belada, M.A. Fanale, A. Janikova, M.S. Czucman, I.W. Flinn, A.V. Kapp, A. Ashkenazi, S. Kelley, G.L. Bray, S. Holden, J.F. Seymour, Dulanermin with rituximab in patients with relapsed indolent B-cell lymphoma: an open-label phase 1b/2 randomised study, Lancet Haematol, 2 (2015) e166-174.

[120] C.Y. Kim, M. Jeong, H. Mushiake, B.M. Kim, W.B. Kim, J.P. Ko, M.H. Kim, M. Kim, T.H. Kim, P.D. Robbins, T.R. Billiar, D.W. Seol, Cancer gene therapy using a novel secretable trimeric TRAIL, Gene Ther, 13 (2006) 330-338.

[121] D.W. Stuckey, K. Shah, TRAIL on trial: preclinical advances in cancer therapy, Trends Mol Med, 19 (2013) 685-694.

[122] M. Jaaskelainen, A. Kyronlahti, M. Anttonen, Y. Nishi, T. Yanase, P. Secchiero, G. Zauli, J.S. Tapanainen, M. Heikinheimo, T.E. Vaskivuo, TRAIL pathway components and their putative role in granulosa cell apoptosis in the human ovary, Differentiation; research in biological diversity, 77 (2009) 369-376.

[123] A.L. Johnson, C. Ratajczak, M.J. Haugen, H.K. Liu, D.C. Woods, Tumor necrosis factor-related apoptosis inducing ligand expression and activity in hen granulosa cells, Reproduction, 133 (2007) 609-616.

[124] A. Farkkila, G. Zauli, U.M. Haltia, M. Pihlajoki, L. Unkila-Kallio, P. Secchiero, M. Heikinheimo, Circulating levels of TNF-related apoptosis inducing-ligand are decreased in patients with large adult-type granulosa cell tumors-implications for therapeutic potential, Tumour Biol, 37 (2016) 11909-11916.

[125] A. Kyronlahti, M. Kauppinen, E. Lind, L. Unkila-Kallio, R. Butzow, J. Klefstrom, D.B. Wilson, M. Anttonen, M. Heikinheimo, GATA4 protects granulosa cell tumors from TRAIL-induced apoptosis, Endocrine-related cancer, 17 (2010) 709-717.

[126] M. Anttonen, L. Unkila-Kallio, A. Leminen, R. Butzow, M. Heikinheimo, High GATA-4 expression associates with aggressive behavior, whereas low anti-Mullerian hormone expression associates with growth potential of ovarian granulosa cell tumors, J Clin Endocrinol Metab, 90 (2005) 6529-6535.

[127] A.E. Moore, Viruses with oncolytic properties and their adaptation to tumors, Ann N Y Acad Sci, 54 (1952) 945-952.

[128] I.R. Eissa, I. Bustos-Villalobos, T. Ichinose, S. Matsumura, Y. Naoe, N. Miyajima, D. Morimoto, N. Mukoyama, W. Zhiwen, M. Tanaka, H. Hasegawa, S. Sumigama, B. Aleksic, Y. Kodera, H. Kasuya, The Current Status and Future Prospects of Oncolytic Viruses in Clinical Trials against Melanoma, Glioma, Pancreatic, and Breast Cancers, Cancers (Basel), 10 (2018).

[129] H.A. Hoster, R.P. Zanes, Jr., E. Von Haam, Studies in Hodgkin's syndrome; the association of viral hepatitis and Hodgkin's disease; a preliminary report, Cancer research, 9 (1949) 473-480.

[130] S.J. Russell, K.-W. Peng, J.C. Bell, Oncolytic virotherapy, Nat. Biotechnol., 30 (2012) 658.

[131] M. Puhlmann, C.K. Brown, M. Gnant, J. Huang, S.K. Libutti, H.R. Alexander, D.L. Bartlett, Vaccinia as a vector for tumor-directed gene therapy: biodistribution of a thymidine kinase-deleted mutant, Cancer Gene Ther, 7 (2000) 66-73.

[132] P. Paszkowski, R.S. Noyce, D.H. Evans, Live-Cell Imaging of Vaccinia Virus Recombination, PLoS Pathog, 12 (2016) e1005824.

[133] C.J. Breitbach, J. Burke, D. Jonker, J. Stephenson, A.R. Haas, L.Q. Chow, J. Nieva, T.H. Hwang, A. Moon, R. Patt, A. Pelusio, F. Le Boeuf, J. Burns, L. Evgin, N. De Silva, S. Cvancic, T. Robertson, J.E. Je, Y.S. Lee, K. Parato, J.S. Diallo, A. Fenster, M. Daneshmand, J.C. Bell, D.H. Kirn, Intravenous delivery of a multi-mechanistic cancer-targeted oncolytic poxvirus in humans, Nature, 477 (2011) 99-102.

[134] D. Haddad, Genetically Engineered Vaccinia Viruses As Agents for Cancer Treatment, Imaging, and Transgene Delivery, Front Oncol, 7 (2017) 96.

[135] G. McFadden, Poxvirus tropism, Nat Rev Microbiol, 3 (2005) 201-213.

[136] S.R. Bidgood, J. Mercer, Cloak and Dagger: Alternative Immune Evasion and Modulation Strategies of Poxviruses, Viruses, 7 (2015) 4800-4825.

[137] H.J. Zeh, S. Downs-Canner, J.A. McCart, Z.S. Guo, U.N. Rao, L. Ramalingam, S.H. Thorne, H.L. Jones, P. Kalinski, E. Wieckowski, M.E. O'Malley, M. Daneshmand, K. Hu, J.C. Bell, T.H. Hwang, A. Moon, C.J. Breitbach, D.H. Kirn, D.L. Bartlett, First-in-man study of western reserve strain oncolytic vaccinia virus: safety, systemic spread, and antitumor activity, Mol Ther, 23 (2015) 202-214.

[138] D.H. Kirn, S.H. Thorne, Targeted and armed oncolytic poxviruses: a novel multi-mechanistic therapeutic class for cancer, Nat Rev Cancer, 9 (2009) 64-71.

[139] M.D. Weitzman, D.A. Ornelles, Inactivating intracellular antiviral responses during adenovirus infection, Oncogene, 24 (2005) 7686-7696.

[140] C.S. Ilkow, S.L. Swift, J.C. Bell, J.S. Diallo, From scourge to cure: tumour-selective viral pathogenesis as a new strategy against cancer, PLoS Pathog, 10 (2014) e1003836.

[141] Y. Yen, Ribonucleotide Reductase Subunit One as Gene Therapy Target, Clinical Cancer Research, 9 (2003) 4304.

[142] P. Nordlund, P. Reichard, Ribonucleotide reductases, Annu Rev Biochem, 75 (2006) 681-706.

[143] M. Fasullo, L. Endres, Nucleotide salvage deficiencies, DNA damage and neurodegeneration, International journal of molecular sciences, 16 (2015) 9431-9449.

[144] C.J. Breitbach, K. Parato, J. Burke, T.H. Hwang, J.C. Bell, D.H. Kirn, Pexa-Vec double agent engineered vaccinia: oncolytic and active immunotherapeutic, Curr Opin Virol, 13 (2015) 49-54.

[145] K.G. Potts, C.R. Irwin, N.A. Favis, D.B. Pink, K.M. Vincent, J.D. Lewis, R.B. Moore, M.M. Hitt, D.H. Evans, Deletion of F4L (ribonucleotide reductase) in vaccinia virus produces a selective oncolytic virus and promotes anti-tumor immunity with superior safety in bladder cancer models, EMBO Mol Med, 9 (2017) 638-654.

[146] M.H. Kim, T.R. Billiar, D.W. Seol, The secretable form of trimeric TRAIL, a potent inducer of apoptosis, Biochem Biophys Res Commun, 321 (2004) 930-935.

[147] J. Foloppe, J. Kempf, N. Futin, J. Kintz, P. Cordier, C. Pichon, A. Findeli, F. Vorburger, E. Quemeneur, P. Erbs, The Enhanced Tumor Specificity of TG6002, an Armed Oncolytic Vaccinia Virus Deleted in Two Genes Involved in Nucleotide Metabolism, Molecular therapy oncolytics, 14 (2019) 1-14.

[148] E. Quoix, H. Lena, G. Losonczy, F. Forget, C. Chouaid, Z. Papai, R. Gervais, C. Ottensmeier, A. Szczesna, A. Kazarnowicz, J.T. Beck, V. Westeel, E. Felip, D. Debieuvre, A. Madroszyk, J. Adam, G. Lacoste, A. Tavernaro, B. Bastien, C. Halluard, T. Palanché, J.-M. Limacher, TG4010 immunotherapy and first-line chemotherapy for advanced non-small-cell lung cancer (TIME): results from the phase 2b part of a randomised, double-blind, placebo-controlled, phase 2b/3 trial, The Lancet Oncology, 17 (2016) 212-223.

[149] A. Idbaih, P. Erbs, J. Foloppe, H. Chneiweiss, J. Kempf, M. Homerin, C. Schmitt, L. Nguyen Them, J.-Y. Delattre, TG6002: A novel oncolytic and vectorized gene pro-drug therapy approach to treat glioblastoma, Journal of Clinical Oncology, 35 (2017) e13510-e13510.

[150] C.J. Breitbach, A. Moon, J. Burke, T.H. Hwang, D.H. Kirn, A Phase 2, Open-Label, Randomized Study of Pexa-Vec (JX-594) Administered by Intratumoral Injection in Patients with Unresectable Primary Hepatocellular Carcinoma, Methods Mol Biol, 1317 (2015) 343-357.

[151] B.C. Vanderhyden, T.J. Shaw, J.F. Ethier, Animal models of ovarian cancer, Reprod Biol Endocrinol, 1 (2003) 67.

[152] M.F. Sanmamed, C. Chester, I. Melero, H. Kohrt, Defining the optimal murine models to investigate immune checkpoint blockers and their combination with other immunotherapies, Ann Oncol, 27 (2016) 1190-1198.

[153] S.Y. Kim, Insights into granulosa cell tumors using spontaneous or genetically engineered mouse models, Clin Exp Reprod Med, 43 (2016) 1-8.

[154] E. Campeau, V.E. Ruhl, F. Rodier, C.L. Smith, B.L. Rahmberg, J.O. Fuss, J. Campisi, P. Yaswen, P.K. Cooper, P.D. Kaufman, A versatile viral system for expression and depletion of proteins in mammalian cells, PloS one, 4 (2009) e6529.

[155] F.A. Kruyt, TRAIL and cancer therapy, Cancer letters, 263 (2008) 14-25.

[156] J.H. Ko, S.G. Lee, W.M. Yang, J.Y. Um, G. Sethi, S. Mishra, M.K. Shanmugam, K.S. Ahn, The Application of Embelin for Cancer Prevention and Therapy, Molecules, 23 (2018).

[157] T. Yang, J. Lan, Q. Huang, X. Chen, X. Sun, X. Liu, P. Yang, T. Jin, S. Wang, X. Mou, Embelin Sensitizes Acute Myeloid Leukemia Cells to TRAIL through XIAP Inhibition and NF-kappaB Inactivation, Cell biochemistry and biophysics, 71 (2015) 291-297.

[158] T. Mori, R. Doi, A. Kida, K. Nagai, K. Kami, D. Ito, E. Toyoda, Y. Kawaguchi, S. Uemoto, Effect of the XIAP inhibitor Embelin on TRAIL-induced apoptosis of pancreatic cancer cells, J Surg Res, 142 (2007) 281-286.

[159] D.V. Rozanov, A.Y. Savinov, V.S. Golubkov, O.L. Rozanova, T.I. Postnova, E.A. Sergienko, S. Vasile, A.E. Aleshin, M.F. Rega, M. Pellecchia, A.Y. Strongin, Engineering a leucine zipper-TRAIL homotrimer with improved cytotoxicity in tumor cells, Molecular cancer therapeutics, 8 (2009) 1515-1525.

[160] C.J. Breitbach, S.H. Thorne, J.C. Bell, D.H. Kirn, Targeted and armed oncolytic poxviruses for cancer: the lead example of JX-594, Curr Pharm Biotechnol, 13 (2012) 1768-1772.

[161] K.G. Potts, M.M. Hitt, R.B. Moore, Oncolytic viruses in the treatment of bladder cancer, Adv Urol, 2012 (2012) 404581.

[162] C.R. Irwin, M.M. Hitt, D.H. Evans, Targeting Nucleotide Biosynthesis: A Strategy for Improving the Oncolytic Potential of DNA Viruses, Front Oncol, 7 (2017) 229.

[163] L. Zhang, B. Fang, Mechanisms of resistance to TRAIL-induced apoptosis in cancer, Cancer Gene Ther, 12 (2005) 228-237.

[164] C.T. Hellwig, M. Rehm, TRAIL signaling and synergy mechanisms used in TRAIL-based combination therapies, Mol Cancer Ther, 11 (2012) 3-13.

[165] C. Voelkel-Johnson, Combination therapy with TRAIL: Recent developments and potential pitfalls, Cancer Biol Ther, 8 (2009) 81-83.

[166] A. Refaat, A. Abd-Rabou, A. Reda, TRAIL combinations: The new 'trail' for cancer therapy (Review), Oncol Lett, 7 (2014) 1327-1332.

[167] M.F. Ziauddin, Z.S. Guo, M.E. O'Malley, F. Austin, P.J. Popovic, M.A. Kavanagh, J. Li, M. Sathaiah, P. Thirunavukarasu, B. Fang, Y.J. Lee, D.L. Bartlett, TRAIL gene-armed oncolytic poxvirus and oxaliplatin can work synergistically against colorectal cancer, Gene Ther, 17 (2010) 550-559.

[168] A.G. El-Shemi, A.M. Ashshi, Y. Na, Y. Li, M. Basalamah, F.A. Al-Allaf, E. Oh, B.K. Jung, C.O. Yun, Combined therapy with oncolytic adenoviruses encoding TRAIL and IL-12 genes markedly suppressed human hepatocellular carcinoma both in vitro and in an orthotopic transplanted mouse model, J Exp Clin Cancer Res, 35 (2016) 74.

[169] W. Zhou, S. Dai, H. Zhu, Z. Song, Y. Cai, J.B. Lee, Z. Li, X. Hu, B. Fang, C. He, X. Huang, Telomerase-specific oncolytic adenovirus expressing TRAIL suppresses peritoneal dissemination of gastric cancer, Gene Ther, 24 (2017) 199-207.

[170] J. Hu, H. Wang, J. Gu, X. Liu, X. Zhou, Trail armed oncolytic poxvirus suppresses lung cancer cell by inducing apoptosis, Acta Biochim Biophys Sin (Shanghai), 50 (2018) 1018-1027.

[171] W. Zhu, H. Zhang, Y. Shi, M. Song, B. Zhu, L. Wei, Oncolytic adenovirus encoding tumor necrosis factor-related apoptosis inducing ligand (TRAIL) inhibits the growth and metastasis of triple-negative breast cancer, Cancer Biol Ther, 14 (2013) 1016-1023.

[172] Z. Han, S. Lee, S. Je, C.Y. Eom, H.J. Choi, J.J. Song, J.H. Kim, Survivin silencing and TRAIL expression using oncolytic adenovirus increase anti-tumorigenic activity in gemcitabine-resistant pancreatic cancer cells, Apoptosis, 21 (2016) 351-364.

[173] X. Yang, B. Huang, L. Deng, Z. Hu, Progress in gene therapy using oncolytic vaccinia virus as vectors, Journal of Cancer Research and Clinical Oncology, 144 (2018) 2433-2440.

[174] K. Kapp, Signal peptide database, Dresden, Germany, 2017.

[175] P.B. Harbury, P.S. Kim, T. Alber, Crystal structure of an isoleucine-zipper trimer, Nature, 371 (1994) 80-83.

[176] S.R. Wiley, K. Schooley, P.J. Smolak, W.S. Din, C.P. Huang, J.K. Nicholl, G.R. Sutherland, T.D. Smith, C. Rauch, C.A. Smith, et al., Identification and characterization of a new member of the TNF family that induces apoptosis, Immunity, 3 (1995) 673-682.

[177] H. Walczak, R.E. Miller, K. Ariail, B. Gliniak, T.S. Griffith, M. Kubin, W. Chin, J. Jones, A. Woodward, T. Le, C. Smith, P. Smolak, R.G. Goodwin, C.T. Rauch, J.C. Schuh, D.H. Lynch, Tumoricidal activity of tumor necrosis factor-related apoptosis-inducing ligand in vivo, Nat Med, 5 (1999) 157-163.

[178] M.J. Prodoehl, N. Hatzirodos, H.F. Irving-Rodgers, Z.Z. Zhao, J.N. Painter, T.E. Hickey, M.A. Gibson, W.E. Rainey, B.R. Carr, H.D. Mason, R.J. Norman, G.W. Montgomery, R.J. Rodgers, Genetic and gene expression analyses of the polycystic ovary syndrome candidate gene fibrillin-3 and other fibrillin family members in human ovaries, Molecular human reproduction, 15 (2009) 829-841.

[179] S. Tian, Q. Huang, Y. Fang, J. Wu, FurinDB: A database of 20-residue furin cleavage site motifs, substrates and their associated drugs, Int J Mol Sci, 12 (2011) 1060-1065.

[180] B.M. Amore, J.P. Gibbs, M.G. Emery, Application of in vivo animal models to characterize the pharmacokinetic and pharmacodynamic properties of drug candidates in discovery settings, Comb Chem High Throughput Screen, 13 (2010) 207-218.

[181] F. Barre-Sinoussi, X. Montagutelli, Animal models are essential to biological research: issues and perspectives, Future Sci OA, 1 (2015) FSO63.

[182] A. Richmond, Y. Su, Mouse xenograft models vs GEM models for human cancer therapeutics, Disease models & mechanisms, 1 (2008) 78-82.

[183] H. Chen, P. Crosley, A.K. Azad, N. Gupta, N. Gokul, Z. Xu, M. Weinfeld, L.M. Postovit, S.A. Pangas, M.M. Hitt, Y. Fu, RUNX3 Promotes the Tumorigenic Phenotype in KGN, a Human Granulosa Cell Tumor-Derived Cell Line, Int J Mol Sci, 20 (2019).

[184] F. Ojima, Y. Saito, Y. Tsuchiya, D. Kayo, S. Taniuchi, M. Ogoshi, H. Fukamachi, S. Takeuchi, S. Takahashi, Runx3 transcription factor regulates ovarian functions and ovulation in female mice, J Reprod Dev, 62 (2016) 479-486.

[185] F. Ojima, Y. Saito, Y. Tsuchiya, M. Ogoshi, H. Fukamachi, K. Inagaki, F. Otsuka, S. Takeuchi, S. Takahashi, Runx3 regulates folliculogenesis and steroidogenesis in granulosa cells of immature mice, Cell and Tissue Research, 375 (2019) 743-754.

[186] V.S. Dhillon, M. Shahid, S.A. Husain, CpG methylation of the FHIT, FANCF, cyclin-D2, BRCA2 and RUNX3 genes in Granulosa cell tumors (GCTs) of ovarian origin, Mol Cancer, 3 (2004) 33.

[187] H. Canada, Guidance Document: Preparation of Clinical Trial Applications for use of Cell Therapy Products in Humans, Government of Canada, 2015.

[188] A.C. Society, Key Statistics for Ovarian Cancer, 2019.

[189] D.R. Camidge, R.S. Herbst, M.S. Gordon, S.G. Eckhardt, R. Kurzrock, B. Durbin, J. Ing, T.M. Tohnya, J. Sager, A. Ashkenazi, G. Bray, D. Mendelson, A phase I safety and pharmacokinetic study of the death receptor 5 agonistic antibody PRO95780 in patients with advanced malignancies, Clin Cancer Res, 16 (2010) 1256-1263.

[190] C.S. Wegner, A. Hauge, L.M.K. Andersen, R. Huang, T.G. Simonsen, J.V. Gaustad, E.K. Rofstad, Increasing aggressiveness of patient-derived xenograft models of cervix carcinoma during serial transplantation, Oncotarget, 9 (2018) 21036-21051.

[191] J.J. Tao, N.A. Cangemi, V. Makker, K. Cadoo, J.F. Liu, D.W. Rasco, W.H. Navarro, C.M. Haqq, D.M. Hyman, First-in-Human Phase I Study of the Activin A Inhibitor, STM 434, in Patients with Granulosa Cell Ovarian Cancer and Other Advanced Solid Tumors, Clin Cancer Res, (2019).

[192] J. Li, R. Bao, S. Peng, C. Zhang, The molecular mechanism of ovarian granulosa cell tumors, J Ovarian Res, 11 (2018) 13.

[193] S.Y. Kim, K. Ebbert, M.H. Cordeiro, M.M. Romero, K.A. Whelan, A.A. Suarez, T.K. Woodruff, T. Kurita, Constitutive Activation of PI3K in Oocyte Induces Ovarian Granulosa Cell Tumors, Cancer research, 76 (2016) 3851-3861.